Stony Brook University

OFFICIAL COPY

The official electronic file of this thesis or dissertation is maintained by the University Libraries on behalf of The Graduate School at Stony Brook University.

© All Rights Reserved by Author.

The Role of Krüppel-like Factor 5 in the Pathogenesis of Pancreatic Ductal Adenocarcinoma

A Dissertation Presented

by

Ping He

to

The Graduate School

in Partial Fulfillment of the

Requirements

for the Degree of

Doctor of Philosophy

in

Molecular and Cellular Biology

(Concentration – Immunology and Pathology)

Stony Brook University

January 2018

Stony Brook University

The Graduate School

Ping He

We, the dissertation committee for the above candidate for the

Doctor of Philosophy degree, hereby recommend

acceptance of this dissertation.

Vincent W. Yang, M.D., Ph.D. – Dissertation Advisor
Professor and Chair, Department of Medicine

Michael A. Frohman, M.D., Ph.D. - Chairperson of Defense
Professor and Chair, Department of Pharmacological Sciences

W. Todd Miller, Ph.D.
Professor and Chair, Department of Physiology and Biophysics

Agnieszka B. Bialkowska, Ph.D.
Assistant Professor, Department of Medicine

Weiqin Lu, Ph.D.
Assistant Professor, Department of Medicine

This dissertation is accepted by the Graduate School

Charles Taber

Dean of the Graduate School

Abstract of the Dissertation

The Role of Krüppel-like Factor 5 in the Pathogenesis of Pancreatic Ductal Adenocarcinoma

by

Ping He

Doctor of Philosophy

in

Molecular and Cellular Biology

(Concentration – Immunology and Pathology)

Stony Brook University

2018

Pancreatic intraepithelial neoplasm (PanIN) is the most common type of precursor lesions of pancreatic ductal adenocarcinoma (PDAC). In the mouse pancreas, oncogenic *Kras* mutations are sufficient for spontaneous PanIN formation, which can be further expedited by cerulein-induced pancreatitis. Krüppel-like factor 5 (KLF5), a triple zinc-finger transcription factor, is differentially upregulated in pancreatic ductal adenocarcinoma (PDAC). Recent evidence shows that KLF5 is normally absent in acinar cells and is expressed in PanIN and PDAC in human tissues. The role of KLF5 in PanIN formation is unknown. To investigate whether KLF5 is required for early oncogenic *Kras*-driven tumorigenesis, I developed genetic engineered mouse models that combined inducible Klf5 knockout with oncogenic *Kras* expression in adult pancreatic acinar cells (*Ptf1a-Cre^{ERTM};Klf5$^{fl/fl}$*, *Ptf1a-Cre^{ERTM};LSL-Kras^{G12D}*, *Ptf1a-Cre^{ERTM};LSL-Kras^{G12D};Klf5$^{fl/fl}$*). *Klf5* knockout reduced oncogenic *Kras*-induced PanIN formation. Furthermore, *Klf5* knockout mice failed to develop acinar-to-ductal metaplasia (ADM), a type of transformation that is triggered by pancreatitis and precedes PanIN formation. Transcriptomic analysis showed that *Klf5* knockout restored normal expression of genes that were altered by oncogenic KRAS signaling. These data showed that KLF5 is required for early pancreatic tumorigenesis induced by oncogenic KRAS. Furthermore, transcriptomic profiling identified NDRG2 as a potential inhibitor of ADM. To investigate the effect of *Klf5* depletion on proliferation of pancreatic cancer cells, I depleted KLF5 in mouse pancreatic cell lines using a system that allows for the expression of *Klf5*-specific shRNA (or proper scrambled shRNA control) upon doxycycline induction. *Klf5* knockdown in mouse pancreatic cancer cells line resulted in dosage-dependent reduction in cancer cell proliferation, possibly due to cell cycle arrests. *Klf5* knockdown in mouse pancreatic cancer cells also increased expression of DNA damage response genes, decreased expression of ductal marker, and decreased

tumor growth in mouse subcutaneous allograft model. In summary, the data showed that KLF5 plays a diverse range of pro-oncogenic roles during initiation as well as progression of pancreatic cancer.

Dedication Page

To my parents, two of the greatest scientists I know, who taught me to believe in hard work and provided me with every opportunity I could wish for.

To my family for their love and support in my journey to pursue my dreams.

Table of Contents

Page

List of Figures

Page

List of Tables

Page

List of Abbreviations

ADM	Acinar-to-ductal metaplasia
AIP	Anterior intestinal portal
ATRA	All-trans retinoid acid
CCND	Cyclin
CDKN	Cyclin dependent kinase inhibitor
ChIP	Chromatin immunoprecipitation
CRISPR	Clustered regularly interspaced short palindromic repeats
E	Embryonic day
EGF	Epidermal growth factor
EMT	Epithelial-to-mesenchymal transition
FFPE	Formalin-fixed paraffin-embedded
FGF	fibroblast growth factor
FOX	Forkhead box
GATA	GATA binding protein
GWAS	Genome-wide association study
HNF	Hepatic nuclear factor
H&E	Hematoxylin & eosin
IC	Immunocytochemistry
IF	Immunofluorescence
IHC	Immunohistochemistry
IPMN	Intraductal papillary mucinous neoplasia
JNK	c-Jun N-terminal kinases
KLF	Krüppel-like factor
KRAS	Kirsten rat sarcoma viral oncogene homolog
KRT19	Keratin-19
LPA	Lysophosphatidic acid
MAPK	Mitogen-activated protein kinase
MCN	mucinous cystic neoplasia
MEK	Mitogen-activated protein kinase kinase
MPC	Multipotent pancreatic progenitor cells
MUC	Mucin
MIZ-1	Myc-interacting zinc finger protein 1
NDRG2	N-Myc downstream-regulated gene 2
NKX	Nirenberg and Kim homeobox factor

PanIN	Pancreatic intraepithelial neoplasia
PDAC	Pancreatic ductal adenocarcinoma
PDX1	Pancreatic and duodenal homeobox factor 1
PI3K	Phosphatidylinositol-3-kinase
PTEN	Phosphatase and tensin homolog
PTF1A	Pancreas specific transcription factor subunit 1A
RA	Retinoic acid
RBPJ	Recombination signal binding protein for immunoglobulin kappa J region
REC8	REC8 meiotic recombination protein
RER	Rough endoplasmic reticulum
SFN	Stratifin
sgRNA	single guide RNA
SHH	Sonic hedgehog
SMAD	SMAD family member
SOX	SRY-box protein
SRY	Sex-determining region Y
TP53	Tumor protein 53

Acknowledgments

First and foremost, I would like to thank Dr. Vincent W. Yang for giving me the opportunity to join his laboratory and for guiding me through every step of my scientific training. I greatly appreciate his patience and guidance in training me to think critically about science and to incorporate clinical knowledge into scientific research. He is a great role model for the physician scientist that I will continue to aspire to become.

I am extremely grateful to Dr. Agnieszka B. Bialkowska for all of the time and effort she has spent on teaching me the scientific rigor that has made me a successful scientist. She has taught me how to be independent in carrying out experiments and how to be specific during presentations. Her enthusiasm for science and optimistic attitude will continue to motivate me throughout my scientific career.

A special thanks goes to my thesis committee members: Dr. Michael Frohman, Dr. Todd Miller, and Dr. Weiqin Lu. I would also like to thank my past committee member, Dr. Jian Cao. I am grateful for their time and commitment in helping me complete my doctoral training with their wonderful scientific questions and advice.

I could not have completed my research without the help of current and past members of the laboratory, my scientific collaborators, as well as members of Dr. Sandeep Mallipattu's laboratory. I am grateful for their willingness to share with me their knowledge and the protocols they have painstakingly optimized. Without their help, this dissertation would have been completed two years later. I learned a great deal from everyone. I am especially thankful to Dr. Yang Liu and Chang-Kyung (Joanna) Kim, my comrades in arms, for their tremendous moral support. I would also like to thank all of the friends I have made at Stony Brook.

I am especially grateful to Drs. Nai-Kong V. Cheung and Irene Cheung for their support and encouragement on my journey to become a physician scientist. Thank you, Dr. Nai-Kong Cheung, for showing me that the more difficult path is sometimes worth taking.

My scientific work was made possible with support from the Stony Brook Medical Scientist Training Program (MSTP), Stony Brook Molecular and Cellular Biology (MCB) Graduate Program, and National Cancer Institute (NCI).

The text of this dissertation in part is a reprint of the materials as it appears in:

Ping He, Jong Won Yang, Vincent W. Yang, Agnieszka B. Bialkowska. Krüppel-like Factor 5, Increased in Pancreatic Ductal Adenocarcinoma, Promotes Proliferation, Acinar to Ductal Metaplasia, Pancreatic Intraepithelial Neoplasia, and Tumor Growth in Mice. In *Gastroenterology*. Accepted for Publication on December 10, 2017.

Chapter 1. Introduction

1.1 Pancreas Physiology

Pancreas is a slender glandular organ located in the retroperitoneum posterior to the stomach. The head of pancreas is found in the curvature of the duodenum. The body of the pancreas extends transversely for approximately 6 inches and ends with its tail found in the hilum of the spleen (1). Genomic analysis has revealed there are highly-conserved pancreas-specific genes across all jawed vertebrates, which supports the theory that the first distinct pancreatic organ evolved through a single, early evolutionary event that predates the vertebrate radiation (2).

Pancreas performs both unique exocrine and endocrine roles that are critical for normal body functions. The three major cell types of the pancreas are the acinar cells, islet cells, and ductal epithelial cells. The endocrine functions of the pancreas are performed by the islet cells found in clusters known as Islets of Langerhans. Specialized islet cells secrete hormones including insulin, glucagon and somatostatin that are required for maintaining glucose levels in the blood. Additionally, specialized islet cells also secrete pancreatic polypeptide hormone, which plays a role in controlling appetite (1). See Figure 1.1 for illustration of the anatomy of pancreas.

The exocrine function of the pancreas is performed by pancreatic acinar cells and ductal epithelial cells. Acinar cell is the most abundant cell type in the pancreas, accounting for 80% of all pancreatic cells. They are pyramid-shaped, polarized, secretory epithelial cells arranged in grape-like acini. Their main function is to synthesize, store and secrete pancreatic enzymes that facilitate the digestion of food in the small intestine. The apical side of each acinar cell faces the

intercellular canaliculi, which connects the acinus to the intercalated duct of the extensive pancreatic ductal network. The basolateral side of each cell faces the interstitial space. At a subcellular level, acinar cells have basolaterally located nuclei surrounded by abundant rough endoplasmic reticulum (RER). The three major types of enzymes synthesized at the RER are α-amylase, lipase, and proteases which are responsible for the hydrolysis of carbohydrate, fat, and proteins, respectively (3). Those enzymes are sorted and packaged in secretory granules through the trans-Golgi network and post-Golgi maturation (1). The mature granules are stored at the apical side of the cells, and the release of their content is regulated by several neuroendocrine secretagogues (1). Cholecystokinin and acetylcholine triggers activation of protein kinase C and Ca2+-dependent exocytosis through inositol triphosphate/diacyl glycerol signaling pathway (1). In contrast, secretin and vasoactive intestinal peptide trigger secretion through increased level of intracellular cAMP and activation of protein kinase A (1). Additionally, angiotensin II can also regulate acinar secretion in a dosage-dependent fashion (1).

Pancreatic ductal epithelial cells form the complex network that collects the enzymes secreted by the acinar cells and deposits them into the duodenum at the ampulla of Vater (also known as duodenal ampulla) (4). The ductal cells of intercalated duct form a simple squamous epithelium which becomes a simple cuboidal epithelium as they join to form the interlobular ducts (4). The epithelium of the larger ducts are lined by cuboidal or columnar epithelial cells surrounded by connective tissue (4). In addition to their function in forming the ductal network, pancreatic ductal epithelial cells are essential for production of bicarbonate that neutralizes the acidity of food enter the duodenum from the stomach (4). Carbonic anhydrase synthesizes bicarbonate and protons from carbon dioxide and water (4). Protons are eliminated from the ductal cells through

basolaterally located Na+/H+ exchanger. Bicarbonate is secreted into the lumen through anionic exchangers on the apical surface of the cells (4).

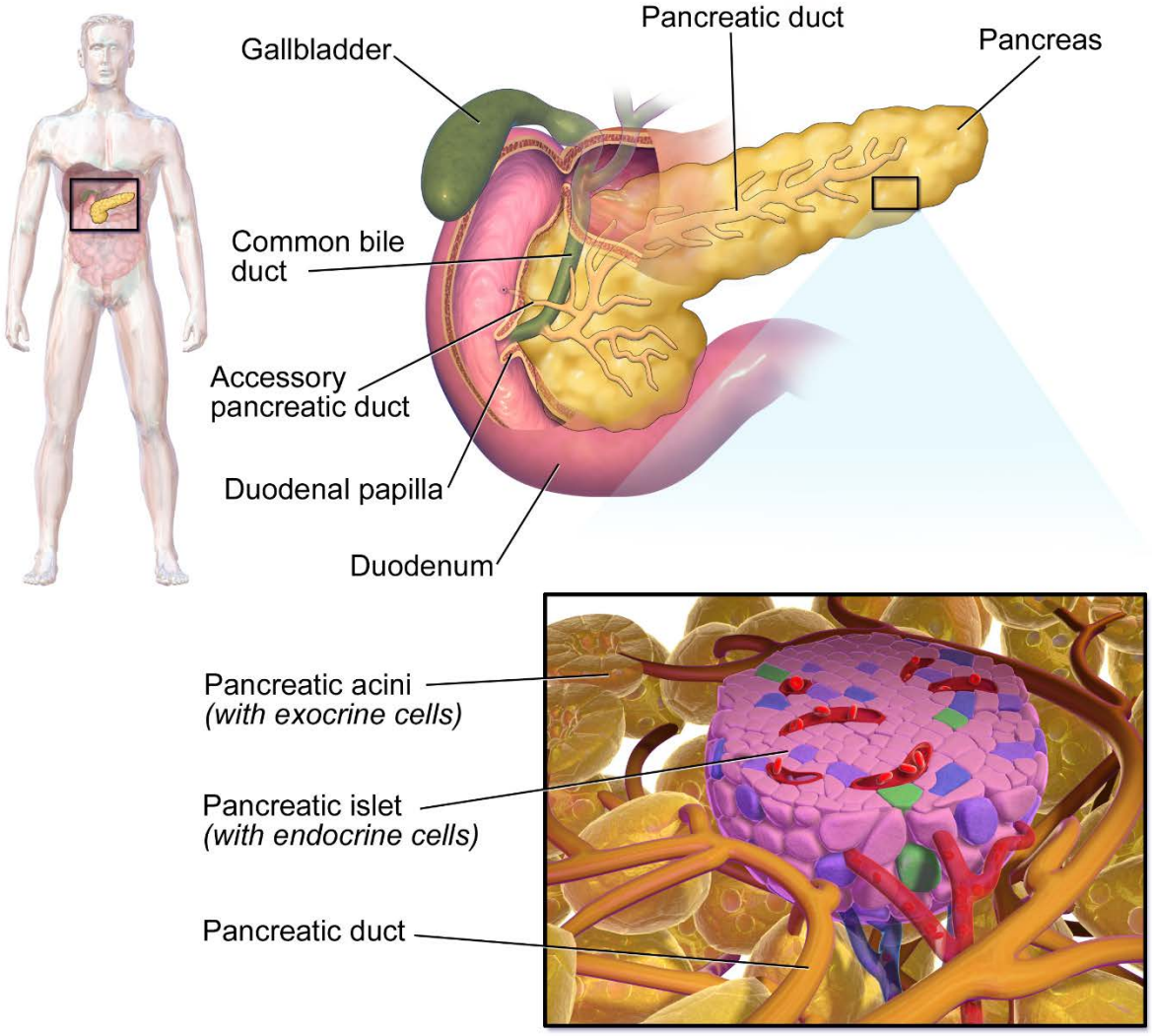

Figure 1.1. Anatomy of the Pancreas
Illustration showing location of the pancreas in the curvature of the duodenum and the arrangement of pancreatic cell types in pancreatic tissue.
Illustration by Bruce Blaus. Blausen.com staff (2014). "Medical gallery of Blausen Medical 2014". WikiJournal of Medicine 1 (2). DOI:10.15347/wjm/2014.010. ISSN 2002-4436. - CC BY 3.0, https://commons.wikimedia.org/w/index.php?curid=28909220

1.2 Signaling Pathways in Pancreatic Development and Adult Pancreas

In mouse, the flat sheet of endoderm folds to form the primitive gut tube, which is divided into foregut, midgut, and hindgut. At embryonic day 7.5 in mouse, the anterior endoderm invaginates to form the anterior intestinal portal (AIP) at the foregut-midgut boundary, the site of pancreatic specification (5). Pancreatic development begins with the condensation of mesenchyme overlying the dorsal aspect of the endodermal gut tube (6). The notochord patterns the adjacent foregut to develop into the dorsal pancreatic bud by excluding sonic hedgehog (SHH), which allows for the expression of the key transcription factor pancreatic and duodenal homeobox factor 1 (PDX1) (5). At approximately 26th day of gestation in human or comparable embryonic day 9.5 in mouse, the endoderm evaginates into the mesenchymal cells giving rise to the initial dorsal bud, which elongates and loses contact with the notochord due to the fusion of dorsal aorta in the midline (5, 6). Approximately 6 days after dorsal bud evagination in human or 16 hours after dorsal bud evagination in mouse, the ventral bud begin to arise from the hepatic/biliary bud evagination (Figure 1.2, A and B) (5, 6).

The molecular control of the ventral pancreas development is markedly different from that of the dorsal pancreas (6). The ventral pancreas fate is induced in the portion of the ventral foregut that has low levels of cardiac fibroblast growth factor (FGF) signaling. The dorsal pancreatic development requires retinoic acid (RA) signaling, as well as Activin and FGF2 secreted from the notochord and dorsal aorta to repress SHH expression during dorsal bud evagination. By approximately 30th day of gestation in human and embryonic day 9.5 in mouse, the multipotent pancreatic progenitor cells (MPCs) are found to occupy both ventral and dorsal buds and are marked by transcription factor SRY (sex-determining region Y)-box 9 (SOX9), PDX1, pancreas

specific transcription factor subunit 1a (PTF1A), and GATA binding protein 4 (GATA4) (Figure 1.2B) (5).

Once evaginated, the pancreatic buds undergo elongation and branching morphogenesis. Pancreas undergoes acute angle branching allowing the new adjacent branches to exclude intervening mesenchyme (6). FGF10 produced by the mesenchymal tissue plays an important role in proliferation of MPCs during this stage (5). Around embryonic day 12 to 13 in mouse or embryonic day 37 to 42 in humans, the ventral and dorsal buds come into contact with one another and fuses (Figure 1.2C). Up until this point there is very little cellular differentiation (6). Proliferation is primarily driven by WNT signaling, which also allows for the maintenance of progenitor status. Epidermal growth factor (EGF) also aids in the proliferative process and further inhibits endocrine differentiation (5). At the tissue level, a dramatic morphogenic reorganization begins in the pancreatic epithelium, which ultimately leads to the formation of two distinct cellular domains. The “tips” of the branching epithelium contain pro-acinar MPCs, which express Nirenberg and Kim homeobox factor (NKX) 6.1, SOX9, and GATA4, while the “trunk” region harbors cells that express NKX6.1 and SOX9 and will give rise to islet and ductal cells (5, 7).

At approximately embryonic day 13.5 in mouse, dramatic cellular changes occur and this marks the beginning of a period known as “secondary transition” (Figure 1.2, D and E) (6, 7). Acinar cell differentiation occurs rapidly with the “tip” cells losing their multipotency and becoming acinar progenitor cells. In mouse, this is marked by the rapid loss of SOX9 in the “tip” cells (5). The differentiation of acinar cells is followed by a rapid expansion and differentiation of endocrine cell number driven by NOTCH signaling via the neurogenin 3 (NGN3) transcription factor (6, 8).

Embryonic development of the pancreas requires a perfectly orchestrated series of complex signaling and gene expression. Many transcription factors are critical for coordinating the expression of genes at the proper time during development. Three of the most important factors required for the maintenance of MPCs are PDX1, PTF1A, and SOX9. PDX1 is an important transcription factor for pancreatic development. Germ-line inactivation of *Pdx1* causes pancreatic agenesis by arresting the growth of the pancreatic epithelium around mouse embryonic day 10.5 (9, 10). How *Pdx1* regulate progenitor expansion remains poorly understood. Microarray analysis found that *Pdx1* mutant mouse embryos exhibit downregulation of several transcription factors including *Nkx6.1* and *Ptf1a* (11). In addition, a decrease in *Sox9* expression has also been observed in those mice (12). Experiments performed in transgenic mice have shown that *Pdx1* DNA binding sites in enhancer of *Gata4* gene are required for its expression *in vivo* at embryonic day 10.5 to promote acinar lineage commitment. Chromatin immunoprecipitation (ChIP) assay have demonstrated that PDX1 protein directly interacts with sequences in both hepatic nuclear factor 1b (*Hnf1b)* and forkhead box A2 (*Foxa2)* genes (13). *Pdx1* expression is maintained in the developing epithelium, and gradually becomes restricted to islet cells in the adult pancreas where it has been shown to regulate proper insulin synthesis (14). *Pdx1* inactivation using a tetracycline-inducible system in mouse during mid-pancreatic development led to pancreatic agenesis and loss of acinar and islet differentiation, suggesting that *Pdx1* activity is required for all cell types throughout the extent of pancreatic development (15). These results suggest that *Pdx1* is important for the specification of pancreatic cells in early development and maintains islet cell differentiation in adult pancreas.

PTF1A is another important transcription factor during pancreatic organogenesis. Loss of *Ptf1a* results in pancreatic agenesis although a rudimentary dorsal bud is present (16). Lineage-

tracing experiments have shown that *Ptf1a*-deficient cells adopt an intestinal fate (16). These results suggest that *Ptf1a* is essential for the commitment and proliferation of pancreatic progenitors. It has been suggested that FGF10 signaling from the mesenchyme cells maintains *Ptf1a* expression in the dorsal pancreatic bud, but the underlying mechanism is unclear (17). PTF1A protein is a subunit of the PTF1 complex, a trimeric complex composed of two PTF1A and either recombination signal binding protein for immunoglobulin kappa J region (RBPJ) or RBPJL (18). The formation of the complex PTF1A-RBPJ is essential for proper pancreatic development. Mutations in PTF1A protein that impairs RBPJ binding cause pancreatic phenotype similar to *Ptf1a* null mice (19). A recent study has identified a significant number of direct targets of PTF1A in pancreatic progenitors (20). Several of these targets are transcription factors also expressed in MPC populations such as *Pdx1, Nkx6.1, Hnf6*, and *Mnx1* (20). It is also important to note that PTF1A maintains its own expression during pancreatic development (21). PTF1A is the master regulator of acinar cell differentiation (22, 23) and initiates it by a mechanism that involves the replacement of the subunit RBPJ by RBPJL (23). The PTF1A-RBPJL complex appears to directly activate the expression of acinar-specific genes including those coding for secreted enzymes, as suggested by ChIP-seq and gene profiling experiments (23). Lineage tracing experiments show that *Ptf1a* expression become limited to acinar cells in adult mice beginning at embryonic day 14.5 (24).

Sox9, a member of the SRY/HMG box family, is expressed in the $Pdx1^{+}$ cells from embryonic day 9.5, and *Sox9*-expressing cells can give rise to all pancreatic cell types (25). During the secondary transition, *Sox9* expression becomes restricted to the trunk ductal/endocrine progenitor domain. At later stages of pancreas development, SOX9 is maintained in ductal cells. Conditional inactivation of *Sox9* in the $Pdx1^{+}$ cells results in severe pancreatic hypoplasia due to

both diminished MPC proliferation and increased MPC cell death (25). In addition to MPC proliferation and survival, SOX9 is required to maintain MPC identity through a feedforward mechanism mediated by mesenchymal FGF signaling (12). Disruption of this results in activation of the liver developmental program in the pancreatic epithelium (12). SOX9 directly regulates the expression of other transcription factors expressed in MPCs, such as *Hnf1b, Hnf6,* and *FoxA2* suggesting a central role for SOX9 in the transcriptional network controlling MPC formation and maintenance (25).

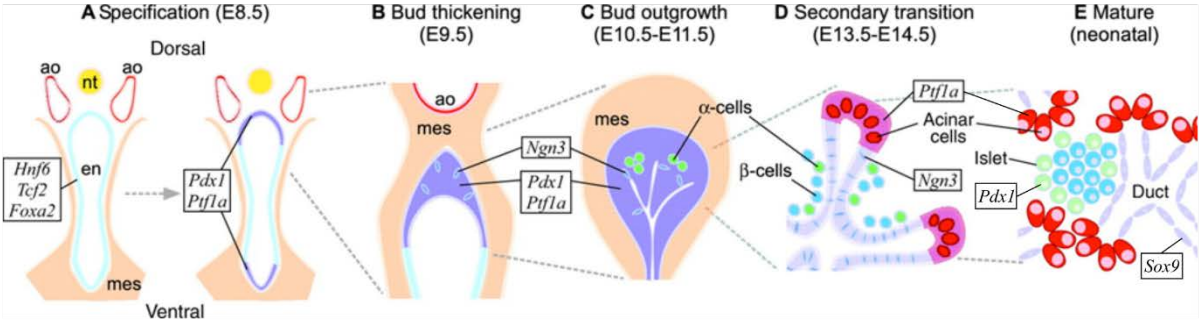

Figure 1.2. Development of the Mouse Pancreas

Illustration showing the developing pancreas in mouse at different embryonic days. **(A)** *Pdx1* and *Ptf1a* initial expression in the dorsal and ventral buds evaginating from the gut endoderm (en). Nearby tissues include notochord (nt) and aorta (ao). **(B)** Mesenchyme (mes) surrounds the thickening buds as the first *Ngn3+* pro-endocrine cells appear. **(C)** Subsequent outgrowth produces a dense epithelial bud, in which early α-cells begin to differentiate. **(D)** The secondary transition marked by massive differentiation and the progressive restriction of *Pdx1* and *Ptf1a* expression. **(E)** The organ has assumed its mature form with *Pdx1* expression in the islet cells, *Ptf1a* expression in the acinar cells, and *Sox9* expression in the ductal cells.

Modified from original figure in: L. Charles Murtaugh. Pancreas and beta-cell development: from the actual to the possible. *Development*. 2007 Feb;134(3):427-38.

Reproduced with permission from Company of Biologists (26)

1.3 Pancreatic Ductal Adenocarcinoma and Its Precursor Lesions

For 2017, the National Cancer Institute estimates that pancreatic cancer will account for 3.2% of cancer cases and 7.2% of cancer-related deaths in the U.S. If incidences of pancreatic cancer continue to rise at the currently rate, pancreatic cancer will be the second leading cause of cancer related death by 2030 (27). Malignant neoplasms of the pancreas are currently classified based on the cellular differentiation into ductal, acinar, or neuroendocrine types (28). Pancreatic ductal adenocarcinoma (PDAC) comprises about 90% of all pancreatic cancer (28). Pancreatic ductal adenocarcinoma is a devastating disease. The overall 5-year survival rate is less than 7%. The majority of patients are diagnosed at an advanced stage. Only about 20% of patient have localized disease and are eligible for radical curative surgery, but the median survival after surgery remains low at only 18 months (28, 29).

PDAC are genetically complex with wide-spread chromosomal abnormalities and numerous mutations (30, 31). Complete analysis of the PDAC exome showed an average of 63 genomic alterations, mainly point mutations (32). These mutations result in the alterations of 12 cellular signaling pathways and processes present in the majority of pancreatic adenocarcinomas. The most notable among those are Kirsten rat sarcoma viral oncogene homolog (KRAS) signaling, regulation of the G_1/S cell cycle transition, TGF-β signaling, integrin signaling, regulation of cell invasion, cell adhesion and small guanine triphosphate (GTPase)-dependent signaling (32). The four most frequently mutated genes are *KRAS* (90%), cyclin dependent kinase inhibitor 2A (*CDKN2A*, p16, 90%), tumor protein P53 (*TP53*, 70%) and SMAD family member 4 (*SMAD4*, 55%) (32). Transcription of the mutant *KRAS* gene determines the production of an abnormal, constitutively-activated KRAS protein, causing the uncontrolled activation of proliferation and survival pathways. Inactivation of the *CDKN2A* gene results in the loss of p16 protein, a master

negative regulator of the G_1/S transition of the cell cycle. TP53 mutations allow the cells to bypass important control checkpoints at the level of DNA damage and apoptosis. Finally, the frequent loss of *SMAD4* gene results in the aberrant signaling by TGF-β. More recent exome sequencing and copy number analyses confirmed the four most frequently mutated genes and identified novel mutant genes involved in chromatin modification (*EPC1* and *ARID2*), DNA damage repair (*ATM*), and axon guidance (33).

Two different progression models have been proposed for the genetic evolution of cancer cells during pancreatic oncogenesis and progression. In one model, comparison of genetic mutations in metastasis to the primary tumor from which they arose showed surprisingly large number of conserved alterations in both. The mutations can be categorized into "founder mutations," present in all samples from a single patient, and "progressor mutations," found only in a subset of samples from each patient. Founder mutations are the four major genes known to be involved in pancreatic carcinogenesis (i.e. *KRAS*, *CDKN2A*, *TP53*, and *SMAD4*). Progressor mutations occur later than founder mutations and are unique to each clonal population in distant metastases that represent heterogeneous subclones also found in the primary tumor (34). Mathematical modeling using this data suggests that genetic evolution of PDAC takes 12 years to progress from the earliest genetic alteration in a precursor lesion to a full-blown invasive cancer, five more years to acquire metastatic ability, and the average patient dies 2 years after metastasis (34).

A more recent study challenges the model of gradual progression in pancreatic oncogenesis with a rapid progression model. Analysis of copy number alterations in PDACs showed that 45% of tumors displayed significant changes in copy number alterations and polyploidization. Mathematical modeling showed that 65% of copy number alterations were caused by a

chromothripsis event, a catastrophic chromosomal damage event leading to high number of rearrangements from incorrect DNA repair (35). Of the chromothripsis events, 11% occur on chromosome 18 resulting in loss of tumor suppressor *SMAD4* and 8% occur on chromosome 12 leading to focal amplification in the region of *KRAS* (35). Polyploid tumors displayed higher frequency of chromothripsis, more *TP53* mutations, and are correlated with worse overall survival (35). Furthermore, most mutations are acquired during diploid phase preceding neoplastic transformation. These data suggest a rapid progression model in which preneoplastic lesions acquire copy number alterations through polyploidization and chromothripsis events leading to rapid neoplastic transformation (35). The number of mutations in founder genes in each tumor has significant prognostic implications (36, 37). Thirty-seven percent of patients have mutations in all 4 founder genes, and patients with mutations in 2 or less founder genes have significantly longer overall survival (36).

During pancreatic oncogenesis, PDAC arises from different types of non-invasive precursor lesions (Figure 1.3A). The most common precursor lesion is pancreatic intraepithelial neoplasia (PanIN) (38). Other less common precursor lesions are intraductal papillary mucinous neoplasia (IPMN) and mucinous cystic neoplasm (MCN) (39). The concept of these lesions being the precursors to PDAC was first established through the analysis of the pancreatic cancer tissues in order to create a pathological progression model for PDAC initiation based on histology (40). Careful genomic studies later supported this model by demonstrating that the precursor lesions share only some of the genetic alterations with their associated infiltrating cancer and the prevalence of shared genetic alterations increases with increasing severity of dysplasia (40, 41).

PanINs are non-invasive microscopic epithelial lesions (<5mm), located in the smaller pancreatic ducts (42). They are composed of a flat or papillary epithelium. PanINs are classified

into different grades according to the extent of histological abnormalities (Figure 1.3B). PanIN-1A and PanIN-1B lesions are low-grade dysplasia, characterized by tall columnar cells with basolateral nuclei and abundant apical mucin. PanIN-1A lesions have flat epithelium, while PanIN-1B lesions have papillary architecture. PanIN-2 lesions are intermediate-grade dysplasia with mostly papillary epithelium with mild to moderate cytological atypia. PanIN-3 lesions are high-grade dysplasia (*carcinoma in situ*) characterized by papillary proliferations of cells with significant cytological atypia (43). PanIN-3 lesions are frequently associated with invasive pancreatic cancer.

Low-grade PanINs are frequently found in normal pancreas. A study using pancreata surgically resected for reasons other than PDAC found PanINs in 26% of 584 cases (44). Most of the lesions were PanIN-1 (50%) and PanIN-2 (41%). PanIN-3 represents 8% of the total PanINs. Genetic studies suggest that PanIN can be a precursor to invasive pancreatic cancer. Increasing grades of PanIN lesions are correlate with accumulating genetic alterations (38). Telomere shortening and activating mutations in the *KRAS* oncogene are the most common alterations in low-grade PanIN lesions (45, 46). Deep sequencing of patient samples showed that *KRAS* mutations are present in >90% of PanIN lesions, including low-grade PanINs, which suggests a gradual expansion of *KRAS*-mutant clone during PanIN progression (47). Mutations in other founder genes, including *CDKN2A, TP53,* and *SMAD4* are associated with progression (46). Loss of *CDKN2A* expression correlates with increasing PanIN grade (30% of PanIN-1A/B, 55% of PanIN-2, and 70% of PanIN-3) (48, 49). Inactivation of *TP53* and *SMAD4* are almost exclusively found in PanIN-3 lesions at 30-50% frequency (50, 51). See summary of mutations in PanINs in Figure 1.3B.

The genetic alterations that are crucial to transition from PanIN-3 lesions to an invasive carcinoma are not very well understood. Currently, it is impossible to trace the PanIN lesions that gave rise to the PDAC since much of the pancreas is quickly overgrown by the PDAC after neoplastic transformation. Furthermore, histological distinction between PanIN-3 and adjacent PDAC can be difficult. Despite these limitations, exome sequencing of PDAC and adjacent PanIN-2 and PanIN-3 lesions have shown that PanINs and invasive carcinomas have similar numbers of mutations (52). Even though there were fewer mutations in PanIN-2 (averaging 30 mutations) compared to the invasive carcinomas (averaging 50 mutations), PanIN-3 showed on average even more mutations (averaging 60 mutations) (52). Careful examination of the specific mutations showed that 66% of mutations were common to the invasive carcinoma and the adjacent PanIN, 10% mutations were only present in the invasive carcinoma, and 25% of the mutations were only present in PanIN lesions (52). The high number of common mutations shared by PanIN and invasive carcinoma supports the progression model, but also raises concerns on whether a lesion is a true PanIN-3 lesion or the ductal spread from adjacent PDAC. It is important to point out that there is no direct clinical evidence showing that presence of PanIN lesions increases the risk or worsen the outcome for PDAC. Clinical studies have shown that PanIN at a resection margin does not affect survival in patients who have a resection for invasive cancer (53). The lack of correlation may be the result of the patients dying from their disease long before residual PanIN has time to progress (53). Study investigating the significance of incidentally discovered PanIN in pancreatic resections for reasons other than PDAC showed that PanIN in the pancreas did not result in an appreciable cancer risk (44).

Intraductal papillary mucinous neoplasia (IPMN) are non-invasive, large, lesions (>5mm in diameter) characterized by mucin-producing epithelium with long papillary projections that

arise within the larger pancreatic ducts (42, 54). IPMN are found with higher frequency in the head of pancreatic (54). Histologically, IPMNs can be categorized as gastric-foveolar, intestinal, pancreatobiliary, or oncocytic type based on the cellular differentiation and morphology of the epithelium (55, 56). Although there are clear differences between IPMN subtypes based on their morphological features, many IPMNs show mixed histology suggesting that the subtypes do not represent completely distinct underlying pathways (56). Although IPMNs share genetic alterations with PanIN and PDAC, some genetic alterations such as activating *GNAS* mutations and inactivating *RNF43* mutations are more specific for the IPMN (57, 58). Genes that are most frequently mutated are *KRAS*, *GNAS*, *CDKN2*A, *RNF43*, *TP53*, and *SMAD4* (57). Virtually all IPMNs (> 90%) harbor at least one mutation in *KRAS* and *GNAS*, suggesting that IPMNs are initiated by a mutation in either of these genes (59). Mutations of oncogene *GNAS* occurs in about 66% of IPMNs, and majority of these mutations are present in the corresponding invasive carcinoma (60). Interestingly, *GNAS* mutations were not found in other types of cystic neoplasms of pancreas or in invasive carcinoma not associated with IPMN lesions (61). A recent study on molecular characterization of a large set of IPMNs showed that 91% of IPMNs display *KRAS* or *GNAS* mutations (47% show mutations in both genes), 38% has *RNF43* mutation, and few have mutations in other adenocarcinoma associated genes: *CDKN2A* (3%), *CTNNB1* (6%), *SMAD4* (5%), and *TP53* (9%) (62).

Mucinous cystic neoplasia (MCNs) are the least common of the precursor lesions that can give rise to PDAC. MCNs are defined as mucin-producing cyst-forming epithelial lesions with an ovarian-type stroma (42, 63). MCNs occur almost exclusively in women and usually in the tail of the pancreas, and they do not communicate with the pancreatic duct system. MCNs is less well-characterized genetically compared to PanINs and IPMNs. Whole-exome sequencing of

microdissected MCNs has revealed an average of 16 somatic mutations with few allelic losses (57). Mutations in *KRAS* are most frequent and are found in 25% of MCNs with low-grade dysplasia, 40% with intermediate-grade dysplasia, and 90% with high-grade dysplasia (57).

The low survival rate in PDAC patients is partially due to the fact that the majority of them are diagnosed at advanced stages (28). There are also extensive stromal involvement creating a protective microenvironment for the cancer cell, which accounts for the high resistance to conventional chemotherapy (64). Understanding the underlying biology of early pancreatic tumorigenesis may be critical for the development of novel diagnostic techniques for early stage detection and of novel therapies for preventive intervention. Genetically engineered mouse models that faithfully recapitulate the initiation of human PDAC have been an important tool used to identify the pancreatic lineages responsible for developing PDAC. The most widely utilized model expresses endogenous $Kras^{G12D}$ oncogene in pancreatic cells during embryonic development by expressing a Cre recombinase under the control of the *Pdx1* or *Ptf1a* promoter (65). This is the only model that recapitulates the full spectrum of PanIN lesions seen in patients (65). However, the limitation is that the expression of the $Kras^{G12D}$ occurs in multipotent pancreatic progenitor cells (MPCs) at embryonic day 8.5 and is maintained in all pancreatic lineages after birth (65).

To better understand the cells of origin for PanIN and PDAC, mutant *Kras* have been expressed in differentiated cells of specific pancreatic lineage in adult mice. One of the earliest studies of this type utilized a mouse model expressing oncogenic $Kras^{G12V}$ through a Cre recombinase under the control of a *Cela1* (gene for pancreatic elastase) promoter and regulated by a tet-off system (66). In this model, oncogenic $Kras^{G12V}$ expression is limited to the acinar cells (66), and the $Kras^{G12V}$ expression can also be kept off from the time of embryonic development to 2 months after birth using tet-off system by continuous administration of doxycycline (66).

Expression of *Kras*^{G12V} before birth resulted in spontaneous generation of PanINs and PDAC indistinguishable from those in human patient (66). However, turning on expression of *Kras*^{G12V} in the adult acinar cells did not allow them to form PanINs unless they were also subjected to chronic pancreatitis induced by cerulein, an oligopeptide analog of cholecystokinin (66). These findings suggested that a non-genetic event such as inflammatory response is required in addition to genetic alteration for the initiation phase of pancreatic tumorigenesis (66). This hypothesis is further supported by well-accepted correlation between chronic pancreatitis and risk of PDAC in patients (67). However, later study using mouse model with expression of oncogenic *Kras*^{G12D} in adult acinar cells using Cre recombinase controlled by *Cela1* promoter or Basic Helix-Loop-Helix Family Member A15 (*Bhlha15*, better known as *Mist1*) promoter showed that inflammation is not essential for the formation of PanINs (68). This discrepancy may be due to the difference in the ability of the two mutant *Kras* alleles to induce senescence (69). Regardless, the study also identified occasional cells with both acinar and ductal phenotypes present in PanINs, which suggest that the differentiated acinar cell with appropriate genetic context is susceptible to spontaneous transdifferentiation into PanIN lesions through an intermediate state (69).

Acinar-to-ductal metaplasia (ADM) is a common and reversible process during pancreatic inflammation, and it is important in facilitating pancreas regeneration after injury (70, 71). During ADM, pancreatic acinar cells undergo genetic reprogramming and transdifferentiate to duct-like progenitor cells (70). Experiments using isolated mouse acini cultured in 3-dimensional (3D) matrices have demonstrated that ADM can be initiated by inflammatory events such as acute and chronic pancreatitis as well as genetic mutations (70, 72-76). Furthermore, recent 3D culture study using human acinar cells demonstrated that ADM in human acinar cells can be induced by TGF-β stimulation (77).

Unlike inflammation, aberrant growth factor signaling, such as oncogenic KRAS signaling, promotes irreversible ADM by preventing re-differentiation and by promoting further progression toward PDAC precursor lesions. Alteration in gene expression caused by oncogenic KRAS signaling includes: silencing of acinar genes such as *PTF1A*, and those for enzymes such as amylase and elastase; induction of ductal genes such as those coding for keratin-19 (*KRT19*) and mucin (*MUC1*); and upregulating expression of multipotent pancreatic progenitor cell genes such *PDX1* and *SOX9* (75). Lineage-tracing experiments in mice demonstrated that ADM cells derived from acinar cells due to persistent expression of oncogenic $Kras^{G12D}$ are incapable of re-differentiation and instead progresses to form PanINs (78). PTF1 transcriptional complex, as mentioned before, has a central role in maintaining acinar cell identity and the production of digestive enzymes (23). *Ptf1a* becomes epigenetically silenced during ADM in mice (79). Furthermore, ablation of *Ptf1a* in mice is sufficient to induce ADM and sensitizing cells to KRAS-mediated transformation (80).

In the normal adult pancreas, SOX9 is expressed in centroacinar cells, at very low levels in acinar cells, and in a subpopulation of ductal cells (81, 82). During inflammation or in the presence of oncogenic KRAS signaling, *Sox9* expression increases in acinar cells and stimulates gene expression that leads to ADM (83) and consequent formation of PanIN (78). In line human tumor samples, *SOX9* expression is elevated at all stages of PanINs and PDAC (84). The absence of *Sox9* expression reduces EGFR signaling and pancreatic tumorigenesis, suggesting a potential mechanism by which SOX9 promotes ADM (85).

In the adult mouse pancreas, *Pdx1* is mainly expressed in islets and only at low levels in acinar cells (86, 87). As shown by lineage tracing, during mouse development, $Pdx1^{+}$ cells represent progenitors of all mature pancreatic cell types (88). When *Pdx1* is persistently

overexpressed during development, the mice develop smaller pancreata filled with duct-like structures (89). *PDX1* is upregulated during pancreatitis, in PanINs, as well as in PDAC in patients (86, 89). PDX1 protein regulates ADM through activation of signal transducer and activator of transcription 3 (STAT3) (89). STAT3 is a regulator of stem cell self-renewal and inflammation, and its activity during ADM in pancreas has also been shown to increase via IL-6 (90) and KRAS–YAP1/TAZ signaling (91, 92). STAT3 signaling is required for ADM, PanIN formation, and PDAC development, and mice with pancreas-specific *Stat3* knockout have reduced $Kras^{G12D}$-induce tumorigenesis (90).

A recent study demonstrated that Krüppel-like factor 4 (KLF4), a member of Krüppel-like factor family of transcription factors (93-95), is also required for oncogenic $Kras^{G12D}$-driven ADM and subsequent PanIN formation (96). *Klf4* is normally expressed in the ductal cell in mouse pancreas, and it transcriptionally regulates the expression of ductal gene *Krt19* (97). In human pancreatic cancer cells, *KLF4* overexpression causes decrease in cell proliferation through upregulation of p21 and the down-regulation of cyclin D1 (98). Another study using mouse models showed that KLF4 functions as a tumor suppressor by suppressing metastasis through downregulation of *CD44*, a marker for cancer stem cell (99). *Klf4* ablation in mouse pancreatic cells attenuates $Kras^{G12D}$-induced ADM and PanIN formation, and *Klf4* overexpression promotes $Kras^{G12D}$-induced ADM and PanIN formation (96). The results suggest that KLF4 promotes ADM and PanIN formation during early pancreatic tumorigenesis, and becomes a tumor suppressor after neoplastic transformation. It is important to point out that neither *Klf4* knockout nor *Klf4* overexpression in pancreatic cells had significant effect on normal pancreatic architecture, suggesting that *Klf4* is dispensable in the context of wild-type KRAS. Furthermore, *Klf4*

overexpression alone is not sufficient to induce ADM or PanIN formation, suggesting that other transcription factors downstream of oncogenic KRAS signaling are required for KLF4 function.

Major signaling targets for oncogenic KRAS signaling during ADM are the mitogen-activated protein kinase (MAPK) pathway and the phosphatidylinositol-3-kinase (PI3K)/AKT pathway. Early studies examining the role of EGFR signaling in oncogenic *Kras*^{G12D}-induced mouse model of PDAC demonstrated that oncogenic KRAS signaling upregulates expression of *Egfr* and activates EGFR signaling (100). When EGFR signaling is inhibited either genetically or pharmacologically, the reduced level of KRAS signaling cannot efficiently promote pancreatic tumorigenesis due to insufficient induction of MEK/ERK activity (100). Further studies showed that inhibition of MAPK signaling using small molecular inhibitors to MEK1 and MEK2 prevents ADM and PanIN formation (75, 101). More recently, MEK activity has been shown to be required for ADM after inflammation in the context of wild-type KRAS (102).

PI3K acts downstream of KRAS, and ADM, PanIN formation, and cancer initiation are all dependent on p110α (also known as PIK3CA, the catalytic subunit of PI3K) (103, 104). ADM, PanIN and the formation of invasive PDAC occurs after expression of a constitutively-active form of p110α (105). PI3K-mediated transdifferentiation of acinar cells is mediated through ERK1/2 signaling (105). To drive these processes, PI3K also initiates actin reorganization orchestrated by Rho GTPases (103, 104, 106). Pancreas-specific deletion of phosphatase and tensin homolog (PTEN), which negatively regulates PI3K signaling, leads to ADM, PanIN, and PDAC in mice (107). In the context of oncogenic *Kras* expression, PTEN loss leads to accelerated formation of PDAC (108, 109). Similarly, expression of a constitutively active allele of *Akt1*, one of the downstream targets for PI3K signaling, induces ADM (110) and cooperates with oncogenic KRAS signaling to drive the progression of PDAC (111). However, only a small set (>3%) of PDAC

patients have mutations in *PIK3CA* (112), which suggests that contribution of PI3K activity is a part of oncogenic KRAS signaling in majority of patients.

ADM in human pancreatic cancer specimens can be observed in proximity to neoplastic precursor lesions (113, 114). Attempts have been made to investigate if human acinar cells that underwent ADM can be precursors to PanIN. Analyses of human ADM lesions for *KRAS* mutations indicated that ADM associated with PanIN lesions harbored the same *KRAS* gene mutation. By contrast, ADM lesions that were not associated with PanIN had wild-type *KRAS*. The conclusion was that the ADM lesion associated with PanIN might represent retrograde extension of the PanIN (115). With the knowledge that inflammation and macrophage-released cytokines can lead to ADM independent of *KRAS* mutations (72), the detection of ADM lesions that are *KRAS* wild-type is not surprising. As human PDAC often has pancreatitis associated, one would expect both ADM lesions that express wild-type *KRAS* and ADM lesions that express mutant *KRAS* (115). Thus, these data can also be interpreted differently: PanIN and ADM lesions associated with PanIN have the same mutations because ADM is a precursor for PanIN; and some of the ADM have progressed to PanIN owing to additional signaling or mutations that ADM did not have. As discussed earlier, it is also possible that the development of human PDAC from ADM might not follow the PanIN progression model, but rather might lead to occurrence of flat lesions (116).

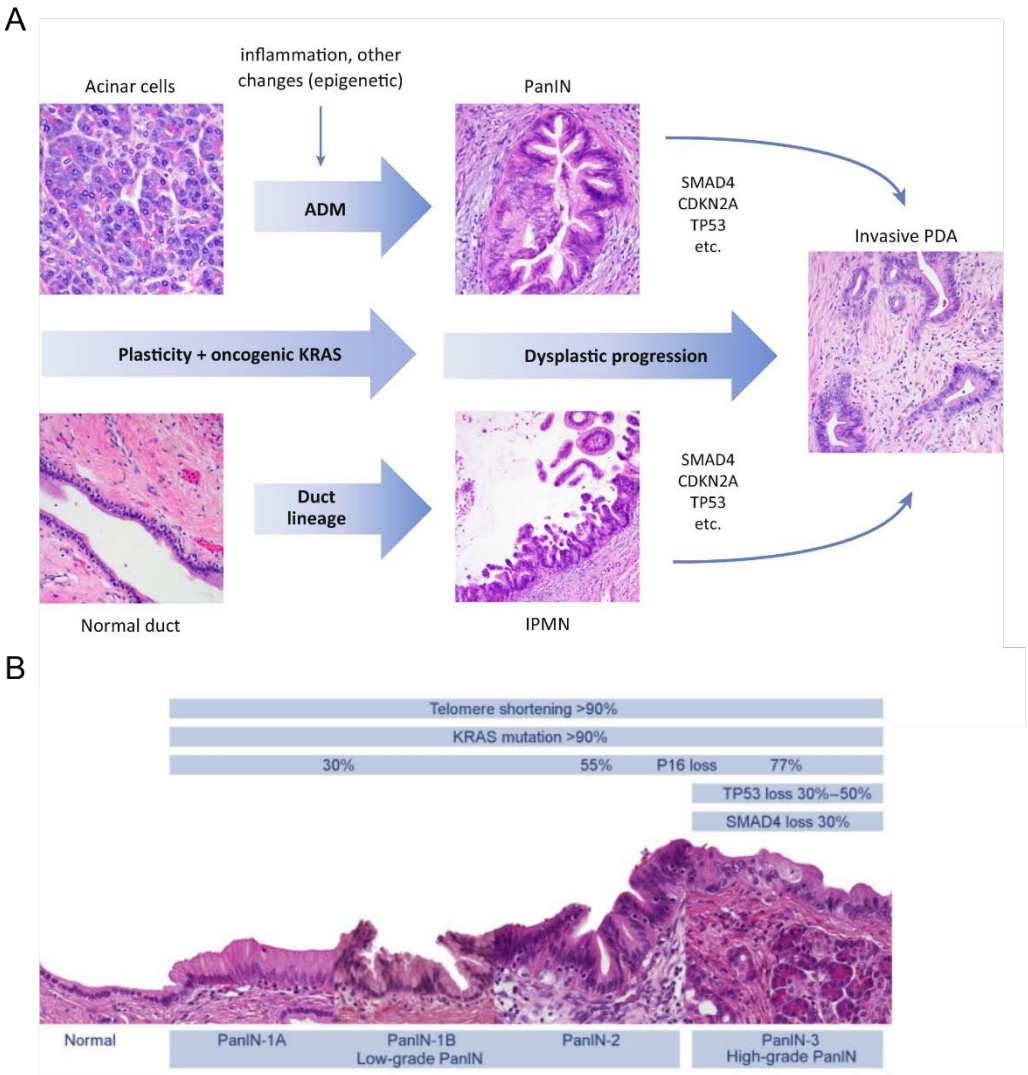

Figure 1.3. Precursor Lesions of Pancreatic Ductal Adenocarcinoma

(A) Acinar cells undergo ADM in response to inflammatory signals or oncogenic KRAS signaling and subsequently gives rise to PanIN lesions. Mature ductal cells may also undergo dedifferentiation to give rise to IPMN lesions. Both PanIN and IPMN lesions accumulate additional molecular alterations during progression to invasive adenocarcinoma. **(B)** The progression of PanIN from low-grade to high-grade are associated with an increased cellular atypia and tissue dysplasia. PanIN-1 and PanIN-2 are low-grade PanIN. PanIN-3 are considered *carcinoma in situ*. Frequency of common mutations are shown.

(A) Modified from original figure in: Timothy R. Donahue and David W. Dawson. Leveraging Mechanisms Governing Pancreatic Tumorigenesis To Reduce Pancreatic Cancer Mortality. *Trends in Endocrinology and Metabolism* 2016 Nov;27(11):770-781. With permission from Elsevier (117)

(B) Reproduced from original figure in: Michaël Noë and Lodewijk A.A. Brosens, Pathology of Pancreatic Cancer Precursor Lesions. *Surgical Pathology Clinics* 2016 Dec;9(4):561-580. With permission from Elsevier (118)

1.4 KLF5 in Gastrointestinal Physiology and Pathophysiology

Krüppel-like factor 5 (KLF5) is a member of family of triple-zinc finger transcription factors, and it has diverse functions in the development and homeostasis of many tissues in the body (See review on mammalian KLFs in *Physiological Reviews* (93)). KLF5 plays an important role during early embryogenesis, and *Klf5* homozygous deletion in mouse embryo is lethal by embryonic day 8.5 (See review on the role of KLFs in stem cell and development in *Development* (94)) (119). The physiological role of KLF5 in the gastrointestinal system is best studied in the context of the intestines (See review on the roles of KLFs in gastrointestinal system in *Gastroenterology* (95)). KLF5 is normally expressed in the stem cells and the transient amplifying progenitor cells at the bottom of the crypt in the intestinal epithelium (120). Intestinal epithelium-specific deletion of *Klf5* in mice through a Cre recombinase under the control of Villin 1 (*Vil1*) promoter showed disruption in intestinal barrier function and increased inflammation due to the impaired epithelial proliferation and differentiation (121). Furthermore, the intestinal pathology is so severe that two-third of the newborn die shortly after birth (121). Interestingly, the surviving animal show a regenerative epithelium with increased expression of SOX9 (121). Similar study deleting *Klf5* from intestinal epithelium using a Cre recombinase drive by *Shh* promoter showed impaired villi formation, possibly due to the lack of decrease in *Sox9* expression normally associated with villi formation (122). The combined data showed that *Klf5* is important for the development of normal intestinal tissue. To examine whether KLF5 is also required for the maintenance of intestinal epithelium in the adult mice, *Klf5* was deleted by a tamoxifen-inducible Cre recombinase and estrogen receptor ligand binding domain fusion protein (Cre^{ERT2}) controlled under *Vil1* promoter (123). Mice with *Klf5* deletion in adult intestinal epithelium showed epithelial distress in the colonic tissue and significant loss of proliferative epithelial cells in the crypts shortly

after tamoxifen induction (123). However, the disruption in epithelial homeostasis was followed by a regenerative response, and the proliferation and *Sox9* expression was restored at day 11 after tamoxifen administration (123). The study showed that KLF5 is important for homeostasis in colonic epithelium in adult mouse.

KLF5 also has important roles in intestinal pathophysiology. Heterozygous *Klf5* knockout mice are less susceptible to murine colonic hyperplasia caused by *Citrobacter rodentium* infection (124). Heterozygous *Klf5* knockout animals are also more susceptible to dextran sulfate sodium (DSS)-induced colitis and have poor recovery after colitis with reduced epithelial proliferation and cell migration at sites of ulceration (125). Further supporting this, exogenous *Klf5* expressed in intestinal epithelium of mice under *Vil1* promoter protects mice from DSS-induced colitis possibly through enhanced cellular repair mediated by the activation of STAT3 signaling in the epithelial cells (126). KLF5 is also upregulated in response to DNA damage, and heterozygous *Klf5* knockout animals are more susceptible to γ irradiation injury (127, 128).

KLF5 functions as a pro-oncogenic factor in many types of gastrointestinal cancers, including oral squamous cell carcinoma (129), gastric cancer (130), pancreatic cancer (131, 132), and colorectal cancer (133, 134). Lysophosphatidic acid (LPA), a mitogen, induce proliferation of human colorectal cancer cell lines SW480 and HCT116 through induction of *KLF5* (135), and all-trans retinoid acid (ATRA) inhibits colorectal cancer cell proliferation by decreasing *KLF5* expression (133). LPA induces proliferation of colorectal cancer cells through activation of β-catenin, the signaling molecule in WNT signaling pathway, and the activity of β-catenin is potentiated by KLF5 (136). KLF5's role in activating the WNT signaling is further supported by data showing that heterozygous deletion of *Klf5* in mice protect them from tumor initiation activity of mutant adenomatous polyposis coli ($Apc^{Min/+}$) by reducing nuclear localization and activity of

β-catenin (137). KLF5 has also been shown to mediate oncogenic RAS signaling in colorectal cancer. KLF5 promotes proliferation through upregulation of *CCND1* and *CCNB1* in oncogenic HRAS transformed mouse fibroblast 3T3 cells and is upregulated in response to elevated MAPK activity and elevated expression of *Egr1* (138, 139). Furthermore, heterozygous deletion of *Klf5* abrogates the cumulative increase in tumor initiation caused by oncogenic $Kras^{G12V}$ in mice expressing $Apc^{Min/+}$ (140). In human colorectal cancer specimens and cell lines, overexpression of *KLF5* correlates with the mutational status of *KRAS*, and inhibition of MAPK signaling using MEK inhibitor reduces KLF5 protein levels and cancer cell proliferation (141).

1.5 KLF5 in Pancreatic Ductal Adenocarcinoma

Since oncogenic KRAS signaling drives expression of *KLF5* in human colorectal cancer cell lines (141), it is possible that KLF5 is a pro-oncogenic factor in human pancreatic cancer. Meta-analysis from four gene expression studies in human PDAC identified *KLF5* as a differentially overexpressed gene in tumor tissue (142). Earliest study on KLF5 in human pancreatic cancer cell line showed that *KLF5* is overexpressed in those cell lines, not through MAPK signaling, but through IL-1β and p38 signaling (131). Furthermore, *KLF5* expression can also be induced by hypoxia through hypoxia-inducible-factor 1α (HIF1α) (131). Lentiviral screening of 185 candidate pro-oncogenic and anti-oncogenic factor in pancreatic cancer cell lines using a pool of 558 shRNA identified *KLF5* as a pro-oncogenic factor (143). Validation of this finding showed *KLF5* knockdown in human PDAC cell line Panc5.04 decreased cancer cell proliferation (143). Transcriptomic analysis and epigenomic analysis identified KLF5 as a transcription factor important for maintaining ductal epithelial phenotype in low-grade human PDAC cell lines by activating the expression of epithelial genes such as keratins and mucins (144).

Furthermore, *KLF5* deletion through CRISPR/Cas9 strategy in low-grade human PDAC cell line CFPAC1 reduced cancer cell proliferation *in vitro* and tumor growth in xenograft model *in vivo* (144). The correlation between KLF5 level and epithelial phenotype is also seen in the context of TGF-β signaling in the mouse model of PDAC (132). In mouse PDAC cells with $Kras^{G12D}$ expression and *Cdkn2a* deletion, TGF-β signaling induces epithelial-mesenchymal transition (EMT) through induction of *Sox4* and *Snai1* (132). However, EMT in those cells were quickly followed by apoptosis, which shows that TGF-β signaling have tumor suppressive effects (132). When *Smad4* is deleted in the same cell line, TGF-β signaling induces *Klf5* expression, and KLF5 protein cooperates with SOX4 to promote tumorigenesis (132).

The results of the previous studies showed that KLF5 is a pro-oncogenic factor and is important in cancer cell proliferation and survival. However, a couple of questions remain unanswered regarding the role of KLF5 in PDAC tumorigenesis. Whether KLF5 is important for early pancreatic tumorigenesis remain unexplored. Genome wide association studies (GWAS) on two independent cohorts of PDAC patients from China and U.S. identified the same SNPs in the noncoding region between *KLF5* and *KLF12* genes that are associated with significantly increased risk for pancreatic cancer (145). Most recent study of those SNPs showed that they are located in a region of super-enhancers and amplification of the region in multiple types of cancers cause oncogenic upregulation of *KLF5* expression (146). These results suggest that KLF5 may have important role in the initiation of PDAC in addition to cancer progression. Furthermore, both shRNA knockdown of *KLF5* and CRISPR/Cas9 knockout of *KLF5* in human PDAC cancer cell line reduced cancer cell proliferation (143, 144). However, the underlying mechanism of the pro-proliferative effects of KLF5 is unknown. In the following study, I tried to fill those gaps in knowledge. I used genetic engineered mouse models of PDAC with inducible acinar-specific *Klf5*

deletion to investigate the role of KLF5 during early pancreatic tumorigenesis. I also used mouse PDAC cell lines with inducible *Klf5* knockdown to investigate the mechanisms underlying the pro-proliferative effect of KLF5 in pancreatic cancer cells.

Chapter 2. Materials and Methods

2.1 Mouse Strains

All animal experiments were approved by Stony Brook University Institutional Animal Care and Use Committee. *Klf5*$^{fl/fl}$ (147), *Ptf1a-Cre*^{ERTM} (Jackson Laboratory, Bar Harbor, Maine; Stock number 019378) (24), and *LSL-Kras*^{G12D} (Jackson Laboratory, Stock Number: 008179) (148) mice have been described previously. All mice are maintained on mixed background. From animals with the above listed genotypes, acinar-specific *Klf5* knockout mice (*Ptf1a-Cre*^{ERTM};*Klf5*$^{fl/fl}$), oncogenic *Kras* expressing mice (*Ptf1a-Cre*^{ERTM};*LSL-Kras*^{G12D}), and mice with combination of both (*Ptf1a-Cre*^{ERTM};*LSL-Kras*^{G12D};*Klf5*$^{fl/fl}$) were generated by cross breeding. For *Klf5* knockout studies, *Ptf1a-Cre*^{ERTM} littermates were used as controls. Experimental mice were euthanized via CO_2 asphyxiation followed by cervical dislocation and necropsy. For subcutaneous allograft experiments, 10 weeks-old C57BL/6J (Stock Number: 008179) mice were purchase from Jackson Laboratory. A list of genetic engineered mouse strains are found in Table 2.1 below.

Table 2.1 Genetically Engineered Mouse Strains

Mouse Line	Official Name
Klf5$^{fl/fl}$	*Klf5*^{tm1Jaw}/J
Ptf1a-Cre^{ERTM}	*Ptf1a*$^{tm2(cre/ESR1)Cvw}$/J
LSL-Kras^{G12D}	*Kras*^{tm4Tyj}/J

2.2 Mouse Genotyping

Mouse tail tips were harvested at postnatal day 21 and digested using Extracta DNA Prep Kit (Quanta Biosciences, Cat. # 95091-250). For <5 mm of tail, add 30 µl of Extraction Reagent (from kit) and heat to 95°C for 30 minutes. Samples were allowed to cool to room temperature

before 30 µl of Stabilization Reagent (from kit) was added. PCR reaction was performed using 1 µl of the DNA extract, 7.5 µl of 2X Choice Taq Blue Mastermix (Denville, Cat. # CB4065-7), PCR primers (1µM final concentration), and water with total volume of 15 µl per reaction. The reactions were subjected to 94°C for 2 minutes, followed by 10 cycles of touchdown PCR (94°C for 20 seconds, 65°C (-0.5°C per cycle) for 15 seconds, then 68°C for 10 seconds), followed by 28 cycles of PCR (94°C for 15 seconds, 60°C for 15 seconds, then 72°C for 10 seconds), followed by 72°C for 2 minutes. Genotyping primers are listed in Table 2.2 below.

Table 2.2 Mouse Genotyping Primers

Ptf1a-Cre^{ERTM}		
Primer	**Sequence 5'->3'**	**Type**
17367	GAA GGC ATT TGT GTA GGG TCA	Forward
17368	GGC TGA GTG AGG GTT GTG AG	Reverse
LSL-Kras^{G12D}		
Primer	**Sequence 5'->3'**	**Type**
22907	TGT CTT TCC CCA GCA CAG T	Wild type Forward
22908	CTG CAT AGT ACG CTA TAC CCT GT	Common
oIMR9592	GCA GGT CGA GGG ACC TAA TA	Mutant Forward
Klf5$^{fl/fl}$		
Primer	**Sequence 5'->3'**	**Type**
Klf5F	GCA TCA GGA GGG TTT CAT GT	Forward
Klf5R	GTC TCG GCC TCA TTG CTA AG	Reverse

2.3 Tamoxifen Administration

To induce Cre recombinase activity in mice with *Ptf1a-Cre^{ERTM}*, tamoxifen was dissolved in corn oil and injected intraperitoneally. 30 mg of tamoxifen (Sigma-Aldrich, Cat. # T5648) was added to 1 ml of corn oil (Sigma-Aldrich, Cat. # C8267), and the mixture was sonicated on ice with 10 second pulses followed by 10 second wait at level 3 on Fisher Scientific Model 550 Sonic Dismembrator with a 1/8 inch probe until the tamoxifen has been fully dissolved. Three 100 µl injections of tamoxifen solution dissolved in corn oil (30 mg/ml, 3 mg/injection) or 100 µl of corn oil as control was injected intraperitoneally on alternating days.

2.4 Cerulein-induced Acute Pancreatitis

To induce acute pancreatitis, mice were injected with cerulein using an injection regiment for 2 consecutive days. 1 mg of cerulein (Bachem, Cat. # H-3220) was dissolved in 1 ml of Dulbecco's Phosphate-Buffered Saline (PBS; Corning, Cat. # 21-031-CV) to make a stock solution. Stock solution (1 mg/ml) was aliquoted and stored at -20°C. On the day of injection, stock solution was dissolved to 20 µg/ml working solution and kept at 4°C until injection. Before each injection, cerulein working solution was allowed to warm to room temperature, and 50 µg of cerulein working solution were injected for each kg of body weight intraperitoneally hourly for 6 hours.

2.5 Histology, Immunohistochemistry and Immunofluorescence

Mouse pancreata were fixed overnight in 10% neutral buffered formalin (Fisher Scientific), processed using automated processor, and paraffin-embedded. 5 µm sections on glass slides were used for histology, immunohistochemistry, and immunofluorescence staining. Hematoxylin and eosin (H&E) staining was performed with standard protocol. Briefly, formalin-fixed paraffin embedded (FFPE) 5 µm sections on glass slides were de-paraffinized by baking for at least 1 hour in 65°C oven. Slides were allowed to cool to room temperature and were incubated twice in xylene for 3 minutes each time. Tissue was rehydrated by consecutive 2 minute incubations in 100% ethanol, 95% ethanol, and 70% ethanol in distilled water. Tissues were incubated for 2 minutes in distilled water, then for 5 minutes in Gill's Hematoxylin III (Poly Scientific R&D Corp., Cat. # s211). Tissues were washed in tap water for 2 minutes, then incubated in lithium carbonate aqueous solution (0.05% w/v) for 30 seconds. Tissues were washed in distilled water for 2 minutes, then

incubated for 2 minutes in Eosin Y Alcoholic Working Solution (Poly Scientific R&D Corp., Cat. # s2186). Tissue was dehydrated in 95% ethanol for 10 seconds then 100% ethanol for 10 seconds. Slides were incubated in in xylene for 3 minutes each time. Finally, slides were mounted using Cytoseal XYL (ThermoFisher, Cat. # 8312-4). All micrographs were analyzed and captured using Nikon Eclipse 90i microscope (Nikon).

Alcian Blue staining was performed as previously described (96). Briefly, Alcian Blue Working Solution was made by dissolving 1 g of Alcian Blue 8GX (Sigma-Aldrich, Cat. # A5268) in 100 ml of 3% acetic acid solution in distilled water (pH adjusted to 2.5). 5 µm FFPE sections on glass slides were de-paraffinized and rehydrated as described above for H&E staining. Tissues were then incubated in Alcian Blue Working Solution for 1 hour. Tissues were washed in distilled water for 2 minutes, then incubated for 2 minutes in Nuclear Fast Red (VECTOR, Cat. # H-3403). Tissue was dehydrated by consecutive 2 minute incubations in 70% ethanol in distilled water, 95% ethanol, and 100% ethanol. Slides were incubated in xylene and mounted as described above. All micrographs were analyzed and captured using Nikon Eclipse 90i microscope (Nikon). Total pancreatic area and Alcian blue stained area were quantified using ImageJ (149). Briefly, the total area is calculated from complete scan of entire pancreatic tissue section by subtraction thresholding of the white background from the total area. Alcian blue stained area was measured using thresholding by hue. For each sample, 2 tissue sections were analyzed.

Immunohistochemistry (IHC) and immunofluorescence (IF) were performed as previously described (150). Briefly, 5 µm FFPE tissue section on glass slides were de-paraffinized as describe above for H&E staining. Tissue was treated in 2% H_2O_2 in methanol for 30 minutes and then rehydrated as described above for H&E staining. Antigen retrieval was performed by subjecting the tissues to Sodium Citrate Buffer (10mM Sodium Citrate, 0.05% Tween 20, pH 6.0) for 10

minutes at 120°C in decloaking chamber (Biocare Medical). Tissue was blocked in 5% w/v bovine serum albumin (BSA, Sigma-Aldrich, Cat. # 3116956001) dissolved in 1X TBST Buffer (20mM Tris Buffer, pH 7.5, 150mM NaCl, 0.1% Tween 20) for 1 hour at 37°C. Tissue was incubated overnight with primary antibody diluted in blocking buffer with gentle rocking at 4°C. After washing three times with 1X TBST, tissue was incubated for 30 minutes at 37°C with the proper corresponding secondary and tertiary antibodies, if applicable, conjugated with horse radish peroxidase (HRP) or fluorophore. Tissue was washed three times with 1X TBST for 5 minutes at room temperature with gentle shaking. For IHC stainings, tissue was developed with Betazoid 3, 3'-Diaminobenzidine (DAB) Chromagen Kit (Biocare Medical, Cat. # BDB2004) for 1 minute. Tissue was washed in distilled water for 2 minutes, then counterstained with hematoxylin for 2 minutes. Tissue was then dehydrated and mounted as previously described for Alcian Blue staining. For IF staining, tissue was counterstained with Hoechst 33258 (ThermoFisher, Cat. # H3569) for 5 minutes at room temperature. Tissue was washed three times with 1X TBST for 5 minutes at room temperature with gentle shaking. Slides were mounted with ProLong™ Gold Antifade Mountant (ThermoFisher, Cat. # P10144).

To examine cellular protein levels using immunocytochemistry (IC), cells were seeded at $1x10^4$ cells per well in 4-welled Millicell EZ Slide (EMD Millipore, Cat. # PEZGS0416). Cells were fixed in 1:1 actone:methanol at -20°C for 20 minutes. After washing in PBS, cells were permeabilized using 0.2% Triton X-100 in PBS at room temperature for 10 minutes. The slides were then blocked using blocking buffer consisting of 3% bovine serum albumin and 0.02% Triton X-100 in PBS at room temperature for 30 minutes. After blocking, the slide were incubated with primary antibody diluted in blocking buffer at 4°C overnight. After washing, fluorescent-labeled secondary antibody was added with the appropriate incubation and washing. The slides were then

counterstained with Hoechst and mounted as described for IF staining. Fluorescent images were captured and analyzed using Nikon Eclipse 90i microscope (Nikon). A list of antibodies used is shown in Table 2.3 below.

Table 2.3 Primary Antibodies for IHC IF, and IC

Antigen	**Host**	**Company**	**Catalog number**
α-SMA	Mouse	Abcam	ab5694
Amylase	Goat	Santa Cruz	Sc-12821
Cyclin D1 (for IC)	Rabbit	Biocare Medical	CRM307AK
KLF5 (for IC)	Mouse	Sigma-Aldrich	SAB4200338
KLF5 (for IHC)	Goat	R&D Systems	AF3758
MKI67	Rabbit	Biocare Medical	CRM325
Keratin-19 (for IF)	Rat	DHSB	TROMA-III
Mac-3	Rat	BD Biosciences	6206131
Vimentin	Rabbit	Cell Signaling	5741

2.6 Human Tissue Microarrays

Human tissue microarrays PA2081a and PA2082 containing de-identified human PDAC tumor samples were purchased from US Biomax, Inc. (Derwood, MD). Combined, these arrays contain duplicate core samples from 191 unique cases with the following breakdown: 129 pancreatic ductal adenocarcinoma, 26 normal tissue adjacent to tumor, 15 normal pancreas, and the remaining are pancreatic adenosquamous carcinoma, acinar cell carcinoma, neuroendocrine carcinoma, pancreatic islet cell tumor, and pancreatic inflammation. IHC staining for KLF5 was performed as described above. Cases were considered positive for KLF5 if both core samples contained positive KLF5 nuclear staining in more than 5% of tumor cells. Each core sample was reviewed for KLF5 positivity by two reviewer blinded to the pathological interpretation.

2.7 Cell Lines

UN-KC-6141, mouse pancreatic cancer cell line derived from KC (*Pdx1-Cre;LSL-Kras^{G12D}*), was obtained from Dr. Surinder Batra (151). UN-KC-6141 were maintained in DMEM medium supplemented with 10% FBS and 1% penicillin/streptomycin at 37°C in 95% air and 5% carbon dioxide (CO_2). The cell line was verified by immunocytochemistry staining for keratin-19, a specific pancreatic ductal epithelial marker, and cell morphology is routinely monitored. HEK 293T cell line was purchased from American Type Culture Collection (ATCC) and cultured according to ATCC instructions. In addition, Mycoplasma tests were performed on all used cell lines.

2.8 Kinase Inhibitor Treatment

Kinase inhibitors LY294002 (Cell Signaling, Cat. # 9901), U0126 (Cell Signaling, Cat. # 9903), PD98059 (Cell Signaling, Cat. # 9900), SB203580 (EMD Millipore, Cat. # 559398), and SP600125 (EMD Millipore, Cat. # 420119) were purchased from their respective manufacturers. For *in vitro* experiments, all kinase inhibitors were solubilized in complete culture media with final concentration of 0.1% dimethyl sulfoxide (DMSO, Fisher Scientific). For kinase inhibition experiments, UN-KC-6141 cells were seeded in culture and treated 24 hours later with medium, 0.01% DMSO, LY294002 (20 μM), U0126 (10 μM), PD98059 (50 μM), SB203580 (20 μM), or SP600125 (10 μM). Cells were collected in 2X Laemmli Buffer (0.125M Tris-HCl, pH 6.8, 4% SDS, 10% 2-mercaptoethanol, 20% glycerol, and 0.004% bromophenol blue) 48 hours post treatment for western blot analysis or for MTS assay 24 hours, 48 hours, and 72 hours post-treatment using CellTiter 96® AQueous One Solution Cell Proliferation Assay (Promega, Cat. # G3582).

2.9 Western Blot Analysis

Western blot was performed as previously described (150). Cells in culture were collected in 2X Laemmli Buffer (0.125M Tris-HCl, pH 6.8, 4% SDS, 10% 2-mercaptoethanol, 20% glycerol, and 0.004% bromophenol blue) for western blot analysis. Sample were subjected to 95°C heating for 10 minutes, followed by cooling to room temperature. Samples were shaken for 1 minute on Genie SI-D248 Disruptor Shaker (Cole-Parmer, Cat. # UX-04724-36). Samples were spun down and used immediately or stored in -20°C for future use. Western blotting was performed using standard protocol. Briefly, samples were run on pre-cast 10% or 4-20% Novex™ Tris-Glycine Midi Protein Gels (ThermoFisher) at 100V. Proteins were transferred in Transfer Buffer (25 mM Tris, 190 mM glycine, 20% methanol, and 0.1% SDS) onto supported nitrocellulose membrane, 0.45 µm (Bio-Rad) for 1 hour at 18V using semi-dry transfer with Trans-Blot® SD Semi-Dry Transfer Cell (Bio-Rad). Ponceau S (0.1% w/v in 5% acetic acid) staining was performed after transfer to verify that the transfer was successful. Membrane was washed with 1X TBST for 5 minutes at room temperature with gentle shaking, blocked in 5% non-fat milk in 1X TBST for 1 hour at room temperature with gentle rocking, and incubated with primary antibody in blocking buffer overnight at 4°C with gentle rocking. After washing three times with 1X TBST, membrane was incubated in the appropriate HRP-conjugated secondary antibody for 1 hour at room temperature with gentle shaking. After washing three times with 1X TBST, membranes were developed using SuperSignal™ West Pico PLUS Chemiluminescent Substrate (ThermoFisher, Cat. # 34580X4) or Immobilon Western Chemiluminescent HRP Substrate (Millipore, Cat. # WBKLS0500). Membrane was images with either X-ray film developer or Azure c300 Imager (Azure Biosystems). A list of primary antibody used for western blot is shown in Table 2.4 below. Densitometry quantification of western blot results was performed using ImageJ (22930834).

Table 2.4 Primary Antibodies for Western Blotting

Antigen	**Host**	**Company**	**Catalog number**
β-actin	Mouse	Sigma-Aldrich	A1978
phospho-AKT Ser473	Rabbit	Life Technologies	44-621G
AKT	Rabbit	Cell Signaling	9272
Cyclin A2	Mouse	Cell Signaling	4656
Cyclin B1	Mouse	Cell Signaling	4135
Cyclin D1 (for Western)	Mouse	Cell Signaling	2926
Cyclin E	Mouse	Millipore	05-363
CDK2	Rabbit	Cell Signaling	2546
CDK4	Rabbit	Cell Signaling	12790
ERK1/2	Rabbit	Millipore	06-182
phospho-ERK1/2 Thr202/Tyr204	Rabbit	Cell Signaling	9101
KLF5 (for Western)	Goat	R&D Systems	AF3758
NDRG2	Rabbit	Abcam	Ab169775
Stratifin (14-3-3σ)	Goat	R&D Systems	AF4424
phospho-STAT3 Y705	Rabbit	Cell Signaling	9145
STAT3	Rabbit	Cell Signaling	4904

Protein from mouse pancreatic tissue was extract using 2X Laemmli Buffer without 2-mercaptoethanol and bromophenol blue (0.125M Tris-HCl, pH 6.8, 4% SDS, and 20% glycerol) containing 1X Halt™ Protease and Phosphatase Inhibitor Cocktail (ThermoFisher, Cat. # 78440). 400 µl of protein extraction buffer was added to 20 mg of mouse pancreatic tissue, and homogenized on ice at maximum speed for 30 seconds using rotor-stator homogenizer. Protein sample was centrifuged at 12,000 x g for 5 minutes. Supernatant containing protein was collected and insoluble debris was discarded. 20 µl of protein sample was used to quantify protein concentration using Pierce™ BCA Protein Assay Kit (ThermoFisher, Cat. # 23225). Remaining sample was frozen at -20°C until use. Before use in western blotting, samples were diluted with 2X Laemmli Buffer containing 2-mercaptoethanol and bromophenol blue at 1:1 ratio and processed as described above.

2.10 Doxycycline-inducible shRNA Expressing Cell Line

Tet-pLKO-puro was a gift from Dmitri Wiederschain (Addgene plasmid # 21915) (152). pLTR-G was a gift from Jakob Reiser (Addgene plasmid # 17532) (153). pCD/NL-BH*ΔΔΔ was a gift from Jakob Reiser (Addgene plasmid # 17531) (154). Doxycycline hyclate (Sigma-Aldrich, Cat. # D9891), was purchased from their manufacturer. UN-KC-6141 cell line with tetracycline inducible expression of shRNA against *Klf5* was generated as previously described (152). All lentiviral experiments were performed under the approval of Stony Brook University Institutional Biosafety Committee. Briefly, shRNA constructs against mouse *Klf5* (shown in Table 2.5 below) and scrambled shRNA construct (155) were synthesized by the Stony Brook University Genomics Core Facility. shRNA constructs were subcloned into *Eco*RI and *Age*I sites of the Tet-pLKO-puro vector. Positive clones were identified using *Xho*I digestion and confirmed using DNA sequencing. For the packaging of lentivirus, HEK 293T cells were seeded and Tet-pLKO-puro vector with shRNA constructs were transfected with pLTR-G vector and pCD/NL-BH*ΔΔΔ using Lipofectamine 2000 (ThermoFisher, Cat. # 11668027). Viral supernatant was harvested 48 hours after transfection. UN-KC-6141 were treated with viral supernatant and 5 µg/ml of polybrene for 72 hours. After 72 hours, medium was replaced with normal culture medium containing 2 µg/ml of puromycin for selection. UN-KC-6141 cells were selected for 9 days with medium change every 3 days. Control cell line with inducible expression of scrambled shRNA construct was also generated using the same methods described.

Table 2.5 shRNA Constructs

Construct	**Sequence**
Scramble shRNA top strand	CCGGCCTAAGGTTAAGTCGCCCTCGCTCGAGCGAG GGCGACTTAACCTTAGGTTTTT
Scramble shRNA bottom strand	AATTAAAAACCTAAGGTTAAGTCGCCCTCGCTCGA GCGAGGGCGACTTAACCTTAGG
TRCN0000055287 top strand (*Klf5* specific shRNA)	CCGGGCAGTAATGGACACCCTTAATCTCGAGATTA AGGGTGTCCATTACTGCTTTTT
TRCN0000055287 bottom strand (*Klf5* specific shRNA)	AATTAAAAAGCAGTAATGGACACCCTTAATCTCGA GATTAAGGGTGTCCATTACTGC

2.11 CRISPR/Cas9 *Klf5* Knockout Cell Line

UN-KC-6141 cell line with *Klf5* knockout was generated as previously described (156). BTEB2 Double Nickase Plasmid (m) (Santa Cruz, Cat. # sc-419372-NIC), BTEB2 Double Nickase Plasmid (m2) (Santa Cruz, Cat. # sc-419372-NIC2), Control Double Nickase Plasmid (Santa Cruz, Cat. # sc-437281), and UltraCruz® Transfection Reagent (Santa Cruz, Cat. # sc-395739) were purchase from their manufacturer and transfection was performed according to the manufacturer's instruction. GFP positive cells were sorted using BD FACSAria cell sorter (BD). After sorting, cells were selected using normal culture medium containing 2 µg/ml of puromycin for 9 days with medium change every 3 days. Isolation of single cell clones was accomplished by serial dilution and protein level of KLF5 was examine using western blot analysis. Clones lacking KLF5 protein were selected and genomic DNA was extracted using GenElute™ Mammalian Genomic DNA Miniprep Kit Protocol (Sigma-Aldrich, Cat. # G1N10) according to the manufacturer's instructions. Genomic DNA extracted were used as template in a PCR reaction using flanking primers designed to detect deletion at the target site (See Table 2.6 below for primer sequences). The PCR reaction was performed using AccuTaq™ LA DNA Polymerase (Sigma-Aldrich, Cat. # D8045) according to the manufacturer's instructions. Deletions were verified by

sequencing using M13 primers (sequencing was performed by Stony Brook University Genomics Core Facility, see Table 2.6 below for primer sequences).

Table 2.6 Sequencing Primers for Checking CRISPR/Cas9 Deletion

Primer or Construct	**Sequence**
Klf5 Double Nickase Plasmid (m) Forward Sequencing Primer	TGTAAAACGACGGCCAGTTCGACCCAGGATCCAA CTCTTCGTGAGCGTCTGGCT
Klf5 Double Nickase Plasmid (m) Reverse Sequencing Primer	CAGGAAACAGCTATGACCATGATCCAGTACTTGA GAGAATCCATCGAGCTTTCATCCCCACGCAAG
Klf5 Double Nickase Plasmid (m2) Forward Sequencing Primer	TGTAAAACGACGGCCAGTTCGACCCAGGATCCAA CTTTAGGAGTTGGCCCCTGTACT
Klf5 Double Nickase Plasmid (m2) Reverse Sequencing Primer	CAGGAAACAGCTATGACCATGATCCAGTACTTGA GAGAATCCATCGGGGTTAAGGCCTGCCATAGAA

2.12 Cell Proliferation and Cell Cycle Progression Assay

For cell proliferation experiments, UN-KC-6141 cell lines with tetracycline inducible expression of shRNA against *Klf5* or scrambled control shRNA were seeded at 5 x 10^3 cells/60 mm culture dish and cultured in medium containing 50 ng/ml of doxycycline. Live cells were collected at 1-6 days post seeding and their numbers were determined by counting using a Coulter counter (Beckman Coulter). Each experiment was done in triplicate. In MTS assay and cell cycle progression assay using UN-KC-6141 cell lines with tetracycline inducible expression of shRNA against *Klf5*, UN-KC-6141 cell lines were pretreated for 3 days with 50 ng/ml of doxycycline before seeding. After additional 24, 48, and 72 hours of culture in 96-well plate, 20 μl of MTS solution (Promega, Cat. # G3582) was added to each well and an analysis was performed according to the manufacturer's protocol. The measurements of the control scrambled shRNA expressing cell line was defined as 100% and the results from other measurements were calculated accordingly. Each experiment was repeated for at least 3 times.

Cell cycle progression assay was performed as described previously (157). Each experiment was done in triplicate. Briefly, cells seeded in 60 mm culture dish were washed with 1

ml of ice-cold PBS and trypsinized with 500 µl of 0.25% (w/v) Trypsin- 0.53 mM EDTA solution. Cells were collected in 4 ml of culture media and centrifuged at 300 x g for 5 minutes. Culture media was aspirated, and cells were fixed in 1 ml of 70% ethanol in PBS overnight at -20°C. Permeabilization buffer was made by adding 1% BSA and 0.2% Triton X-100 (Sigma-Aldrich, Cat. # X-100) to PBS. Staining buffer was made by adding 0.1% Triton X-100 and 1 mg/ml of RNase A in water. 5 ml of Permeabilization buffer was added to fixed cells, and cells were centrifuged at 300 x g for 5 minutes. After aspirating the supernatant, the cell pellet was re-suspended in 200 µl of Staining Buffer and transferred into 12mm x 75mm FACS tubes. 20 µl of 2 mM stock solution of propidium iodide (Sigma-Aldrich, Cat. # P4170) in water was added to make the final concentration 200 µM. Flow cytometry was performed by Stony Brook Research Flow Cytometry Core Facility using BD FACSCalibur cell analyzer.

For proliferation recovery experiments, UN-KC-6141 cell lines with tetracycline inducible expression of shRNA against *Klf5* or scrambled control shRNA were seeded at 1 x 10^4 cells/60 mm culture dish and cultured in medium with and without 50 ng/ml of doxycycline for the first 6 days. Live cells were collected at 1-6 days post seeding and their numbers were determined by counting using a Coulter counter (Beckman Coulter). UN-KC-6141 cell lines with tetracycline inducible expression of shRNA against *Klf5* and control treated with media containing 50 ng/ml of doxycycline for the first 6 days were reseeded as before and were either continued on media containing 50 ng/ml of doxycycline or cultured in media without doxycycline for 6 days. Again, live cells were collected and counted at 1-6 days after seeding (7-12 days after the start of doxycycline treatment) as described. For the third cycle, UN-KC-6141 cell lines with tetracycline inducible expression of shRNA against *Klf5* and treated with media containing 50 ng/ml of doxycycline for 6 days and recovered in media without doxycycline for 6 days were compared

with cells that were treated for 12 continuous days. The cells were seeded as already described and live cells were collected and counted at 1-6 days after seeding (13-18 days after the start of doxycycline treatment) as described.

2.13 RNA Isolation and Expression Analysis

Total RNA from UN-KC-6141 cell lines was extracted using TRIzol Reagent (ThermoFisher, Cat. # 15596026) per manufacturer's protocol. DNase digestion was performed using RNase-Free DNase Set (Qiagen, Cat. # 79254) according to manufacturer's protocol. RNA was then cleaned up using RNeasy MinElute Cleanup Kit (Qiagen, Cat. # 74204) according to manufacturer's protocol. cDNA synthesis was performed using SuperScript VILO cDNA Synthesis Kit (ThermoFisher, Cat. # 11754050) according to manufacturer's protocol. qRT-PCR analysis were performed using TaqMan Gene Expression Primers Mm00456521_m1 (ThermoFisher, Cat. # 4331182) for *Klf5*, Mm03024075_m1 (ThermoFisher, Cat. # 4331182) for *Hprt1*, Mm99999915_g1 (ThermoFisher, Cat. # 4331182) for *Gapdh*, and Mm00443483_m1 for *Ndrg2*. qPCR assay was performed using TaqMan Gene Expression Master Mix (ThermoFisher, Cat. # 4369016) and QuantStudio 3 qPCR machine (ThermoFisher). qPCR arrays were performed using Mouse Cell Cycle RT^2 Profiler PCR Array (Qiagen, Cat. # 330231) and RT^2 SYBR Green ROX qPCR Mastermix (Qiagen, Cat. # 330524).

For RNA sequencing performed by New York Genome Center, RNA sequencing libraries were prepared using the KAPA Stranded RNA-Seq Kit with RiboErase (kapabiosystems) in accordance with the manufacturer's instructions. Briefly, 500 ng of total RNA was used for ribosomal depletion and fragmentation. Depleted RNA underwent first and second strand cDNA synthesis. cDNA was then adenylated, ligated to Illumina sequencing adapters, and amplified by

PCR (using 9 cycles). Final libraries were evaluated using fluorescent-based assays including PicoGreen (Life Technologies) or Qubit Fluorometer (Life Technologies) and Fragment Analyzer (Advanced Analytics) or BioAnalyzer (Agilent 2100), and were sequenced on an Illumina HiSeq2500 sequencer (v4 chemistry, v2 chemistry for Rapid Run) using 2 x 125bp cycles.

Reads were aligned to the NCBI GRCm38 mouse reference using STAR aligner (v2.4.2a).8 Quantification of genes annotated in Gencode vM5 were performed using featureCounts (v1.4.3) and quantification of transcripts using Kalisto (158). QC were collected with Picard (v1.83) and RSeQC (http://broadinstitute.github.io/picard/) (159). Normalization of feature counts and statistical modeling using negative binomial distribution was done using the DESeq2 package (160). *P*-value were adjusted for multiple comparisons using Bonferroni correction. Significant genes have a minimum log2 fold-change of 1 and a maximum adjusted P-value of 0.05.

2.14 Chromatin Immunoprecipitation

ChIP-PCR was performed using SimpleChIP Enzymatic Chromatin IP Kit (Cell Signaling, Cat. # 9003) using manufacturer's protocol. Briefly, UN-KC-6141 cell lines with tetracycline inducible expression of shRNA against *Klf5* or scrambled control shRNA after 5 days of 50 ng/ml doxycycline treatment were fixed with formaldehyde and DNA was digested with Micrococcal nuclease. Digested protein-DNA was incubated with anti-KLF5 antibody (Abcam Cat. # ab137676) and precipitated using Protein G coated magnetic beads. Rabbit IgG (Cell Signaling, Cat. # #2729) and anti-Histone 3 (Cell Signaling, Cat. #4620) antibodies were used as negative and positive controls, respectively. PCR were ran using primers sets specific for potential binding site. See Table 2.7 below for list of primers.

Table 2.7 Primer for Potential KLF5 Binding Sites

Primer	**Sequence**
Ndrg2 Promoter Site 1 Forward Sequence Primer	TGCAGTCTCTAGTCTCCGGG
Ndrg2 Promoter Site 1 Reverse Sequence Primer	AGCGTTCACACTCAATCTTGT
Ndrg2 Promoter Site 2 Forward Sequence Primer	GGATGAAAGGGGCATTGATGT
Ndrg2 Promoter Site 2 Reverse Sequence Primer	CAATGTCCAATGGAACCGGA
Ndrg2 Promoter Site 3 Forward Sequence Primer	GTCTCCCCACTTTACCCGTC
Ndrg2 Promoter Site 3 Reverse Sequence Primer	CGTGGGGGATCCCTTAAACC
Ndrg2 Promoter Site 4 Forward Sequence Primer	GAGCCTATGAGCATCACCTCT
Ndrg2 Promoter Site 4 Reverse Sequence Primer	AAACACGCCCCGTAACTCG
Ndrg2 Promoter Site 5 Forward Sequence Primer	GCGGACCTAAGTCAAAGGCA
Ndrg2 Promoter Site 5 Reverse Sequence Primer	CCGAACTACAGCCAGGAGAC
Krt19 Promoter Site Forward Sequence Primer	GGTGGGGCAACCTTGTCTCAGAA
Krt19 Promoter Site Reverse Sequence Primer	ACCCCTCTGAGCCCCAACTCA

2.15 Subcutaneous Allograft Model of Tumor Growth

One flank of each is injected with *Klf5* shRNA cells and the opposite flank with scrambled shRNA control cells. The tumors were allowed to grow undisturbed for 7 days. 7 days after implantation, the mice (8 males and 8 females, n = 16) were given water containing 1mg/ml of doxycycline and 5% sucrose to induce shRNA expression. Animal weight and tumor volume, measured by external caliper measurements (2544306), were monitored daily from the onset of doxycycline treatment (7 days after implantation) to 14 days after implantation. The animals were euthanized at 14 days after implantation, and the tumors were collected for formalin-fixed paraffin embedded preparation.

2.16 LightSwitch Luciferase Promotor Activity Assay

GoClone® reporter vectors without promoter (pLightSwitch-empty prom) or with human *KRT19* (pLightSwitch-*KRT19* prom) were purchased from their manufacturer (Active Motif). Vector containing human *KLF5* cDNA with an N-terminal HA tag inserted into pEGFP-N1 after excision of gene encoding EGFP was previously described (KLF5-OE) and was used to

overexpress human KLF5 protein (161). Similar vectors containing human *SP1* cDNA (SP1-OE) and *KLF4* cDNA (KLF4-OE) available in the lab were used to overexpress human SP1 and KLF4 proteins, respectively. pEGFP-N1 after excision of gene encoding EGFP was used as negative control. HEK293T cells were seeded at $1x10^4$ cells per well in 96-well white tissue culture plate and cultured in culture media without antibiotics for 24 hours after seeding to obtain 70% confluency at transfection. The cells were co-transfected using Lipofectamine 2000 (ThermoFisher, Cat. # 11668027) with either pLightSwitch-*KRT19* prom or pLightSwitch-empty prom and a combination of two of the overexpression vectors (KLF5-OE, SP1-OE, KLF4-OE, or pEGFP-N1 after excision of gene encoding EGFP). Media was replaced with fresh media without antibiotics 6 hours after transfection. Cells were assayed 24 hours after transfection using LightSwitch Reporter Assay Kit (Active Motif, LS010) according to the manufacturer's protocol.

2.17 Statistical Methods

Two-sided Student's T-tests, two-sided Mann-Whitney tests, and Spearman's Rank Correlation were performed when appropriate using GraphPad Prism version 5.00 for Windows (GraphPad Software, Sand Diego, CA). A *P*-value of < 0.05 was considered significant. For subcutaneous allograft experiments, statistical analysis was performed using a linear mixed model for longitudinal data. Dependence of tumor on both flanks of a mouse was modeled using unstructured covariance matrix and dependence of 7 volumes over time from a tumor was modeled using compound symmetry structure. This type of dependence matrix was selected based on Akaike Information Criteria. Volumes at Day 7 after implantation was used as a covariate.

Chapter 3. KLF5 Knockout in Early Pancreatic Tumorigenesis

This chapter in part is a reprint of the materials as it appears in:

Ping He, Jong Won Yang, Vincent W. Yang, Agnieszka B. Bialkowska. Krüppel-like Factor 5, Increased in Pancreatic Ductal Adenocarcinoma, Promotes Proliferation, Acinar to Ductal Metaplasia, Pancreatic Intraepithelial Neoplasia, and Tumor Growth in Mice. In *Gastroenterology*. Accepted for Publication on December 10, 2017

3.1 Introduction

Pancreatic tumorigenesis is a complex process involving transformation, followed by dysplasia and invasion. The best known genetic initiators of this process are mutations in *KRAS* (162). *KRAS* mutations are the earliest and most common mutations found in patient tumors (162). Mouse models with pancreas-specific expression of mutant *Kras* have become widely adopted in the study of early pancreatic tumorigenesis due to their ability to recapitulate the processes of acinar-to-ductal metaplasia (ADM) and pancreatic intraepithelial neoplasm (PanIN) formation (65). Activation of oncogenic KRAS signaling trigger pathological changes by disrupting the complex of transcriptional network that regulates normal cellular identity. Until the recent advances in sequencing technology and transgenic mouse models, it was impossible to study the complex transcriptional regulation involved in the cellular transformation in mammals in a spatiotemporal manner and on a transcriptome-wide basis. With the current technology, we have only begun to identify key transcription factors induced by oncogenic KRAS (e.g. SOX9 and KLF4) that are required for ADM and PanIN formation (78, 96).

Krüppel-like Factor 5 (KLF5) is an important factor in gastrointestinal physiology and pathophysiology, and its dysregulation has been implicated in the oncogenesis in almost every type of gastrointestinal tissue (95). Very little is known about the role KLF5 plays in the early pancreatic tumorigenesis. The only study implicating KLF5 as a mediator of pancreatic tumorigenesis was conducted in the context of TGF-β tumor suppression and *SMAD4* mutations (132). In pancreatic cancer cell lines and mouse models with wild-type *SMAD4* and oncogenic *KRAS*, TGF-β stimulation induces cancer cells to express *SOX4* and undergo epithelial-to-mesenchymal transition (EMT) through transcriptional activation of *SNAI1* (132). SNAI1 protein transcriptionally represses *KLF5*, and this in turn allows SOX4 protein to induce apoptotic gene expression (132). When the function of SMAD4 is disrupted due to genetic deletion, *SOX4* is upregulated independent of *SNAI1* expression, and the concomitant expression of *SOX4* and *KLF5* promotes tumorigenesis (132). This study demonstrated the importance of KLF5 in promoting oncogenesis and challenged the conventional notion of EMT as a pro-oncogenic event linked to metastasis and oncogenic progression (132). However, the study does not address the role of KLF5 and TGF-β signaling in ADM and PanIN formation during early pancreatic tumorigenesis, because both the mouse models and the human cancer cell lines used in the study have already undergone neoplastic transformation (132). A more recent study showed that the TGF-β stimulation triggers ADM in acinar cells isolated from human pancreas using flow cytometry, suggesting that the TGF-β signaling has complex effect during early pancreatic tumorigenesis that might be opposite of its effect after neoplastic transformation (77). Furthermore, *SMAD4* mutations are almost exclusively found in PanIN-3 lesions, suggesting that the TGF-β/SMAD/SNAI1 pathway described may be more relevant to the role of KLF5 during pancreatic cancer progression and less important during PanIN formation.

KLF5 is required for multiple processes during the development of the embryo. Homozygous deletion of *Klf5* in mouse is embryonically lethal at E8.5 (119). Since the role of KLF5 in pancreatic development during embryogenesis is unknown, constitutive deletion of *Klf5* in the pancreas of the mouse could have the unforeseeable effects. Furthermore, the effects of *Klf5* knockout in the pancreas or in whole-body of the adult mouse had not been studied. To overcome this limitation, a tamoxifen-inducible Cre recombinase fused to mutant estrogen receptor ligand binding domain (Cre^{ERTM}) expressed under Pancreas-specific Transcription Factor, Subunit 1a (*Ptf1a*) promoter (*Ptf1a-Cre*^{ERTM} allele) can be used to trigger Cre-mediated recombination in adult acinar cells in a spatiotemporal manner and bypassing the undesirable effects of deletion of *Klf5* during embryogenesis (24). Previous experiment characterizing the efficiency and specificity of this system using eYFP lineage tracing has shown that activation of Cre function by tamoxifen injections after E18.5 gave rise to eYFP tracing limited to the acinar cell population (24). In adult mice at 5 weeks of age, three injections of tamoxifen at 3mg per injection given over 6 days induced 60-80% recombination of *Rosa26*^{LacZ} and *Rosa26*^{eYFP} alleles (24).

To address the gap in the knowledge on the role of KLF5 during ADM and PanIN formation, I utilized *Ptf1a-Cre*^{ERTM}, *LSL-Kras*^{G12D} and *Klf5*$^{fl/fl}$ mouse models to examine the effects of *Klf5* deletion during those processes (24, 147, 148). By crossbreeding, I generated mice with acinar cell-specific *Kras*^{G12D} expression and *Klf5* deletion that are induced with precise spatiotemporal control by tamoxifen injections. The experiments using those mice demonstrated that KLF5 is required for spontaneous *Kras*^{G12D}-induced PanIN formation and PanIN formation following acute pancreatitis. Furthermore, acinar cells with deletion of *Klf5* failed to undergo pancreatitis-induced ADM. Changes in gene expression due to *Klf5* deletion during ADM were identified using RNA-sequencing, showing *Ndrg2* as a potential target gene. The upregulation of

NDRG2 after *Klf5* deletion was validated, and the physical interaction between KLF5 and *Ndrg2* promoter was shown. The results demonstrated that KLF5 is a critical factor required for the complex transcriptional network involved in cellular transformation during ADM and PanIN formation. Furthermore, the results also implicated NDRG2 as a novel regulator of the signaling pathways underlying ADM.

3.2 Characterization of Mice with *Klf5* Knockout in Pancreatic Acinar Cells

To study whether KLF5 is expressed during $Kras^{G12D}$-induced PanIN formation, I performed IHC analyses in the pancreata of wild-type (C57BL/6) and *Ptf1a-Cre;LSL-*$Kras^{G12D}$ mice. *Ptf1a-Cre;LSL-*$Kras^{G12D}$ mice are born with morphologically normal pancreas and spontaneously develop PanINs as they age (Figure 3.1, A and B) (65). In wild-type mouse pancreas, KLF5 staining was localized to the nuclei of ductal cells (Figure 3.1C). Acinar cells did not express KLF5, and the islet cells had low levels of nuclear KLF5 (Figure 3.1C). In *Ptf1a-Cre;LSL-*$Kras^{G12D}$ mouse pancreas, both ADM and PanIN lesions displayed high levels of nuclear KLF5 (Figure 3.1D). The data suggest that KLF5 is upregulated in response to oncogenic KRAS signaling and may mediate ADM and PanIN formation.

To examine the requirement for KLF5 in spontaneous $Kras^{G12D}$-induced PanIN formation, I crossbred mice with the *Ptf1a-*Cre^{ERTM}, *LSL-*$Kras^{G12D}$ and $Klf5^{fl/fl}$ alleles to generated mice that combine oncogenic $Kras^{G12D}$ expression and *Klf5* deletion in acinar cells upon tamoxifen administration (Figure 3.2A). I obtained mice with four different combinations of transgenic alleles: *Ptf1a-*Cre^{ERTM}, *Ptf1a-*Cre^{ERTM};$Klf5^{fl/fl}$, *Ptf1a-*Cre^{ERTM};*LSL-*$Kras^{G12D}$, and *Ptf1a-*Cre^{ERTM};*LSL-*$Kras^{G12D}$;$Klf5^{fl/fl}$. There were no differences in the overall health and weight among the mice of different genotypes at 5-7 weeks of age. Pancreatic tissue collected two days after

administration of corn oil (vehicle for tamoxifen) from mice at 5-7 weeks of age showed normal pancreatic histology in all four genotypes (Figure 3.2B). Animals were followed up until 6 months after corn oil injection (7-8 months of age), and mice of all four genotypes showed normal overall health, weight, and pancreatic histology (Figure 3.2B).

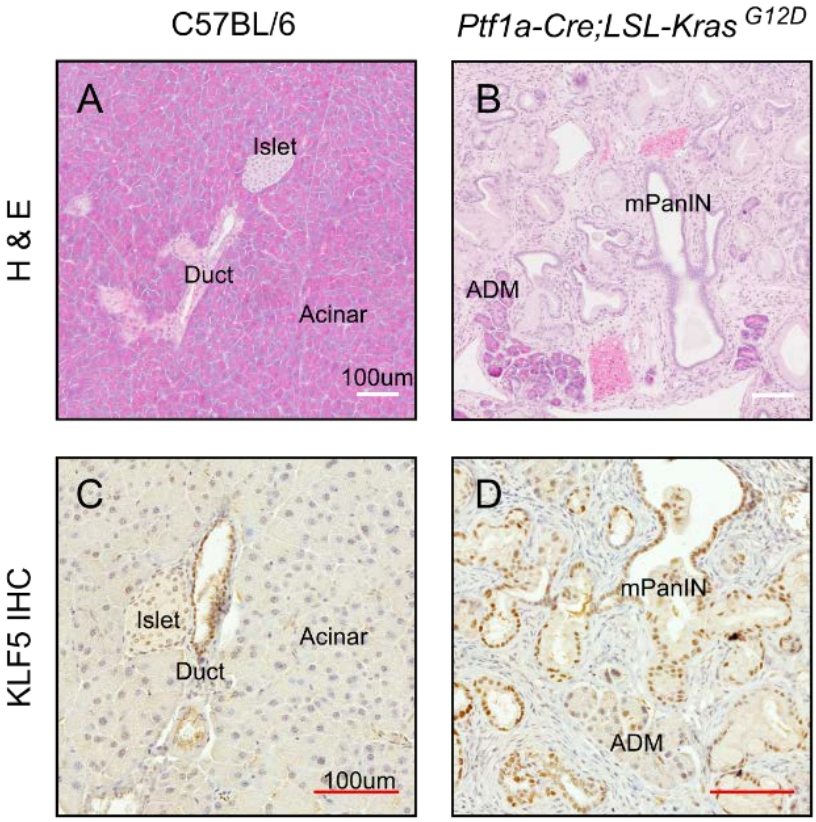

Figure 3.1. Expression of KLF5 in Normal Mouse Pancreas and Mouse Model of PDAC
H&E staining of normal pancreas from 6 months-old C57BL/6 mice (**A**) and diseased pancreas from 6 months-old *Ptf1a-Cre;LSL-Kras*^{G12D} mouse (**B**). Immunohistochemical analysis of KLF5 in pancreas from 6 months-old C57BL/6 strain mouse (**C**) and in pancreas from 6 months-old *Ptf1a-Cre;LSL-Kras*^{G12D} mouse (**D**). Scale bars = 100 µm.

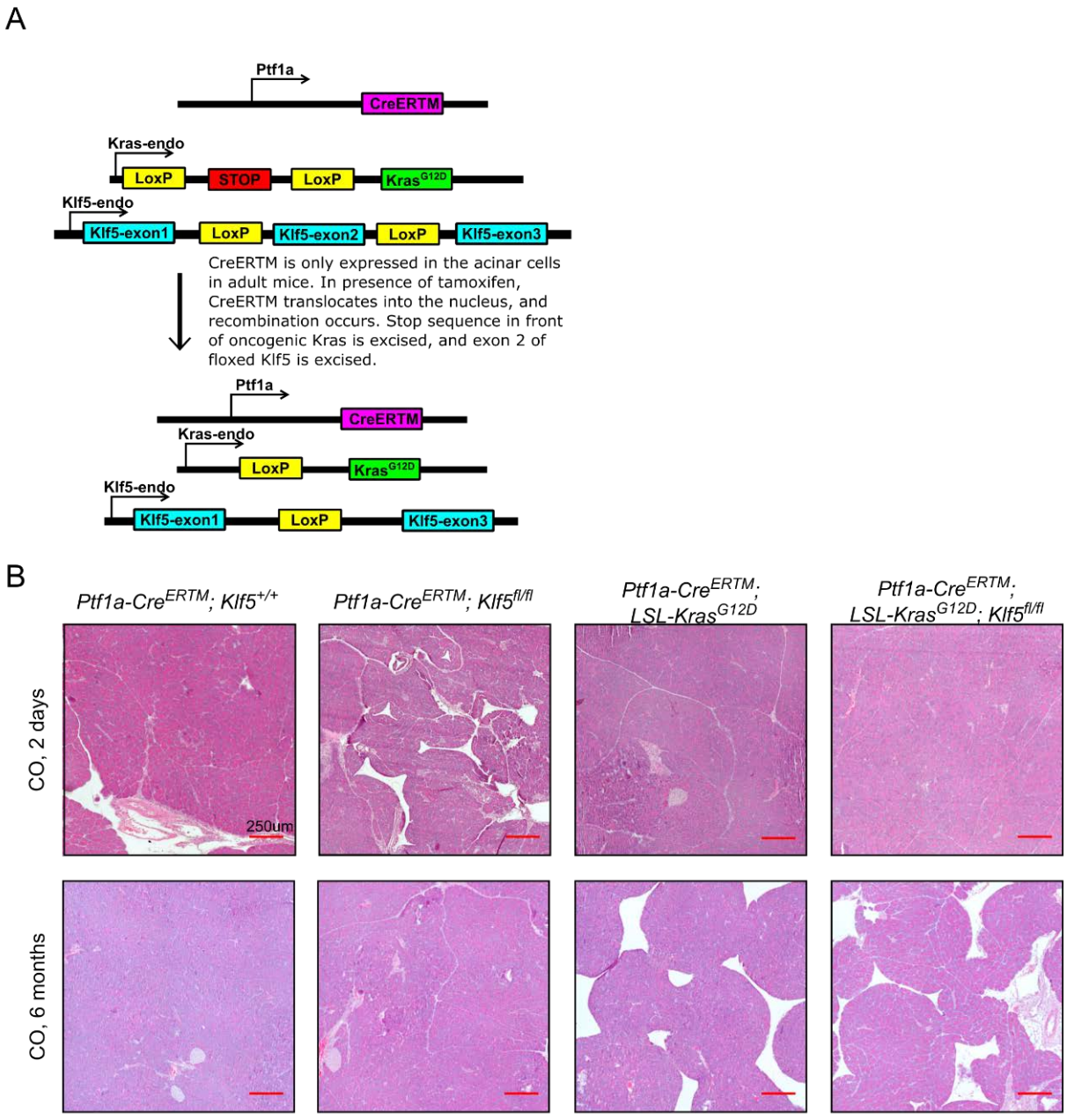

Figure 3.2 *Ptf1a-Cre^{ERTM}/LoxP* System
(A) Outline of the models that allow for the expression of *Kras^{G12D}* and deletion of *Klf5* after tamoxifen induction. **(B)** H&E staining of pancreatic tissue from mouse of indicated genotypes 2 days and 6 months after corn oil (CO) injections. Scale bars = 250 µm.

3.3 *Klf5* Knockout Reduces KRAS^{G12D}-induced PanIN Formation

Previous study characterizing *Ptf1a-Cre^{ERTM}* mouse model showed that the recombination efficiency of *Rosa26^{LacZ}* allele by Cre^{ERTM} fusion protein increases with dosage of tamoxifen in a dosage-dependent manner (24). Validation of inducible Cre recombinase activity showed that three 3 mg tamoxifen injections given over 6 days starting at 5 weeks of age induced up to 80% recombination of *Rosa26^{LacZ}* alleles in pancreatic acinar cells (24). Based on these published data, I adopted this tamoxifen injection regimen and collected pancreatic tissue from mice to examine spontaneous PanIN formation at 3 months after the last tamoxifen injection (Figure 3.3A). As shown in the control experiment above, mice injected with corn oil alone do not develop PanINs when observe up to 6 months after injection (Figure 3.2B). At 3 months after tamoxifen administration, histological analysis showed morphologically normal acini in *Ptf1a-Cre^{ERTM}* and *Ptf1a-Cre^{ERTM};Klf5$^{fl/fl}$* mice (Figure 3.3B). In contrast, pancreata of *Ptf1a-Cre^{ERTM};LSL-Kras^{G12D}* mice contained large regions comprising of ductal structures embedded in extensive desmoplasia (Figure 3.3B). The ductal lesions stained positive for Alcian Blue, a marker for mucin production in PanINs, *Ptf1a-Cre^{ERTM};LSL-Kras^{G12D}* mice (Figure 3.3C). These finding are consistent with earlier reports of spontaneously formed mouse PanIN in oncogenic *Kras^{G12D}*-induced models (65, 78). In comparison, *Ptf1a-Cre^{ERTM};LSL-Kras^{G12D};Klf5$^{fl/fl}$* mice had fewer ductal lesions, without extensive desmoplasia (Figure 3.3B). Quantifications of the percentage of total pancreatic area stained positive for Alcian Blue, a measure of the area affected by PanIN, showed no difference between *Ptf1a-Cre^{ERTM}* and *Ptf1a-Cre^{ERTM};Klf5$^{fl/fl}$* mice (0.20% ± 0.13%, n = 3 vs. 0.27% ± 0.11%, n = 8, respectively; Mean ± SD) (Figure 3.3C). On the other hand, *Ptf1a-Cre^{ERTM};LSL-Kras^{G12D};Klf5$^{fl/fl}$* mice had significantly reduced Alcian Blue positive area compared to *Ptf1a-Cre^{ERTM};LSL-Kras^{G12D}* (2.62% ± 1.66, n = 6 vs. 0.45% ± 0.11%, n = 4, respectively; Mean ± SD)

(Figure 3.3C). IHC staining for KLF5 shows nuclear staining localized to the ductal cells in *Ptf1a-Cre^{ERTM}* and *Ptf1a-Cre^{ERTM};Klf5$^{fl/fl}$* mice (Figure 3.3D). PanIN lesions in *Ptf1a-Cre^{ERTM};LSL-Kras^{G12D}* mice had positive nuclear KLF5 staining (Figure 3.3D). Rare ductal lesions in *Ptf1a-Cre^{ERTM};LSL-Kras^{G12D};Klf5$^{fl/fl}$* mice retained partial nuclear KLF5 staining, suggesting that those cells escaped *Klf5* deletion. The results indicate that KLF5 is required for the spontaneous formation of *Kras^{G12D}*-induced PanIN *in vivo*.

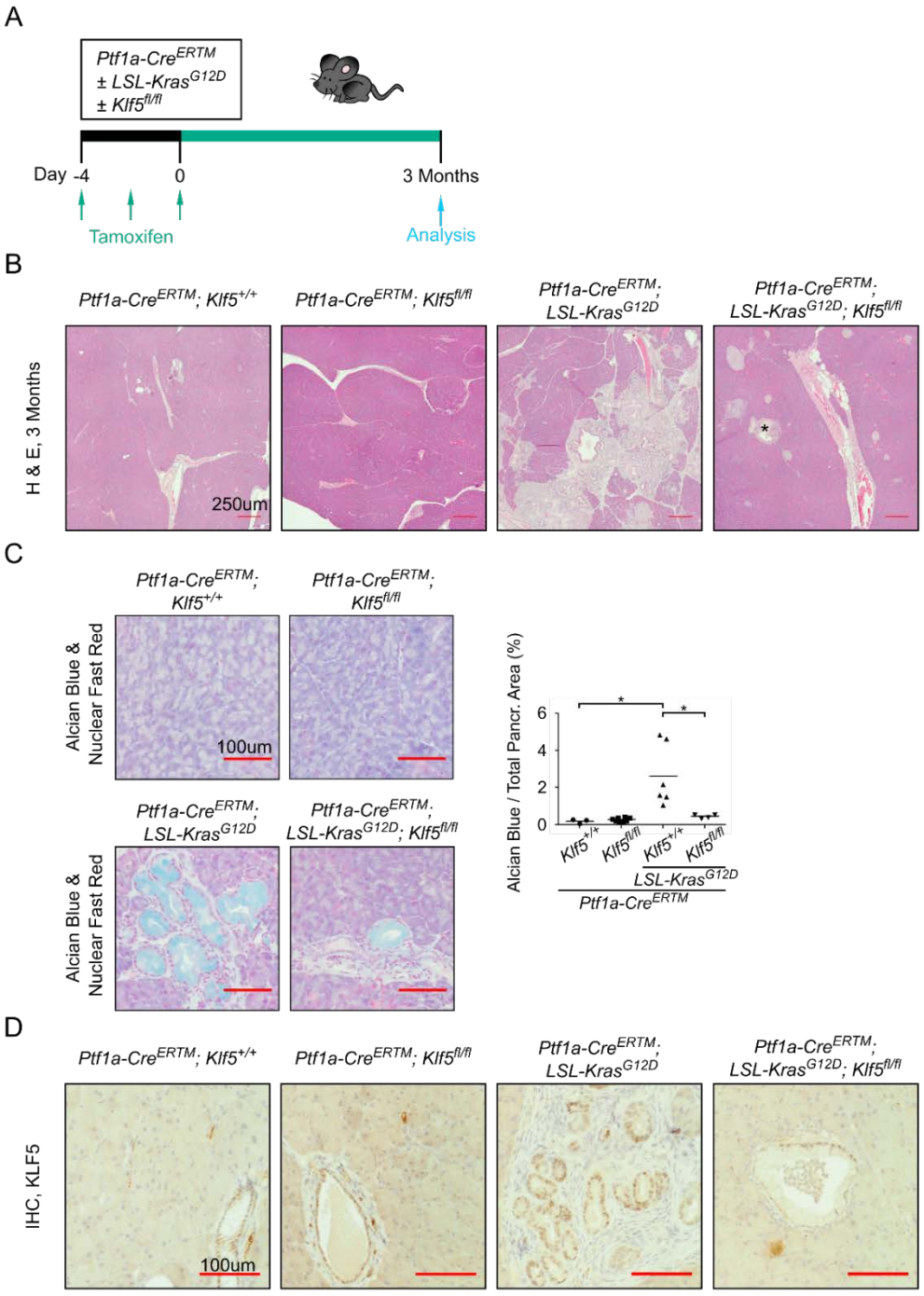

Figure 3.3 *Kras*^{G12D}-induced PanIN Formation after *Klf*5 Deletion

(A) Scheme showing inducible model of *Kras*^{G12D} expression and inactivation of *Klf5*. **(B)** H&E staining of pancreata from mice of each genotype. Scale bar = 250 µm. * in image indicate residual PanIN. **(C)** Alcian Blue staining counterstained with Nuclear Fast Red of pancreata from mice of each genotype. Scale bar = 100 µm. Graph showing quantification of percent Alcian Blue^{+} pancreatic area. Data represents mean, * $P < 0.05$ by Mann-Whitney test. **(D)** Immunohistochemical analysis of KLF5 in pancreata from mice of each genotype. Scale bars = 100 µm.

3.4 *Klf5* Knockout Reduces Acute Pancreatitis-induced ADM

Chronic inflammation is a major risk factor associated with pancreatic cancer in human (163). Pancreatitis induced by cerulein, an oligopeptide secretagogue, can accelerate $Kras^{G12D}$-induced PanIN formation by promoting inflammation-induced ADM (164). In this model of pancreatitis, acute pancreatitis is observable in the pancreas during and immediately after cerulein injections (164). ADM is observable in the pancreas at 2 days after cerulein injections (164). Pancreas of mice with wild-type *Kras* recover when examined at 7 days after cerulein injections (164). At 21 days after cerulein injections, the pancreata of mice with $Kras^{G12D}$ mutation are predominantly filled with PanIN lesions (164). To examine the role of KLF5 in pancreatitis-induced ADM and PanIN formation, I examined pancreata from the mouse model at 1 hour, 2 days, and 2 weeks after cerulein treatment (Figure 3.4A). H&E staining of pancreata from mice of all four genotypes at 1 hour time-point showed disrupted acinar morphology and infiltration of inflammatory cells consistent with acute pancreatitis (Figure 3.4B). Acute pancreatitis was verified by serum amylase measurement 1 hour after last injection of cerulein (Figure 3.4B), and there was no significant difference in the serum amylase level between different genotypes treated with cerulein (Figure 3.4C). Pancreata from $Ptf1a\text{-}Cre^{ERTM}$ control mice 2 days after cerulein treatment contain ADM (Figure 3.5A), characterized by appearance of duct-like structures with large lumen consistent with previous reports (78, 164). Pancreata from $Ptf1a\text{-}Cre^{ERTM};LSL\text{-}Kras^{G12D}$ mice at 2 days after cerulein treatment contain more extensive ADM compared to the control (Figure 3.5A). In contrast, $Ptf1a\text{-}Cre^{ERTM};Klf5^{fl/fl}$ and $Ptf1a\text{-}Cre^{ERTM};LSL\text{-}Kras^{G12D};Klf5^{fl/fl}$ mice at 2 day time-point failed to form ADM (Figure 3.5A). By 2 week time-point, pancreata from $Ptf1a\text{-}Cre^{ERTM}$ and $Ptf1a\text{-}Cre^{ERTM};Klf5^{fl/fl}$ mice were indistinguishable from PBS-treated control mice based on histology (Figure 3.5A). $Ptf1a\text{-}Cre^{ERTM};LSL\text{-}Kras^{G12D}$ mice developed large regions containing

PanINs. In contrast, pancreata from *Ptf1a-Cre^{ERTM};LSL-Kras^{G12D};Klf5$^{fl/fl}$* mice have significantly fewer PanINs. Quantifications of ductal lesions in *Ptf1a-Cre^{ERTM};LSL-Kras^{G12D}* and *Ptf1a-Cre^{ERTM};LSL-Kras^{G12D};Klf5$^{fl/fl}$* mice showed a 77% reduction in the number of lesions after *Klf5* inactivation (Figure 3.5A) (205 ± 33, n = 5 vs. 47 ± 20, n = 4, respectively; Mean ± SD; $P < 0.05$ by Mann-Whitney test). Quantification of Alcian Blue positive area showed minimal difference between *Ptf1a-Cre^{ERTM}* and *Ptf1a-Cre^{ERTM};Klf5$^{fl/fl}$* mice in comparison to the significant difference between *Ptf1a-Cre^{ERTM};LSL-Kras^{G12D}* and *Ptf1a-Cre^{ERTM};LSL-Kras^{G12D};Klf5$^{fl/fl}$* mice (7.16% ± 3.55%, n = 5 vs. 0.64% ± 0.41%, n = 4, respectively; Mean ± SD; $P < 0.05$ by Mann-Whitney test) (Figure 3.5B). These results demonstrated that KLF5 is important for ADM formation and its inactivation in the context of activated KRAS reduces pancreatitis-induced ADM formation *in vivo*.

To understand the role of KLF5 in ADM and PanIN formation after pancreatitis, I examined expression pattern of KLF5 by IHC staining and those of amylase and keratin-19 (KRT19) by immunofluorescence (IF) staining in tissues from mouse treated with cerulein. Amylase, an enzyme produced specifically by acinar cells, and KRT19, a structure protein in ductal cells, can be used to identify cells undergoing ADM, which will be double-positive for both markers (164). Pancreata from *Ptf1a-Cre^{ERTM}* and *Ptf1a-Cre^{ERTM};LSL-Kras^{G12D}* mice at 1 hour time-point showed strong nuclear KLF5 expression in acinar cells compared with negative expression in acinar cells of PBS-treated control mice (Figure 3.6). The heterogeneity in the level of KLF5 upregulation by the acinar cells suggests cell-to-cell variability in the response to cerulein stimulation. Acinar cells in *Ptf1a-Cre^{ERTM};Klf5$^{fl/fl}$* and *Ptf1a-Cre^{ERTM};LSL-Kras^{G12D};Klf5$^{fl/fl}$* mice at 1 hour time-point did not express KLF5, which demonstrated effective deletion of *Klf5* in the model (Figure 3.6). At 2 day time-point, pancreata from *Ptf1a-Cre^{ERTM}* mice contained ADM with

positive nuclear KLF5 staining (Figure 3.6). Acinar cells in the regions with normal morphology no longer express nuclear KLF5. Pancreata from *Ptf1a-Cre^{ERTM};LSL-Kras^{G12D}* mice at 2 day time-point contained more ADM with strong nuclear KLF5 staining compared to *Ptf1a-Cre^{ERTM}* mice (Figure 3.6). On the other hand, *Ptf1a-Cre^{ERTM};Klf5$^{fl/fl}$* and *Ptf1a-Cre^{ERTM};LSL-Kras^{G12D};Klf5$^{fl/fl}$* mice failed to develop KLF5-postive ADM (Figure 3.6). Pancreata from *Ptf1a-Cre^{ERTM}* and *Ptf1a-Cre^{ERTM};Klf5$^{fl/fl}$* mice at 2 week time-point were indistinguishable on KLF5 IHC staining from pancreata of PBS-treated control (Figure 3.6). Pancreata from *Ptf1a-Cre^{ERTM};LSL-Kras^{G12D}* mice at 2 week time-point contained large regions of PanINs with strong nuclear KLF5 staining (Figure 3.6). Some isolated PanINs with nuclear KLF5 staining remains in pancreata of *Ptf1a-Cre^{ERTM};LSL-Kras^{G12D};Klf5$^{fl/fl}$* mice at 2 week time-point (Figure 3.6).

Amylase and KRT19 staining of pancreata from mice of all genotypes at the 1 hour time-point showed disrupted acinar morphology characteristic of acute pancreatitis (Figure 3.7). IF staining confirmed ADM found at 2 day time-point with amylase and KRT19 double positive ductal lesions (Figure 3.7), consistent with previous reports (78, 164). Pancreata of *Ptf1a-Cre^{ERTM};Klf5fl/fl* and *Ptf1a-Cre^{ERTM};LSL-Kras^{G12D};Klf5$^{fl/fl}$* mice were mainly comprised of amylase-positive and KRT19-negative acini with normal morphology at 2 day time-point (Figure 3.7). Pancreata from *Ptf1a-Cre^{ERTM}* and *Ptf1a-Cre^{ERTM};Klf5$^{fl/fl}$* mice at 2 week time-point were comprised of normal amylase positive acini and KRT19 positive ducts, while pancreata from *Ptf1a-Cre^{ERTM};LSL-Kras^{G12D}* mice contained large numbers of KRT19 positive PanINs (Figure 3.7). Pancreata from *Ptf1a-CreE^{RTM};LSL-Kras^{G12D};Klf5$^{fl/fl}$* mice contained reduced number of residual KRT19-positive PanINs compared to *Ptf1a-Cre^{ERTM};LSL-Kras^{G12D}* mice (Figure 3.7). The results verified that *Klf5* deletion reduces *Kras^{G12D}*-induced PanIN formation through inhibition of ADM.

KLF4 and SOX9 are other transcription factors that have been shown to be required for PanIN formation (78, 96). To examine whether *Klf5* deletion causes changes in the levels of KLF4 and SOX9, I performed IF staining for the two factors on the mouse tissue at 2 week time-point. Both IF staining of KLF4 and SOX9 showed increased percentage of nuclei stained in *Ptf1a-Cre^{ERTM};LSL-Kras^{G12D}* mice compared with *Ptf1a-Cre^{ERTM}* mice at 2 week time-point (n = 3), and those increases were reversed in *Ptf1a-Cre^{ERTM};LSL-Kras^{G12D};Klf5$^{fl/fl}$* mice (Figure 3.8).

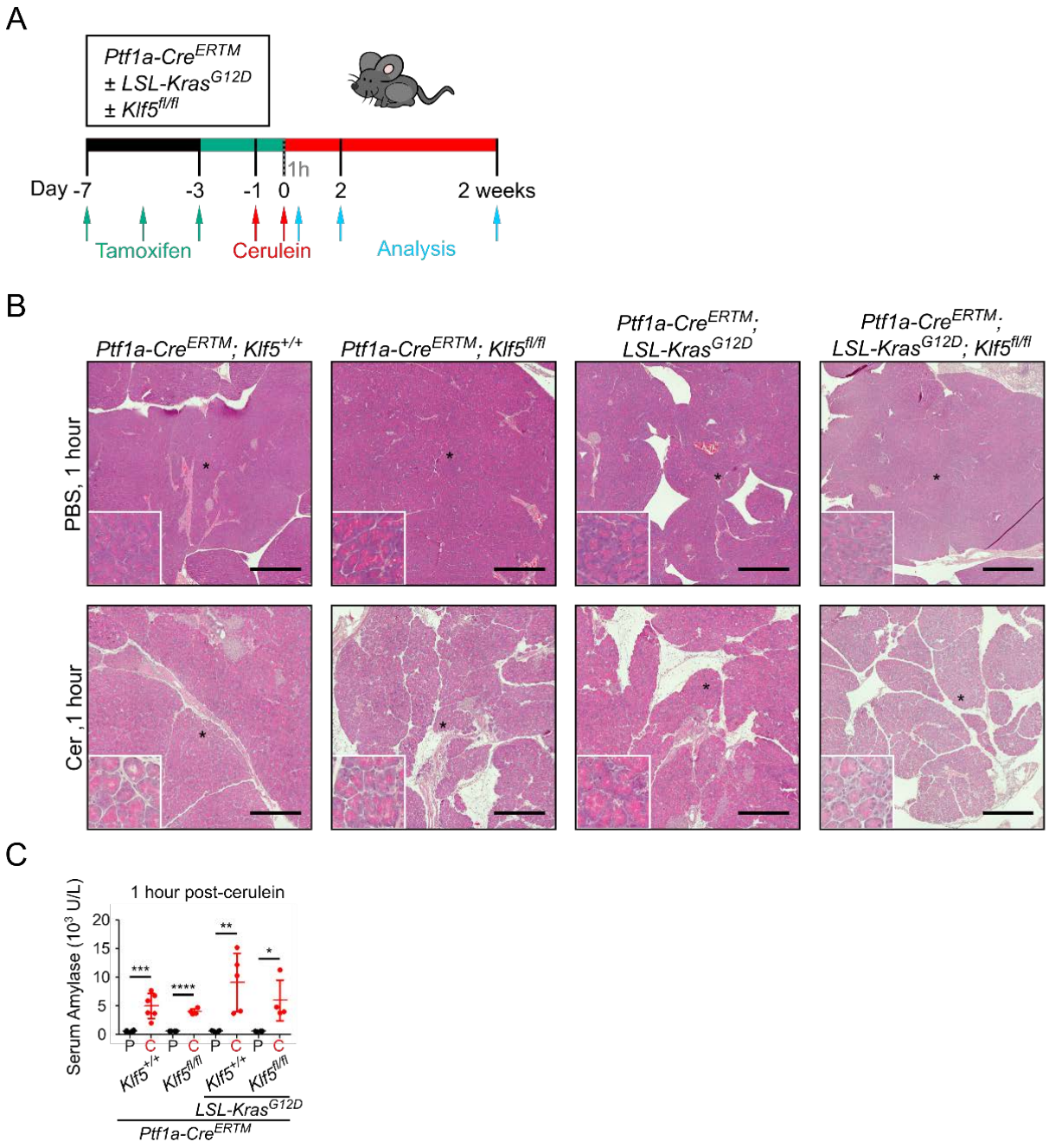

Figure 3.4. Cerulein-induce Acute Pancreatitis

(A) Scheme showing experimental design of cerulein-induced pancreatitis in combination with tamoxifen-inducible *Kras*^{G12D} expression and *Klf5* inactivation. **(B)** H&E staining of pancreata from mice of indicated genotype and at 1 hour after last cerulein injection. Scale bar = 500 µm. Inset: Enlargement of area marked by asterisk. **(C)** Graph showing quantification of serum amylase measurement at 1 hour time-point from cerulein-treated animals (C) and PBS-treated controls (P). Data represent mean ± SD. * *P* < *0.05; ** P < 0.01; *** P < 0.001; **** P < 0.0001* by Mann-Whitney test.

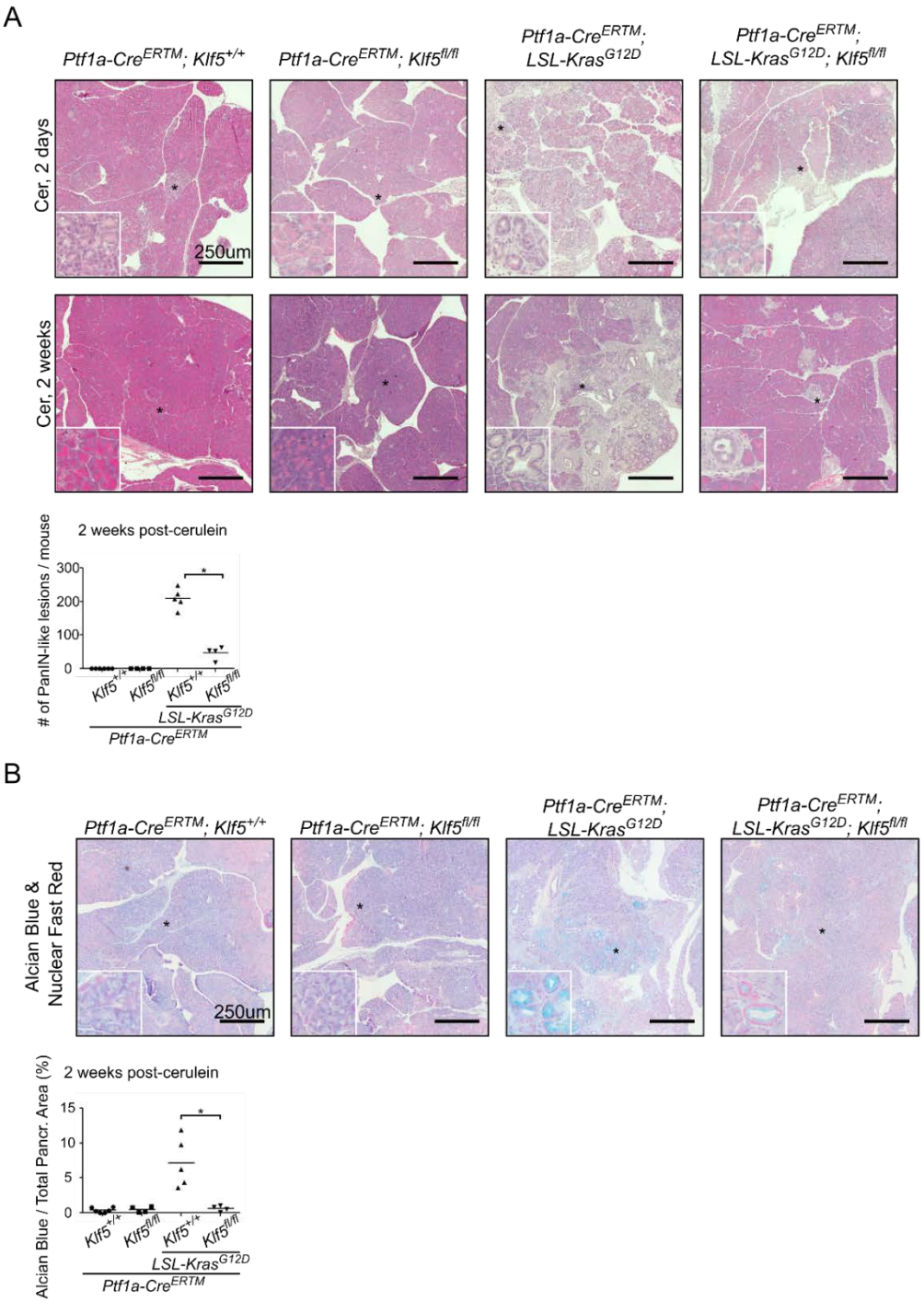

Figure 3.5. *Kras^{G12D}*-induced PanIN Formation Following Acute Pancreatitis
(A) H&E staining of pancreata from mice of indicated genotypes at 2 day and 2 week time-point. Scale bar = 500 μm. Inset: Enlargement of area marked by asterisk. Graph showing quantification of PanIN-like ductal lesions per pancreas from mice at 2 week time-point. **(B)** Alcian Blue staining counterstained with Nuclear Fast Red of pancreata from mice of each genotype at 2 week time-point. Scale bar = 500 μm. Inset: Enlargement of area marked by asterisk. Graph showing quantification of percentage of Alcian Blue^{+} pancreatic area. Data represent mean. * $P < 0.05$ by Mann-Whitney test.

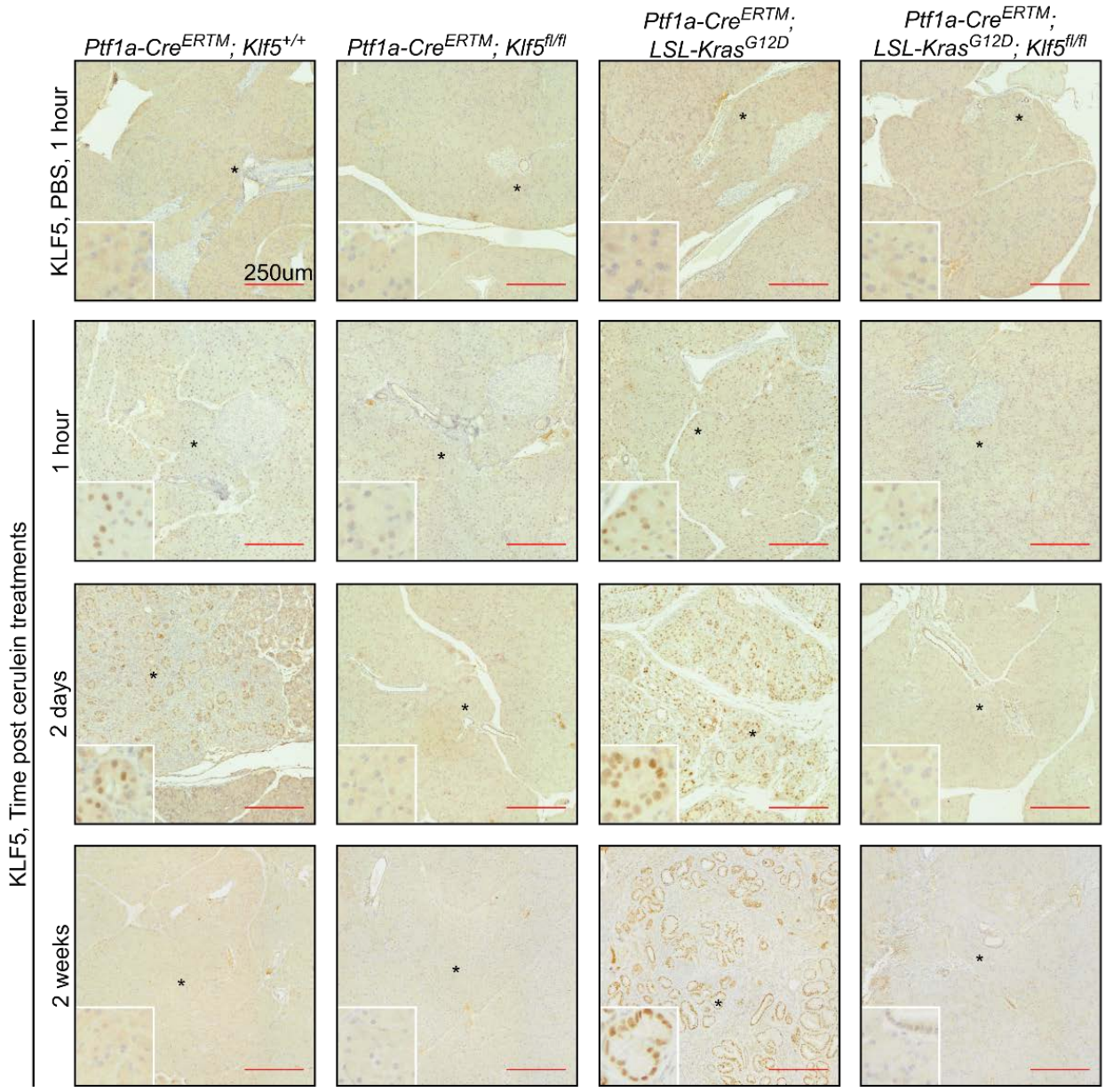

Figure 3.6. KLF5 Expression Following Acute Pancreatitis
Immunohistochemical analysis of KLF5 in pancreata from mice of indicated genotypes and time-points. Scale Bar = 250 μm. Inset: Enlargement of area marked by asterisk.

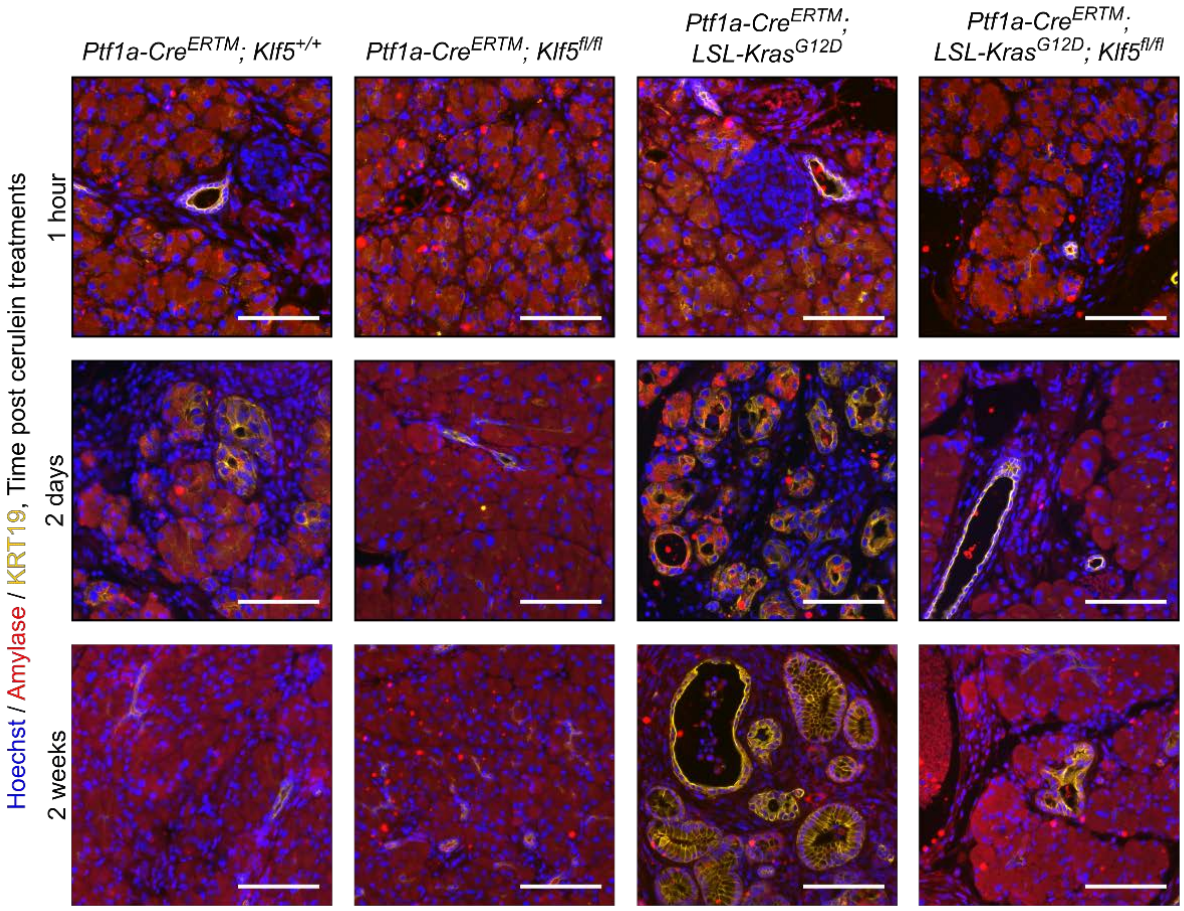

Figure 3.7. Amylase and KRT19 Expression Following Acute Pancreatitis
Multicolor immunofluorescence (IF) analysis of Hoechst nuclear staining (blue), amylase (red), and KRT19 (yellow) in pancreata from mice of indicated genotypes and time-points. Scale = 100 µm. Inset: Enlargement of area marked by asterisk.

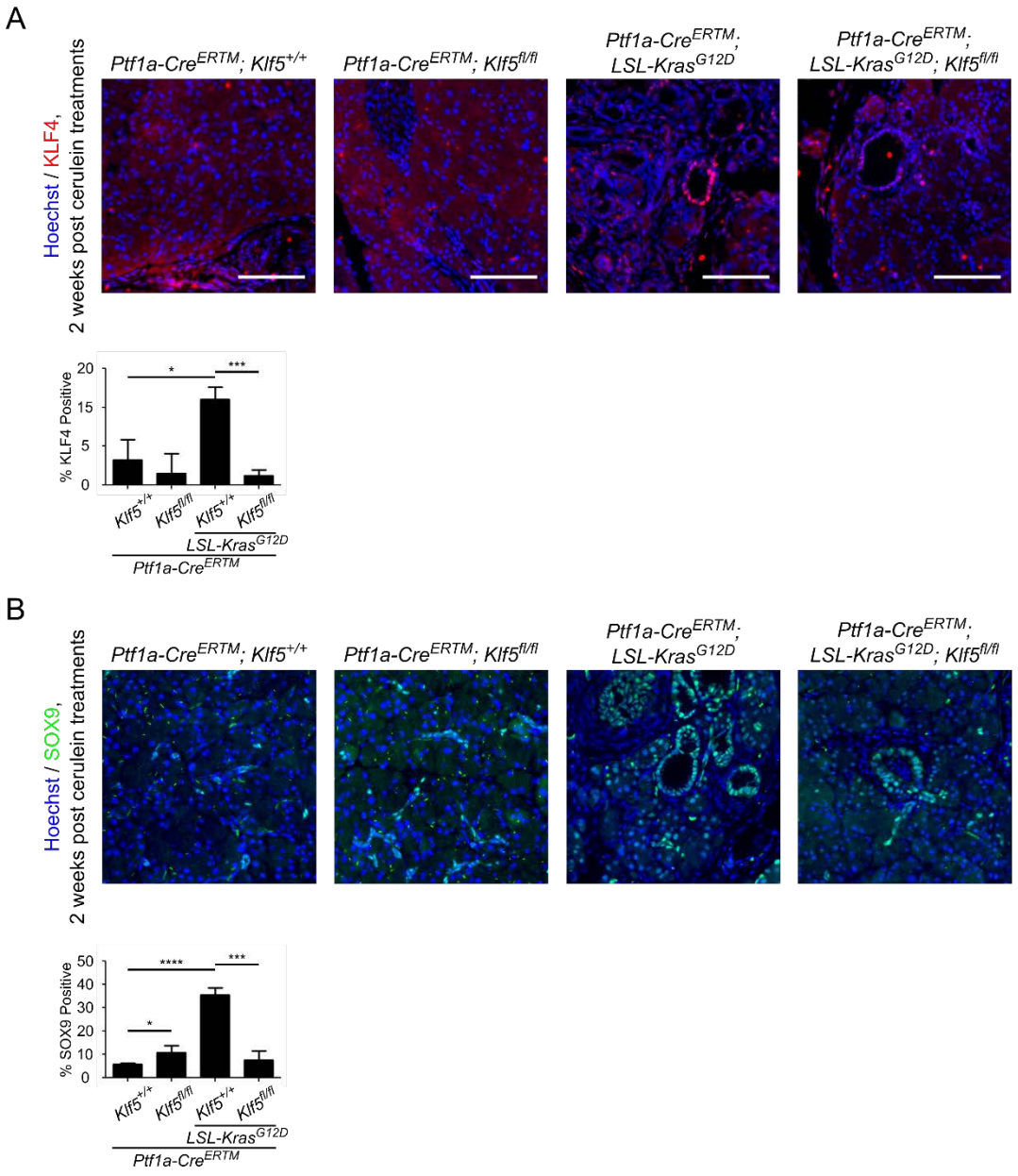

Figure 3.8. KLF4 and SOX9 Expression After Acute Pancreatitis Following *Klf5* Deletion
(A) Multicolored IF staining showing Hoechst nuclear staining (blue) and KLF4 (red). Graph showing quantification for percent (%) of total nuclei that are KLF4 positive. **(B)** Multicolored IF staining showing Hoechst nuclear staining (blue) and SOX9 (green). Graph showing quantification for percent (%) of total nuclei that are SOX9 positive. Scale = 100 µm. * $P < 0.05$; *** $P < 0.001$; **** $P < 0.0001$ by Mann-Whitney test.

3.5 Regulation of Transcriptome Reprogramming by KLF5

To elucidate the transcriptional mechanism by which *Klf5* deletion blocks pancreatitis-induced ADM, I performed a complete transcriptomic profiling of RNA extracted from mice at 2-day time-point after cerulein. Changes in gene expression were considered significant in each pairwise comparison if the fold-change > 2 and adjusted $P < 0.05$. I identified three significantly differentially expressed genes with concordance in both pairwise comparisons of *Ptf1a-Cre^{ERTM};Klf5$^{fl/fl}$* to *Ptf1a-Cre^{ERTM}* genotypes and *Ptf1a-Cre^{ERTM};LSL-Kras^{G12D};Klf5$^{fl/fl}$* to *Ptf1a-Cre^{ERTM};LSL-Kras^{G12D}* genotypes. In addition to those 3 genes, 41 genes (e.g. *Fmo2*) are significantly differentially expressed in only one comparison (Figure 3.9A). A summary of differentially expressed genes from pairwise comparison can be found in Appendix A, and full data can be found at Gene Expression Omnibus (Accession Number: GSE104055). The analysis showed that REC8 Meiotic Recombination Protein (*Rec8*) is downregulated, and Glyoxalase I (*Glo1*) and N-myc down-regulated gene 2 (*Ndrg2*) are upregulated after *Klf5* deletion (Figure 3.9B).

Among those, NDRG2 is a tumor suppressor and has been shown to be downregulated in numerous cancers (165). NDRG2 inhibits STAT3 signaling (166), which is important for oncogenic *Kras*-induced pancreatic tumorigenesis including ADM (91). qRT-PCR validation of RNA sequencing results showed decreased *Klf5* mRNA level (Figure 3.9C) and increased *Ndrg2* mRNA level (Figure 3.9D) upond comparing *Ptf1a-Cre^{ERTM};Klf5$^{fl/fl}$* to *Ptf1a-Cre^{ERTM}* genotypes and *Ptf1a-Cre^{ERTM};LSL-Kras^{G12D};Klf5$^{fl/fl}$* to *Ptf1a-Cre^{ERTM};LSL-Kras^{G12D}* genotypes at the 2 day time-point. Western blot analysis of mouse pancreatic lysate also showed an increase in NDRG2 protein, a decrease in phosphorylated, active form of STAT3 (Y705), and no change in total

STAT3 (Figure 3.10). These results indicate that *Klf5* deletion leads to upregulation of NDRG2 and reduction of STAT3 activation *in vivo*.

To examine whether *Ndrg2* is a direct transcriptional target of KLF5, I performed a search for potential KLF5 binding sites in a 4.5 kb sequence upstream of the translation start site of mouse *Ndrg2* gene using JASPAR database. The result showed 5 potential binding sites in the *Ndrg2* promoter region. I then performed Chromatin Immunoprecipitation (ChIP) assay on *Klf5* shRNA cells with doxycycline-inducible *Klf5* knockdown (see details in Methods) and scrambled shRNA cells as control after 5 days of doxycycline treatment using anti-KLF5 antibody followed by PCR using primers sets designed for each of the potential binding sites. The results showed that endogenous KLF5 physically interact with all 5 potential sites and binding was reduced after *Klf5* knockdown by RNA interference (Figure 3.11).

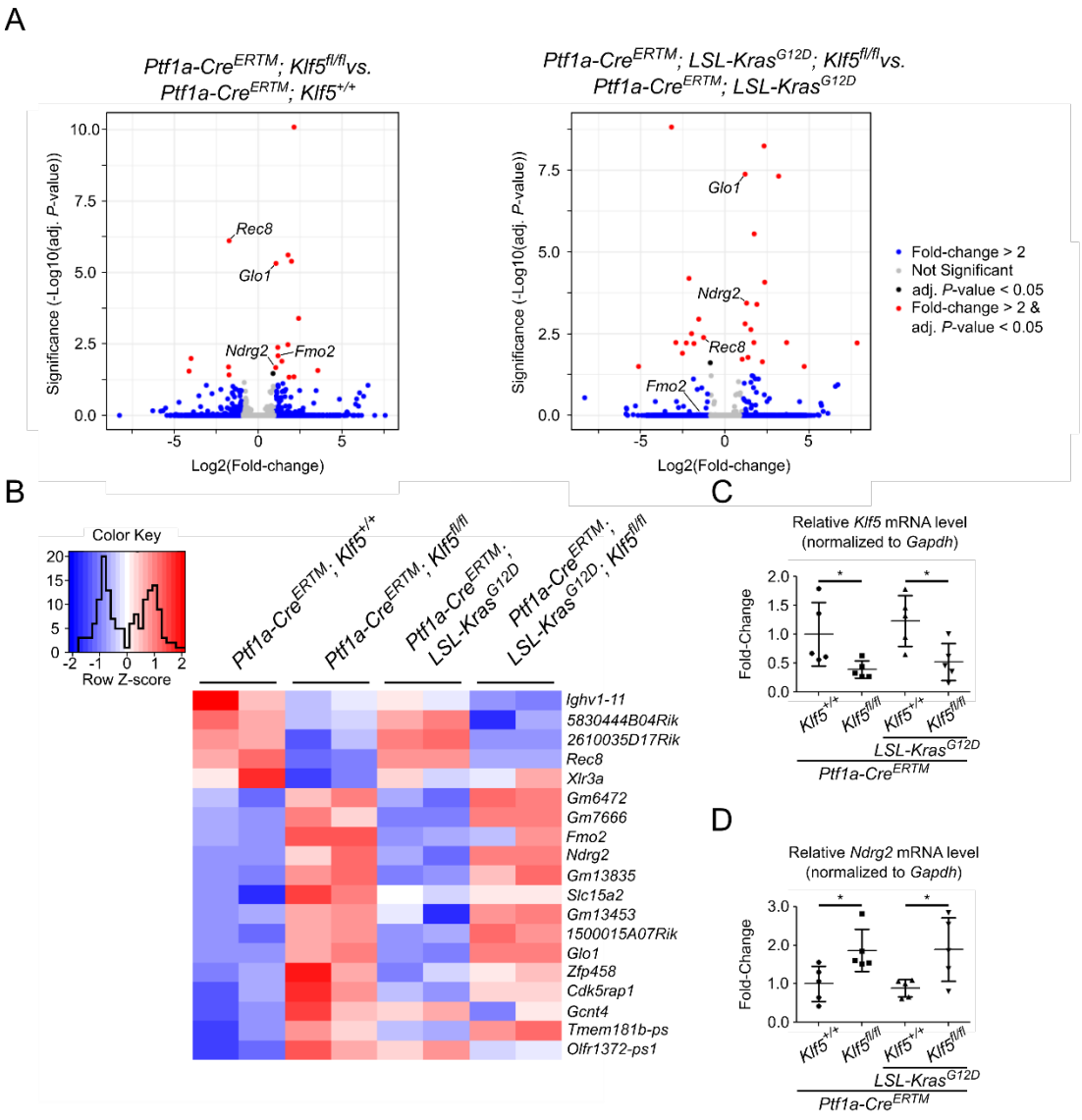

Figure 3.9. Transcriptomic Changes and *Ndrg2* Upregulation after *Klf5* Deletion
(A) Volcano plots of RNA-seq data showing differential expression of genes in pairwise comparison of *Ptf1a-Cre^{ERTM};Klf5$^{fl/fl}$* vs. *Ptf1a-Cre^{ERTM}* mice (left) and *Ptf1a-Cre^{ERTM};LSL-Kras^{G12D};Klf5$^{fl/fl}$* vs. *Ptf1a-Cre^{ERTM};LSL-Kras^{G12D}* mice (right). **(B)** Heatmap showing *Z*-score of normalized read counts of 19 most significant gene (*P < 0.05)* identified by pairwise comparison of *Ptf1a-Cre^{ERTM};Klf5$^{fl/fl}$* to *Ptf1a-Cre^{ERTM}* genotype. qRT-PCR analysis of *Klf5* mRNA level **(C)** and *Ndrg2* mRNA level **(D)** in mice at 2-day time-point and indicated genotypes (n = 5). * *P < 0.05* by two-sided, parametric t-test.

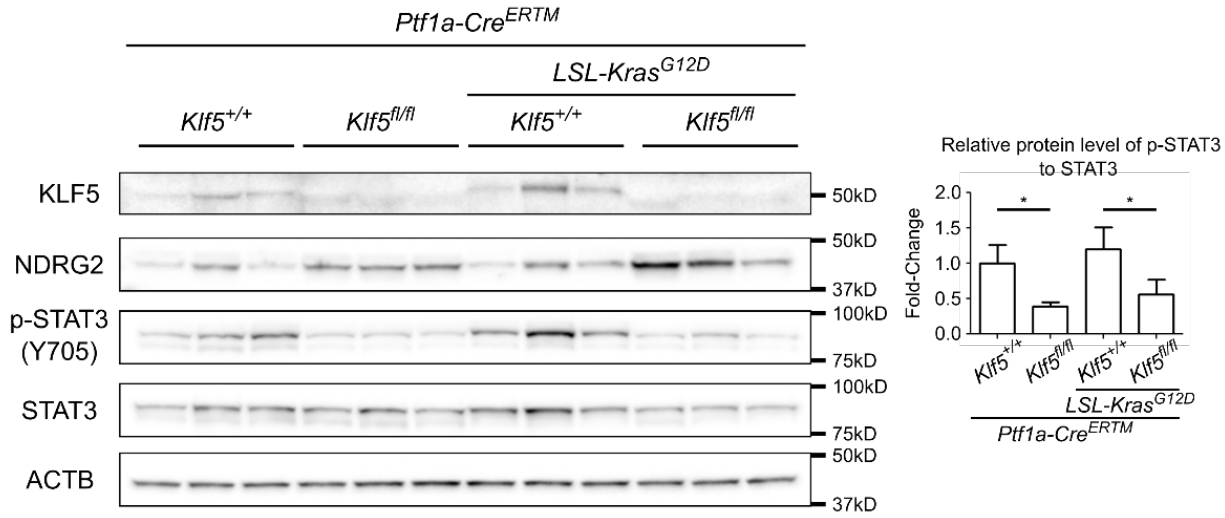

Figure 3.10. Inhibition of STAT3 Activation after *Klf5* Deletion
Western blot analysis of protein extracted from pancreata of mice at 2-day time-point showing changes in proteins levels of KLF5, NDRG2, p-STAT3(Y705), total STAT3, and ACTB (loading control) (n = 3). Graph of densitometry showing relative protein levels of p-STAT3 to STAT3. * $P < 0.05$ by two-sided, parametric t-test.

A

Predicted Binding Sites of KLF5 in mouse *Ndrg2* Promoter

Site	Matrix ID	Name	Score	Relative score	Start	End	Strand	Predicted sequence
1	MA0599.1	KLF5	15.4291	0.999533	-4389	-4380	-	GCCCCACCCC
2	MA0599.1	KLF5	12.9637	0.96817	-3209	-3200	-	CCCCCTCCCC
3	MA0599.1	KLF5	11.612	0.950974	-2087	-2078	-	CCCACGCCCA
4	MA0599.1	KLF5	14.8528	0.992201	-1955	-1946	+	GCCCCTCCCC
5	MA0599.1	KLF5	14.8528	0.992201	-1777	-1768	-	GCCCCTCCCC

B

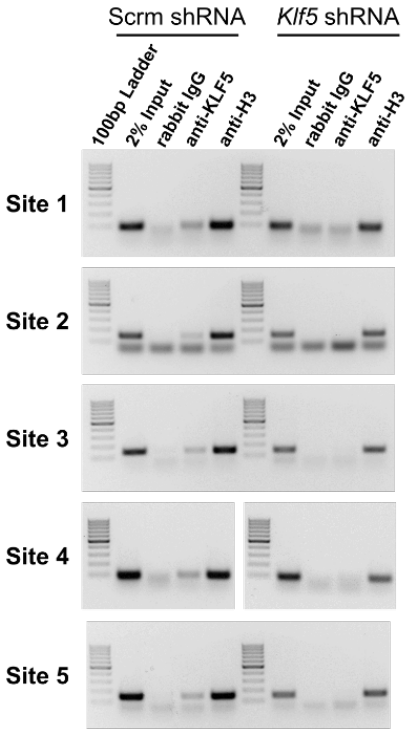

Figure 3.11. Physical Binding of KLF5 to *Ndrg2* Promoter

ChIP-PCR was performed on Klf5 shRNA and Scrm shRNA cells after 5 days of 50 ng/ml doxycycline treatment to examine whether endogenous KLF5 can bind to *Ndrg2* promoter. **(A)** Predicted binding sites for KLF5 in sequence 4.5kb upstream of *Ndrg2* translation start site using JASPAR database. **(B)** PCR amplification of site specific sequences in DNA product of ChIP using anti-KLF5 antibody.

3.6 Discussion

The progression of pancreatic acinar cells to premalignant PanIN lesions with acinar-to-ductal metaplasia (ADM) as an intermediary step is an accepted model of early pancreatic tumorigenesis (164, 167). I hypothesized that KLF5 is an essential factor required for early pancreatic tumorigenesis. Using a tamoxifen-inducible, acinar cell-specific mouse model, I demonstrated that *Klf5* deletion in adult pancreatic acinar cells reduces spontaneous $Kras^{G12D}$-induced PanIN formation (Figure 3.3). Acinar cells with *Klf5* deletion also failed to form ADM following cerulein-induced pancreatitis (Figure 3.5). Interestingly, KLF5, which is normally absent in acinar cells, was expressed in the nuclei of acinar cells during pancreatitis and was maintained during ADM in *Ptf1a-*Cre^{ERTM} and *Ptf1a-*Cre^{ERTM}*;LSL-*$Kras^{G12D}$ mice and $Kras^{G12D}$-induced PanIN formation in *Ptf1a-*Cre^{ERTM}*;LSL-*$Kras^{G12D}$ mice (Figure 3.6). The findings in ADM and PanIN formation are supported by the results of staining for amylase and KRT19, biomarkers for acinar and ductal phenotype, respectively (Figure 3.7). Together the data suggest that KLF5 is required for ADM and oncogenic KRAS-induced PanIN formation.

Ndrg2 is a gene of interest detected by the RNA sequencing and validated by qRT-PCR and Western blot (Figure 3.9D & 3.10). It is upregulated in the pancreas of *Klf5* deleted mice 2 days after cerulein-induced pancreatitis (Figure 3.9). NDRG2 is a member of a family of alpha/beta hydrolase that do not have hydrolytic site and enzymatic activity (165). Several studies have shown that low levels of NDRG2 are associated with poor clinical prognosis in pancreatic cancer (168, 169). In breast cancer cell lines, NDRG2 can functions as a tumor suppressor by inhibiting STAT3 signaling through the upregulation of *SOCS1* (166, 170). STAT3 signaling is required during ADM and PanIN formation (90, 91). I showed that the ratio of active, phosphorylated STAT3 (Y705) to total STAT3 is reduced after *Klf5* deletion *in vivo* (Figure 3.10). The results suggest that *Klf5*

deletion inhibits STAT3 signaling, possibly through increased expression of NDRG2. NDRG2 can potentially inhibit ADM and PanIN formation through additional mechanisms, including the inhibition of NFkB activation and expression of *MMP9* (165).

I have shown that endogenous mouse KLF5 can bind to the mouse *Ndrg2* promoter, suggesting that KLF5 can directly regulate *Ndrg2* expression (Figure 3.11). One potential mechanism for the direct regulation of *Ndrg2* expression by KLF5 is through the known interaction between KLF5 and Myc-Interacting Zinc Finger Protein 1 (Miz-1, ZBTB17). KLF5 associates with Miz-1 to repress expression of genes such as *CDKN2B* (171). Furthermore, Miz-1 is known to be essential for the c-Myc mediated repression of human *NDRG2* expression, a process which KLF5 may also participate in (172). Alternatively, previous studies in human pancreatic cancer cell lines showed that histone deacetylase (HDAC) inhibitor can increase expression of *NDRG2* (169). HDAC1 is known to directly interact with KLF5 by binding to the first zinc finger in KLF5 DNA binding domain and inhibit its activity as a transcriptional activator, but whether KLF5 is important for HDAC1 activity is unclear (173). Therefore, KLF5 could also be regulating *NDRG2* expression epigenetically by recruiting HDAC1 to the *NDRG2* promoter. Further studies are needed to confirm that human KLF5 can bind to the human *NDRG2* promoter and identify the mechanism by which KLF5 is regulating *NDRG2* expression.

In addition to Miz-1, KLF5 potentially interact with other transcription factors such as KLF4 and SOX9 to promote PanIN formation. When *Klf5* is deleted in the context of $Kras^{G12D}$ expression in acinar cells at 2 weeks after cerulein treatment, the protein levels of both KLF4 and SOX9 are also reduced (Figure 3.8). Like KLF5, KLF4, another Krüppel-like factor, is required for PanIN formation (96). ChIP-seq study showed that KLF4 and KLF5 share majority of their binding targets, which might explain their similar function during PanIN formation (144). While

constitutive deletion of *Klf5* is embryonically lethal, deletion of *Klf4* is not, which suggests that other KLFs, possibly KLF5, can compensate for KLF4 functions (93). This hypothesis is further supported by the fact that KLF4 can be substituted with KLF5 when generating induced pluripotent stem cells (174). Additionally, see Chapter 4 for regulation of *KRT19* expression by KLF4 and KLF5 as an example of cooperative activation of the same target gene by two different KLFs. Unlike KLF5, KLF4 becomes a tumor suppressor after malignant transformation (98). This switch in function from pro-oncogenic to anti-oncogenic factor for KLF4 is not observed for KLF5. Finally, the interaction between KLF4 and KLF5 when they are bound to the same target gene is unknown. SOX9 is also required for PanIN formation (78). In intestine, SOX9 is a direct target of KLF5 and is upregulated during regenerative response following disruption of intestinal epithelial homeostasis after KLF5 loss (123). Physical interaction between SOX9 and KLF5 in context of gene regulation has not been studied.

Chapter 4. KLF5 and Pancreatic Cancer Cell Proliferation

This chapter in part is a reprint of the materials as it appears in:

Ping He, Jong Won Yang, Vincent W. Yang, Agnieszka B. Bialkowska. Krüppel-like Factor 5, Increased in Pancreatic Ductal Adenocarcinoma, Promotes Proliferation, Acinar to Ductal Metaplasia, Pancreatic Intraepithelial Neoplasia, and Tumor Growth in Mice. In *Gastroenterology*. Accepted for Publication on December 10, 2017

4.1 Introduction

Krüppel-like Factor 5 (KLF5) is highly overexpressed in patient pancreatic tumors and pancreatic cancer cell lines compared to normal tissue (142). The high levels of KLF5 in cancer cells suggest that it may have important role in maintaining oncogenic functions in addition to its role in early tumorigenesis (See Chapter 3). The earliest study conducted using human pancreatic cancer cell lines to elucidate the role of KLF5 in pancreatic cancer cells showed that KLF5 is important for cancer cell proliferation and survival by inducing the expression of platelet-derived growth factor A (PDGFA) and Survivin, respectively (131). Furthermore, KLF5 expression in those cell lines was shown to be regulated by Interleukin 1β (IL-1β) and Hypoxia Inducible Factor 1 α (HIF-1α) and not by oncogenic KRAS signaling through MAPK pathway (131). The results of the study suggest that there is a subset of pancreatic cancer with high levels of KLF5 but are *KRAS* wild-type.

More recent studies corroborated the early findings showing that KLF5 promotes proliferation and survival of pancreatic cancer cells. RNAi screen in human pancreatic cancer cell

lines using lentiviral library identified KLF5 as a pro-oncogenic factor (143). Further validation of this hypothesis showed pancreatic cancer cells with *KLF5* knockdown by shRNA had decreased cell proliferation *in vitro* and decreased tumor growth in subcutaneous xenograft model (143). Study using CRISPR/Cas9 system to knockout *KLF5* in human pancreatic cancer cell line also showed decreased cell proliferation *in vitro* and tumor growth in subcutaneous xenograft model after *KLF5* knockout (144). The same study demonstrated that KLF5 is required for the recruitment of other transcription factors to activate genes associated with epithelial phenotype specific to low-grade pancreatic cancer (144).

Many gaps in the knowledge on the roles of KLF5 in pancreatic cancer remain. The results from the experiments using $Kras^{G12D}$ mouse model suggest that KLF5 expression within the acinar cells can be dependent on the oncogenic KRAS signaling. To address this, I used a mouse pancreatic cancer cells line derived from $Kras^{G12D}$-driven mouse model of PDAC to show that inhibiting downstream pathways of KRAS (i.e. MAPK and PI3K pathway) reduces KLF5 expression (151). I then established a stable mouse pancreatic cancer cell line with inducible expression of *Klf5*-specific shRNA and studied the effects of KLF5 depletion in mouse pancreatic cancer cell line on cell proliferation, cell cycle, expression of epithelial gene, and tumor growth.

4.2 Expression of KLF5 in Human PDAC

To examine the prevalence of KLF5 expression in human PDAC tumors, my colleague Jong Won Yang and I performed immunohistochemical (IHC) analyses on human tissue microarrays (PA2081a and PA2082), which contain a combined 129 cases of PDAC with two core samples per case (Figure 4.1A). Cases were considered positive for KLF5 if both core samples contained positive KLF5 nuclear staining in more than 5% of tumor cells. 33 cases missing core

samples were excluded. Of the 96 remaining cases of PDAC, 73% (70/96) were positive for KLF5. KLF5-positive cases were found across all tumor grades and comprise 100% (8/8) of Grade 1 tumor, 66% (36/54) of Grade 2 tumors, and 76% (26/34) of Grade 3 tumors. Analysis of The Cancer Genome Atlas data by the Human Protein Atlas show that survival is negatively correlated with *KLF5* expression (Figure 4.1B) (175). In this analysis, each case was categorized as high or low *KLF5* expression by comparing to the median *KLF5* expression. This data suggests that KLF5 has a function in cancer cells after neoplastic transformation and not just in PanIN formation.

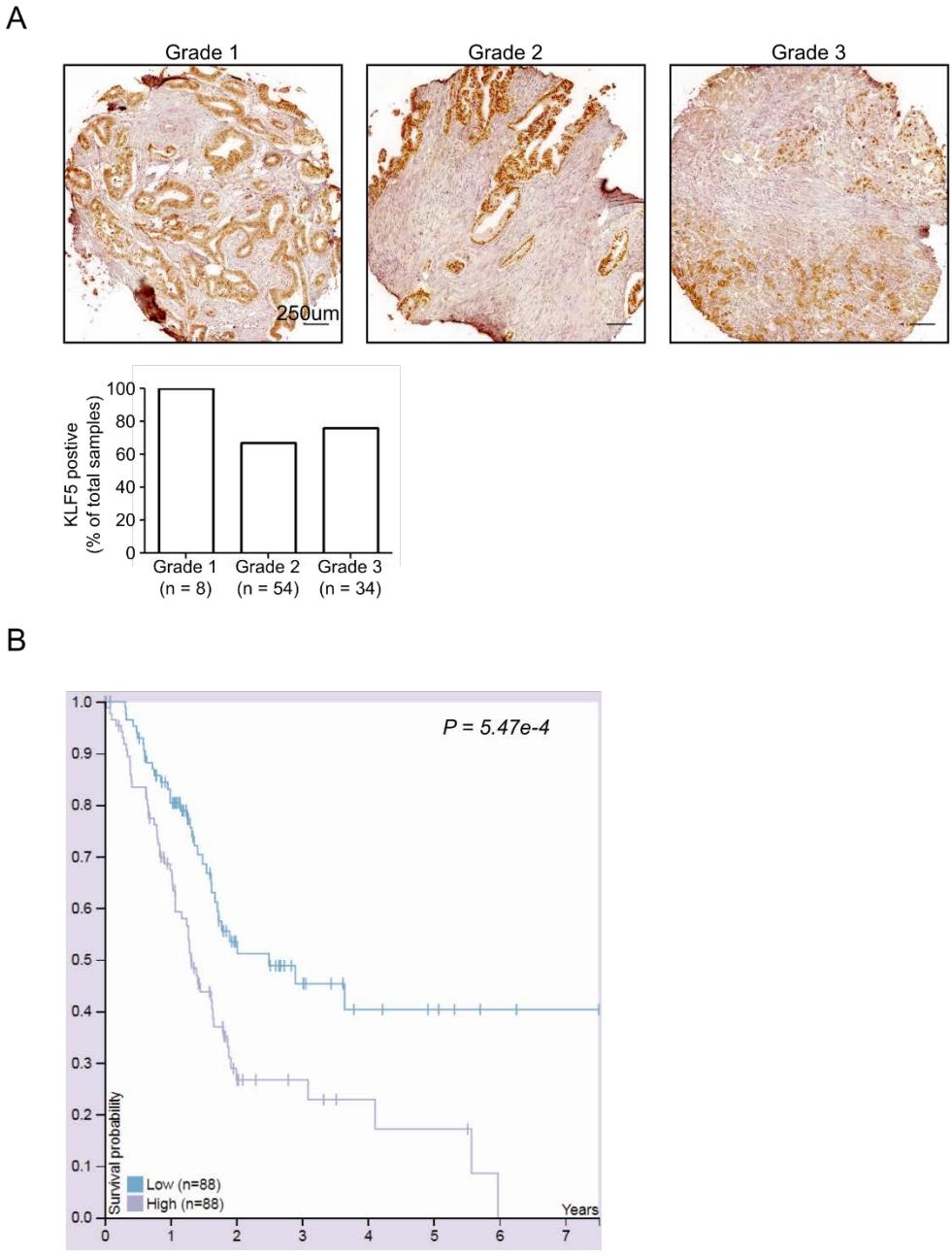

Figure 4.1. KLF5 Expression in Human Pancreatic Tumors
(A) Immunohistochemical analysis of KLF5 on human pancreatic cancer tissue microarray. Scale bars = 250 µm. Graph showing quantification of percent KLF5+ across tumor grades. n = number of cases (2 tissue core per case). **(B)** Kaplan-Meier curve showing survival of patient with high or low expression of *KLF5* based on TCGA data (high and low expression separated by median). *P = 5.47e-4.* Image credit: Human Protein Atlas. (28818916)
Survival Analysis/ KLF5/pathology/tissue/pancreatic cancer available from v18.proteinatlas.org. URL:
https://www.proteinatlas.org/ENSG00000102554-KLF5/pathology/tissue/pancreatic+cancer

4.3 Regulation of *Klf5* expression by $KRAS^{G12D}$

Although KLF5 overexpression correlates with *KRAS* mutation and MEK activity in human colorectal cancer (141), the earliest study of KLF5 in human pancreatic cell lines demonstrated that oncogenic *KRAS* expression and MEK signaling may not be required for KLF5 overexpression in pancreatic cancer cells *in vitro* (131). To identify the signaling pathways downstream of KRAS responsible for regulating *Klf5* expression in the mouse model, I used a battery of kinase inhibitors to inhibit those pathways in UN-KC-6141 mouse pancreatic cancer cell line, a cell line derived from $Kras^{G12D}$-induced mouse model of PDAC (151), comparable to the mouse model I developed. I treated UN-KC-6141 cells with kinase inhibitors, LY294002, U0126, PD98059, SB203580, and SP600125 to target phosphatidylinositide 3-kinases (PI3Ks), mitogen-activated protein kinase kinase 1/2 (MEK1/2), MEK1, p38 mitogen-activated protein kinases (p38), and c-Jun N-terminal kinases (JNKs), respectively. After 48 hours of treatment, UN-KC-6141 cells treated with LY294002, U0126, and PD9859 had decreased protein level of KLF5, suggesting that PI3K and MEK signaling is involved in regulating *Klf5* expression (Figure 4.2A). Decreased phospho-AKT level in LY294002 treated cells without decreases in total AKT level, phospho-ERK1/2 level, or total ERK1/2 level indicate that LY294002 specifically inhibited PI3K activity without affecting MEK activity (Figure 4.2A). Similarly, U0126 and PD98059 specifically decreased phospho-ERK1/2 level without changing the level of phospho-AKT level (Figure 4.2A). Densitometry shows that LY294002 and U0216 significantly decreased KLF5 protein level (Figure 4.2B).

The number of UN-KC-6141 cells substantially decreased after 48-hour treatment with several kinase inhibitors. Quantification showed significant decreases in the cell proliferation after treatment with LY294002, U0126, PD9859, and SP600125 comparing to DMSO-treated control

cells (Figure 4.2C). The decrease in proliferation closely correlated with the decrease in KLF5 expression (Spearman's Rank Correlation, r=0.9429, P=0.0164). These results suggest that *Klf5* overexpression in *Kras*^{G12D}-induced model of PDAC is maintained by both PI3K and MEK signaling, and high protein level of KLF5 promotes cancer cell proliferation (Figure 4.2D).

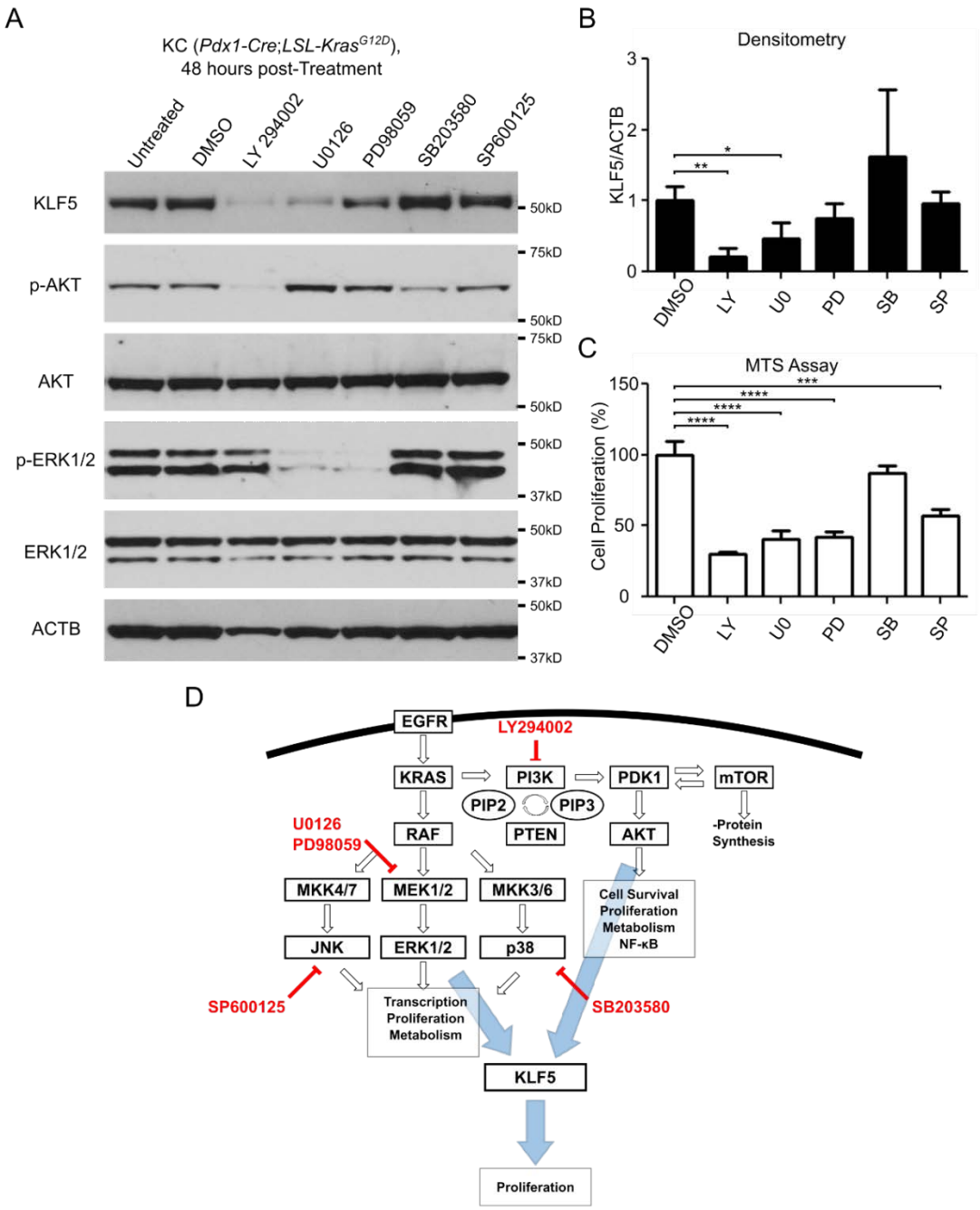

Figure 4.2. Regulation of KLF5 by MEK and PI3K Signaling

UN-KC-6141 cells were treated for 48 hours with kinase inhibitors, LY294002, U0126, PD98059, SB203580, SP600125, or DMSO (Control). **(A)** Western blot analysis of KLF5, phospho-AKT (p-AKT), total AKT, phospho-ERK1/2 (p-ERK1/2), ERK, and ACTB (loading control) **(B)** Graph showing densitometry analysis of Western blot results in fold change normalized to DMSO treated control (n = 3). **(C)** Cell proliferation after kinase inhibition examined by MTS assay shown as percentage normalized to DMSO treated control (n=4). Data represent mean ± SD for **(B)** and **(C)**. ** $P < 0.05$; ** $P < 0.01$; *** $P < 0.001$; **** $P < 0.0001$* by two-sided, parametric t-test. **(D)** Scheme showing targets of kinase inhibitors downstream of KRAS signaling and regulation of KLF5 by the signaling pathways.

4.4 Effect of KLF5 Depletion on Pancreatic Cancer Cell Proliferation

Consistent with the findings using kinase inhibitors, previous reports demonstrated reduction in proliferation of human pancreatic cancer cell lines after KLF5 is either depleted by RNA interference (RNAi) using short hairpin RNA (shRNA) or deleted by targeted genomic editing using CRISPR/Cas9 (143, 144). To examine whether decrease of cell proliferation in UN-KC-6141 cell line was a direct consequence of KLF5 depletion, I established stable UN-KC-6141 cell line with tetracycline-inducible expression of shRNA targeting *Klf5* (referred to from here on as *Klf5* shRNA cells). A stable UN-KC-6141 cell line with tetracycline-inducible expression of scrambled shRNA was established as a negative control (referred to from here on as scrambled shRNA cells). *Klf5* knockdown after 5 days of doxycycline treatment was verified using qRT-PCR and Western blot analysis (Figure 4.3A and B, respectively). Cell proliferation and MTS assays showed significant cell proliferation decrease after *Klf5* knockdown (Figure 4.3C and D, respectively).

Flow cytometric analysis of cell cycle using propidium iodide showed a significant decrease in the number of cells in G0/G1 phase and increase in S and G2/M phases (Figure 4.3E). qRT-PCR array analysis was performed on mRNA extracted from *Klf5* shRNA cells and scrambled shRNA cells after 5 days of doxycycline treatment. Twelve genes were significantly upregulated after *Klf5* depletion, and *Ccnd2* was the only gene significantly downregulated (Figure 4.3F; Appendix B). Among genes upregulated are positive cell cycle regulators *Cdk4, Ccne1, Ccnb1, Cdc25a, Smc1a, and Cdk2* (Figure 4.3F). Negative regulators of cell cycle that are upregulated includes *Sfn, Gpr132, Gadd45a, Rb1, and Pmp22* (Figure 4.3F). Western blot analysis showed decrease in cyclin D1 (CCND1), and increase in cyclin E (CCNE), cyclin A2 (CCNA2),

cyclin B1 (CCNB1), cyclin-dependent kinase 4 (CDK4), cyclin-dependent kinase 2 (CDK2), and stratifin (SFN) (Figure 4.3B).

To examine whether the decrease in cellular proliferation after *Klf5* knockdown is reversible, I examined cellular growth curve of *Klf5* shRNA cells and scrambled shRNA cells during 6 days of doxycycline treatment and during 2 cycles of 6-day recovery (Figure 4.4). The results showed marked decrease in proliferation of *Klf5* shRNA cells treated with doxycycline compared to the scrambled shRNA cells and untreated *Klf5* shRNA cells. Cell proliferation was not restored during the first 6-day recovery cycle, but was restored during the second 6 day recovery cycle (Figure 4.4). These results showed that the decrease in proliferation after *Klf5* depletion is rescuable.

To examine the effect of chronic KLF5 loss on the UN-KC-6141 cell line, I deleted *Klf5* through CRISPR/Cas9 double nickase system, which uses two different single guide RNA (sgRNA) that targets sequences in close proximity in the targeted gene to enhance specificity (176). Using this technique, I established a clone of UN-KC-6141 cell line with *Klf5* knockout (referred to from here on as *Klf5* KO) using mouse *Klf5*-specific sgRNAs. For control, I established a clone of UN-KC-6141 cell line using the same system and selection process, except replaced the *Klf5*-specific sgRNAs for nonspecific sgRNAs. Knockout of *Klf5* was validated using qRT-PCR and Western blotting (Figure 4.5, A and B, respectively). More moderate decreases in cell proliferation and changes in cell cycle were also found when *Klf5* is deleted from UN-KC-6141 cell line using CRISPR/Cas9 system. The decrease in cell proliferation of *Klf5* KO cells compared to control cells is less pronounce than the decrease in proliferation of cells after *Klf5* knockdown (Figure 4.5C). Cell cycle analysis shows a significant decrease in proportion of cells in G0/G1 phase and corresponding increase in S phase alone (Figure 4.5D).

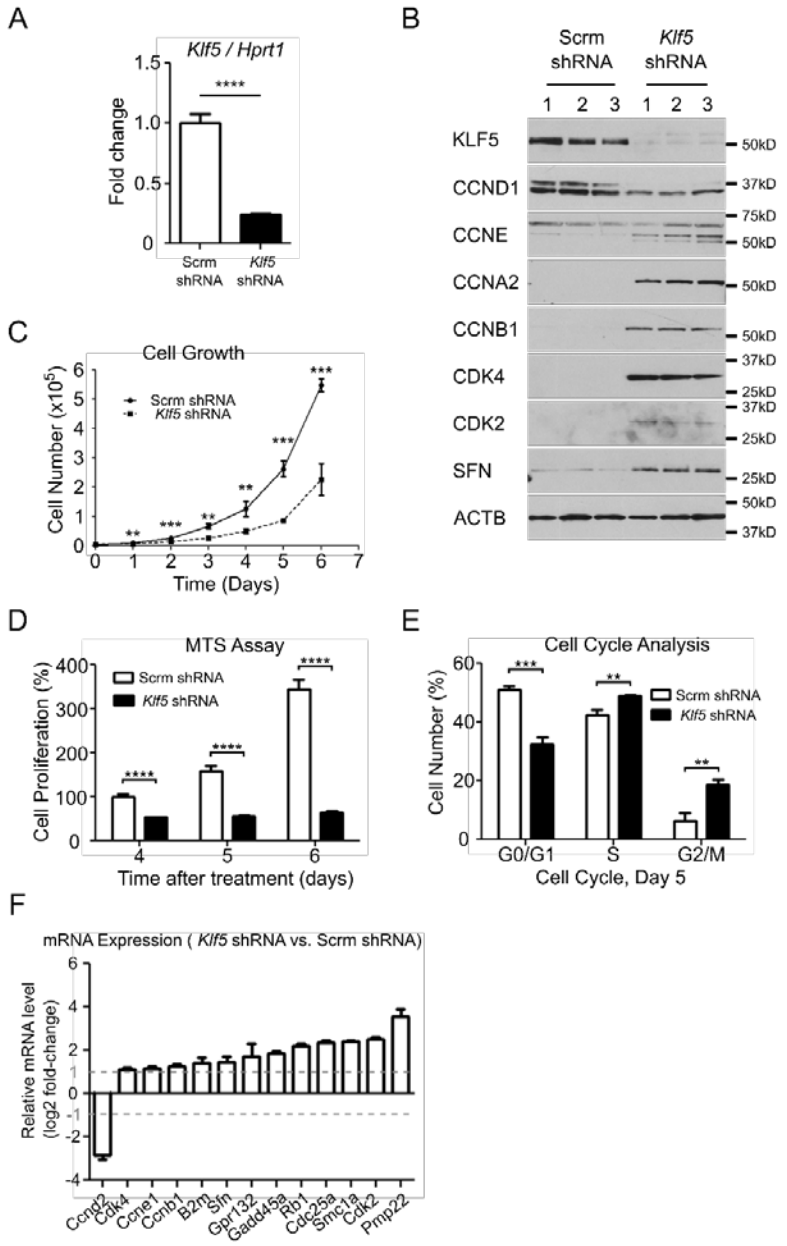

Figure 4.3. Effects of *Klf5* Knockdown on Cancer Cell Proliferation and Cell Cycle

(A) Results of qRT-PCR showing *Klf5* mRNA levels in *Klf5* shRNA and Scrm shRNA cells after 5 days of 50 ng/ml doxycycline treatment, normalized to Scrm shRNA control. Hprt1 was used as housekeeping gene. **(B)** Western blot analysis of KLF5, CCND1, CCNE, CCNA2, CCNB1, CDK4, CDK2, SFN, and ACTB (loading control) in *Klf5* shRNA and Scrm shRNA cells after 5 days of doxycycline treatment. (n=3). **(C)** Cellular growth curve of *Klf5* shRNA and Scrm shRNA cells treated with doxycycline (n = 3). **(D)** Cell proliferation measured by MTS assay at specific time-points (n = 4). Results normalized to Scrm shRNA cells at Day 4. **(E)** Cell cycle analysis of *Klf5* shRNA and Scrm shRNA cells at day 5 (n = 3). **(F)** Graph representing significant gene expression changes detected by PCR array targeting 83 cell cycle regulatory genes. (n=3, $P < 0.05$). Data represent mean ± SD for **(A)**, **(C)**, **(D)**, **(E)**, and **(F)**. ** $P < 0.01$; *** $P < 0.001$; **** $P < 0.0001$ by two-sided, parametric t-test.

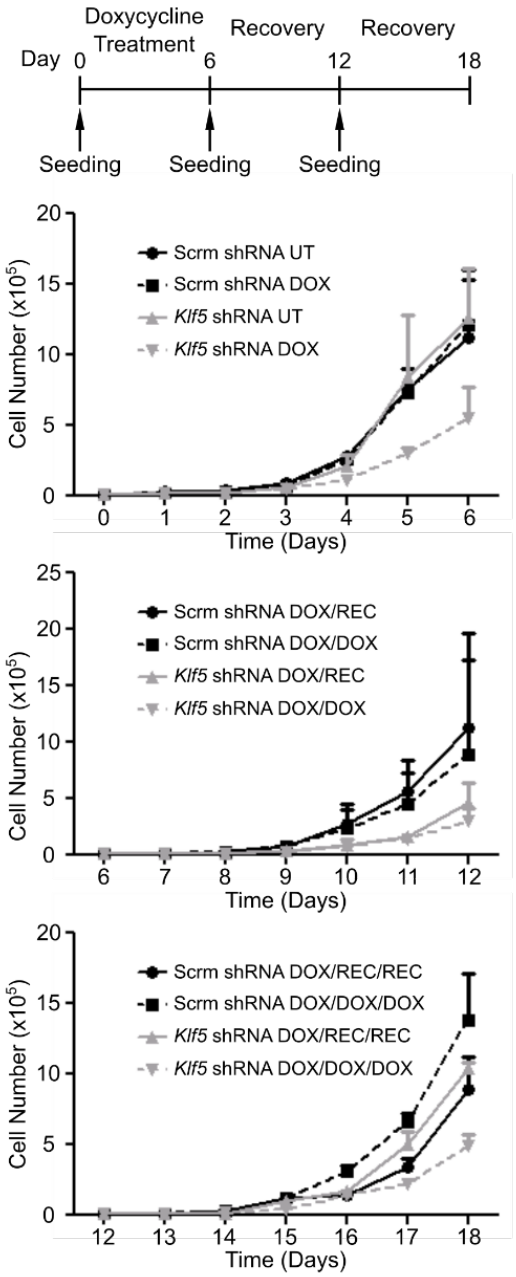

Figure 4.4. Recovery of Cell Proliferation after Transient *Klf5* Knockdown
Cellular growth curve of *Klf5* shRNA and Scrm shRNA cells during 6-day doxycycline treatment (top graph), during 6 days of recovery after 6 days of doxycycline treatment (middle graph), and during additional 6 days of recovery (bottom graph). Data represent mean ± SD.

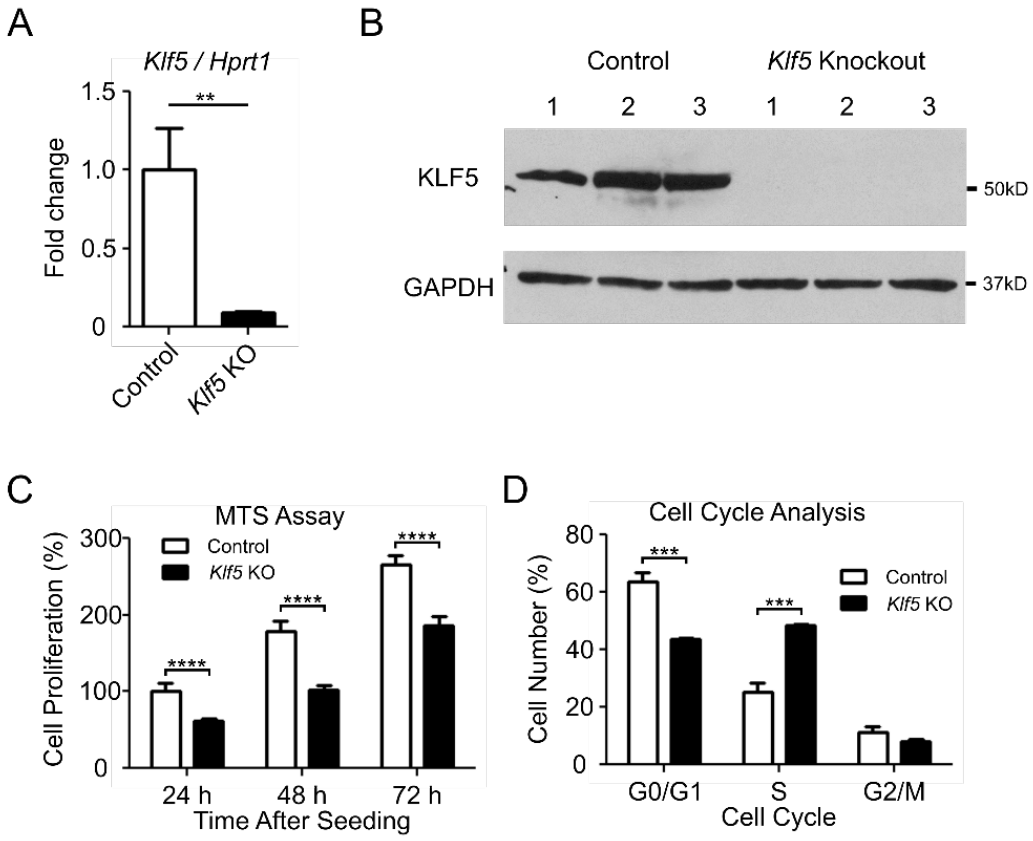

Figure 4.5. Effects of *Klf5* Knockout on Cancer Cell Proliferation and Cell Cycle
UN-KC-6141 cell line with *Klf5* knockout (*Klf5* KO) was established using CRISPR/Cas9 system with guide RNA targeting mouse *Klf5*. UN-KC-6141 control cell line (Control) was established using CRISPR/Cas9 system with non-specific guide RNA. **(A)** qRT-PCR analysis for *Klf5* mRNA level of Control and *Klf5* KO cell lines (n = 3). **(B)** Western blot analysis for KLF5 protein in Control and *Klf5* KO cell lines (n =3). **(C)** Cell proliferation of Control (white bar) and *Klf5* KO (black bar) cells measured by MTS assay at 24, 48, and 72 hours after seeding (n = 4). **(D)** Cell cycle analysis of Control (white bar) and *Klf5* KO (black bar) cells 72 hours after seeding (n = 3). Data represent mean ± SD for (A), **(C)** and **(D)**. ***P < 0.01, *** P < 0.001; **** P < 0.0001* by two-sided, parametric t-test. n values represent replicates of the same clone.

4.5 KLF5 as a Regulator of Ductal Phenotype in Pancreatic Cancer Cell

I examined the expression of CCND1, a known transcriptionally regulated gene target of KLF5 by IF analysis of CCND1 and KLF5 in *Klf5* shRNA cells and scrambled shRNA cells after doxycycline treatment. The results showed a marked decrease in CCND1 in cells after *Klf5* knockdown (Figure 4.6A). Together with the Western blotting and qRT-PCR data, these results confirmed effective depletion of KLF5 and downregulation of a KLF5 target gene in UN-KC-6141 cell line. *Klf5* shRNA cells also displayed changes in cell morphology (Figure 4.6B). It has been reported that KLF5 is important for maintaining ductal epithelial phenotype of human low-grade PDAC cell lines (144). To examine whether cells with *Klf5* knockdown also have decreased expression of ductal marker, I performed IF analysis for KLF5 and KRT19, which showed loss of KRT19 staining in cells with *Klf5* knockdown (Figure 4.6C). *Klf5* KO cells also has decreased level of CCND1 compared to the control cells, similar to the effects of *Klf5* knockdown (Figure 4.7A). However, KRT19 levels only decreased slightly in *Klf5* KO cells compared to the control cells.

To test whether *KRT19* is a direct target of KLF5, I performed ChIP-PCR assay to examine the physical interaction between endogenous mouse KLF5 and *Krt19* promoter. The results show PCR amplification of product from ChIP using anti-KLF5 antibody in scrambled shRNA cells (Figure 4.8A). No amplification was observed when KLF5 is depleted in *Klf5* shRNA cells. The data showed that KLF5 physically interact with mouse *Krt19* promoter and corroborate previous data showing physical interaction between KLF5 and cluster of keratin genes located on human chromosome 17 (144). To examine the effect of KLF5 on *KRT19* promoter activity, I performed luciferase reporter assay using pLightSwitch construct containing RenSP luciferase driven by the human *KRT19* promoter. pLightSwitch with empty promoter was used as negative control. When

SP1 overexpression construct is co-expressed with pLightSwitch construct in HEK293T cells, *KRT19* promoter activity increase by 2-fold from its basal level (Figure 4.8B). Overexpression of either human KLF4 or KLF5 increased *KRT19* promoter activity by 4-fold from its basal level (Figure 4.8B). Furthermore, combined overexpression of any two factors among SP1, KLF4 and KLF5 increased *KRT19* promoter activity by 10-13 fold from its basal level (Figure 4.8B). These data demonstrated that KLF5 can act cooperatively with SP1 and KLF4 to promote expression of *KRT19.*

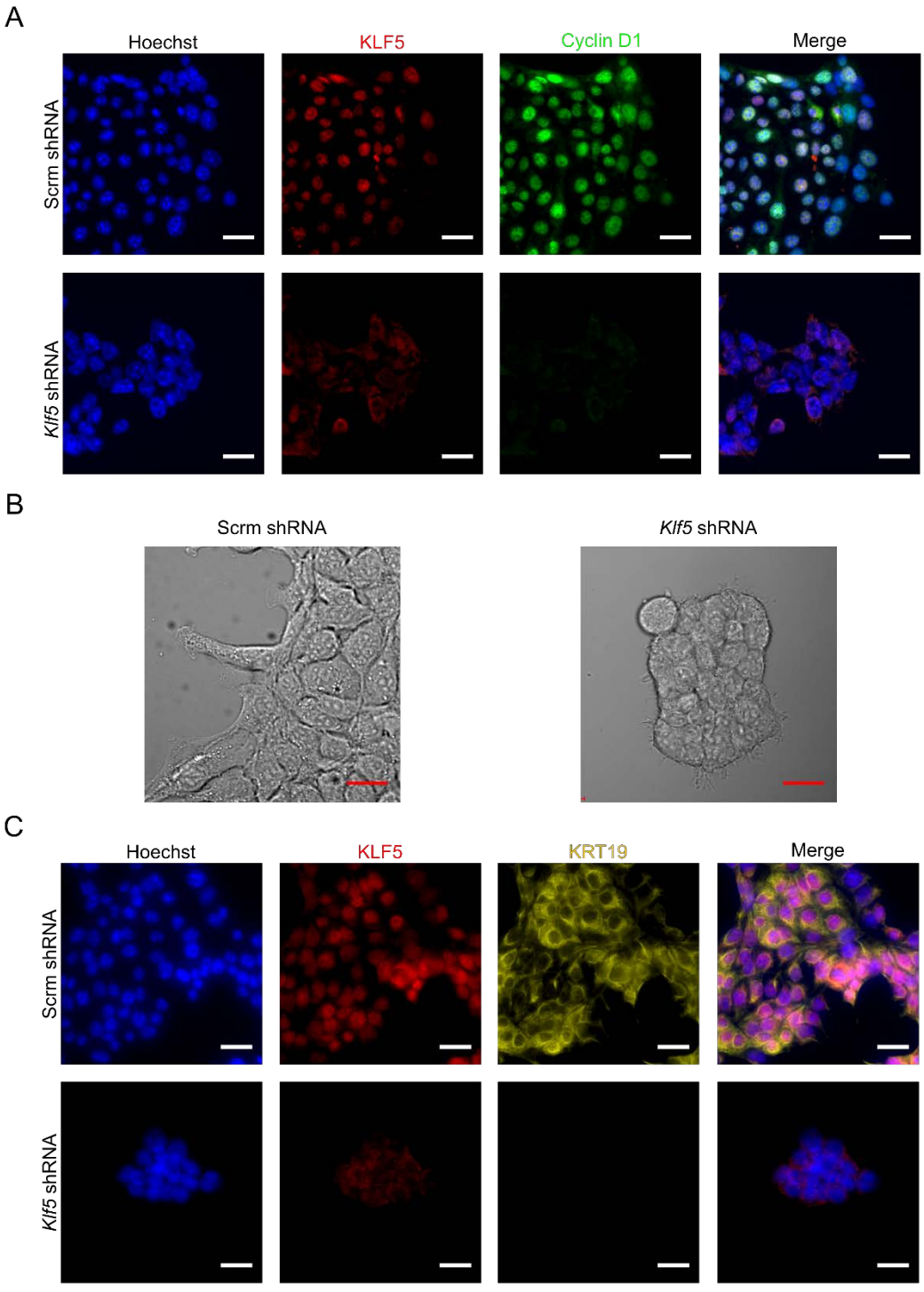

Figure 4.6. Reduction of CCND1 and KRT19 Levels after *Klf5* Knockdown
(A) Multicolor IF staining of KLF5 (red) and CCND1 (green) in *Klf5* shRNA and Scrm shRNA cells. **(B)** Phase-contrast microscopy image of *Klf5* shRNA and Scrm shRNA cells. **(C)** Multicolor IF staining of KLF5 (red) and KRT19 (yellow) in *Klf5* shRNA and Scrm shRNA expressing cells. Scale Bar = 25 µm for **(A)** and **(C)**; Scale Bar = 20 µm for **(B)**.

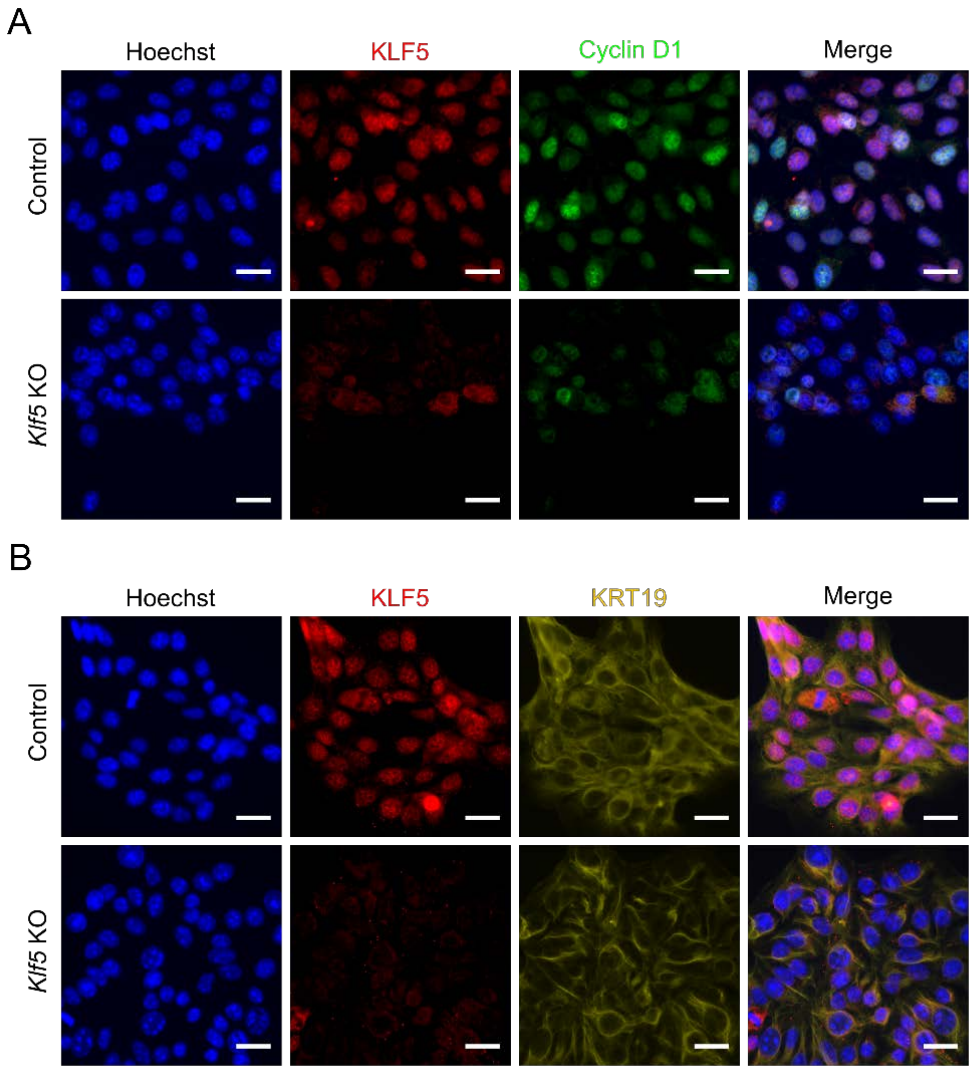

Figure 4.7. Reduction of CCND1 and KRT19 Levels after *Klf5* Knockout
(A) Multicolor IF staining of KLF5 (red) and CCND1 (green) in Control and *Klf5* KO cells. **(B)** Multicolor IF staining of KLF5 (red) and KRT19 (yellow) in Control and *Klf5* KO cells. Scale Bar = 25μm for **(A)** and **(B)**.

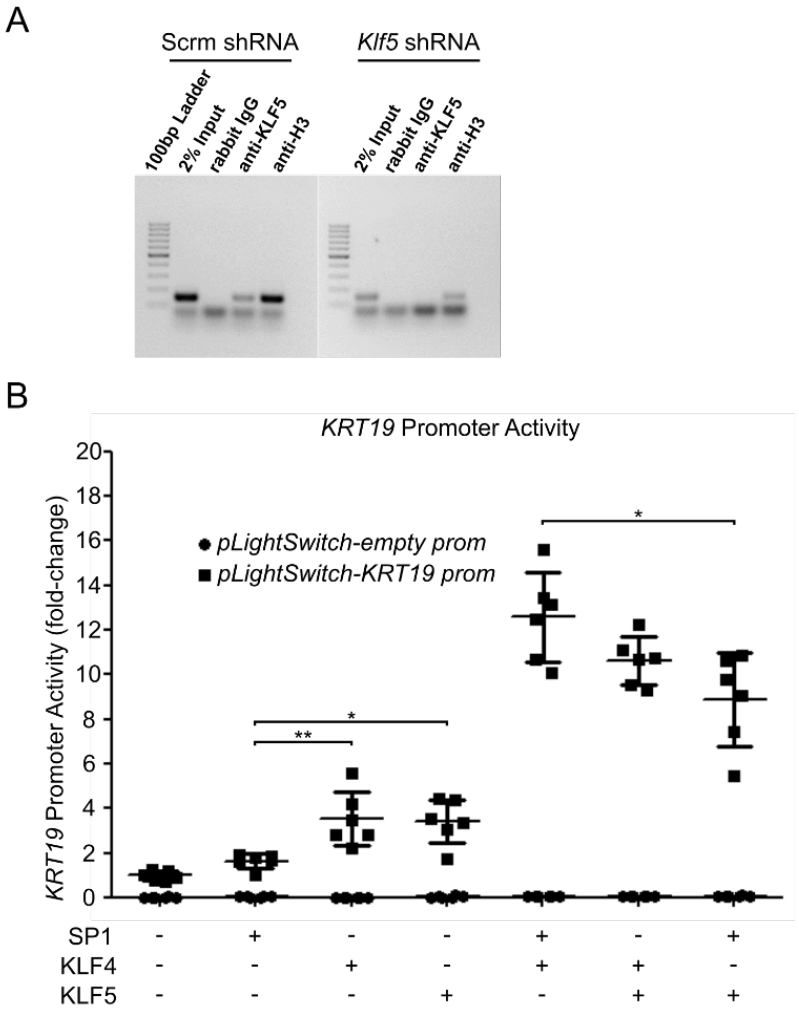

Figure 4.8. Regulation of *KRT19* Expression by KLF5
(A) ChIP-PCR assay showing PCR amplification of DNA product from ChIP by anti-KLF5 antibody in Scrm shRNA and *Klf5* shRNA cells. Rabbit IgG and anti-Histone 3 were used as negative control and positive control, respectively. **(B)** Luciferase promoter activity assay using pLightSwitch construct driven by human *KRT19* promoter in HEK293T cells (n = 6). pLightSwitch construct without promoter were used as experimental negative control. Human SP1, KLF4 and KLF5 were overexpressed in combinations indicated. *$P < 0.05$, ** $P < 0.01$ by two-sided, parametric t-test.

4.6 KLF5 as a Regulator of Pancreatic Cancer Tumorigenesis

To study the effects of *Klf5* depletion on $Kras^{G12D}$-driven tumorigenesis, I subcutaneously implanted *Klf5* shRNA cells and scrambled shRNA cells on two flanks of the same syngeneic immunocompetent mice (n = 16, 8 males and 8 females). All of the mice implanted with cancer cells had subcutaneous tumors on both flanks at 7 days after implantation. Tumors derived from *Klf5* shRNA cells were smaller than the corresponding tumors derived from scrambled shRNA cells before the start of doxycycline treatment (71.61 mm^3 ± 30.79 mm^3 vs. 121.44 mm^3 ± 34.90 mm^3, respectively; Mean ± SD, $P < 0.0001$). At 7 days after implantation, mice were given water containing doxycycline to induce shRNA expression. Tumor growth curve of the 7 day period following doxycycline administration showed that the scrambled shRNA tumors continued to grow while the *Klf5* shRNA tumors shrunk on average of 55% by volume (Figure 4.9A). Statistical analysis of the tumor growth showed that the difference between *Klf5* shRNA tumors and scrambled shRNA control tumors is highly significant ($P < 0.0001$). At 14 days after implantation, there was a substantial reduction in the volumes of *Klf5* shRNA tumors compared with that of their paired scrambled shRNA control tumors (Figure 4.9B; 39.75 mm^3 ± 15.93 mm^3 vs. 143.94 mm^3 ± 46.64 mm^3, respectively; Mean ± SD, $P < 0.0001$). Three out of 16 *Klf5* shRNA tumors had complete regression, but none of the control tumors regressed. H&E staining of the collected tumors showed that scrambled shRNA tumors contained moderately to poorly differentiated adenocarcinoma with tubular morphology and focal necrosis, while the paired *Klf5* shRNA tumors contained minimal amounts of poorly differentiated adenocarcinoma if any tumor tissue is present at all (Figure 4.9C). IHC staining for KLF5 confirmed reduced KLF5 protein levels in *Klf5* shRNA tumors. Staining for vimentin and αSMA, two fibroblast-specific markers, showed minimal fibrosis in scrambled shRNA tumors and increased fibrosis in *Klf5* shRNA tumors (Figure 4.9C

and D). IHC staining for Mac-3, a macrophage-specific marker, revealed focal infiltration of macrophage present in the *Klf5* shRNA tumors but absent in scrambled shRNA control tumors (Figure 4.9C). Staining for CCND1 and KRT19 show significant decrease in CCND1 and KRT19 protein level in *Klf5* shRNA tumors (Figure 4.9D). IF staining for MKI67, a marker for cells not in G0 phase, show no difference in the percentage of MKI67-positive cells between *Klf5* shRNA tumors and scrambled shRNA control tumors (Figure 4.9D).

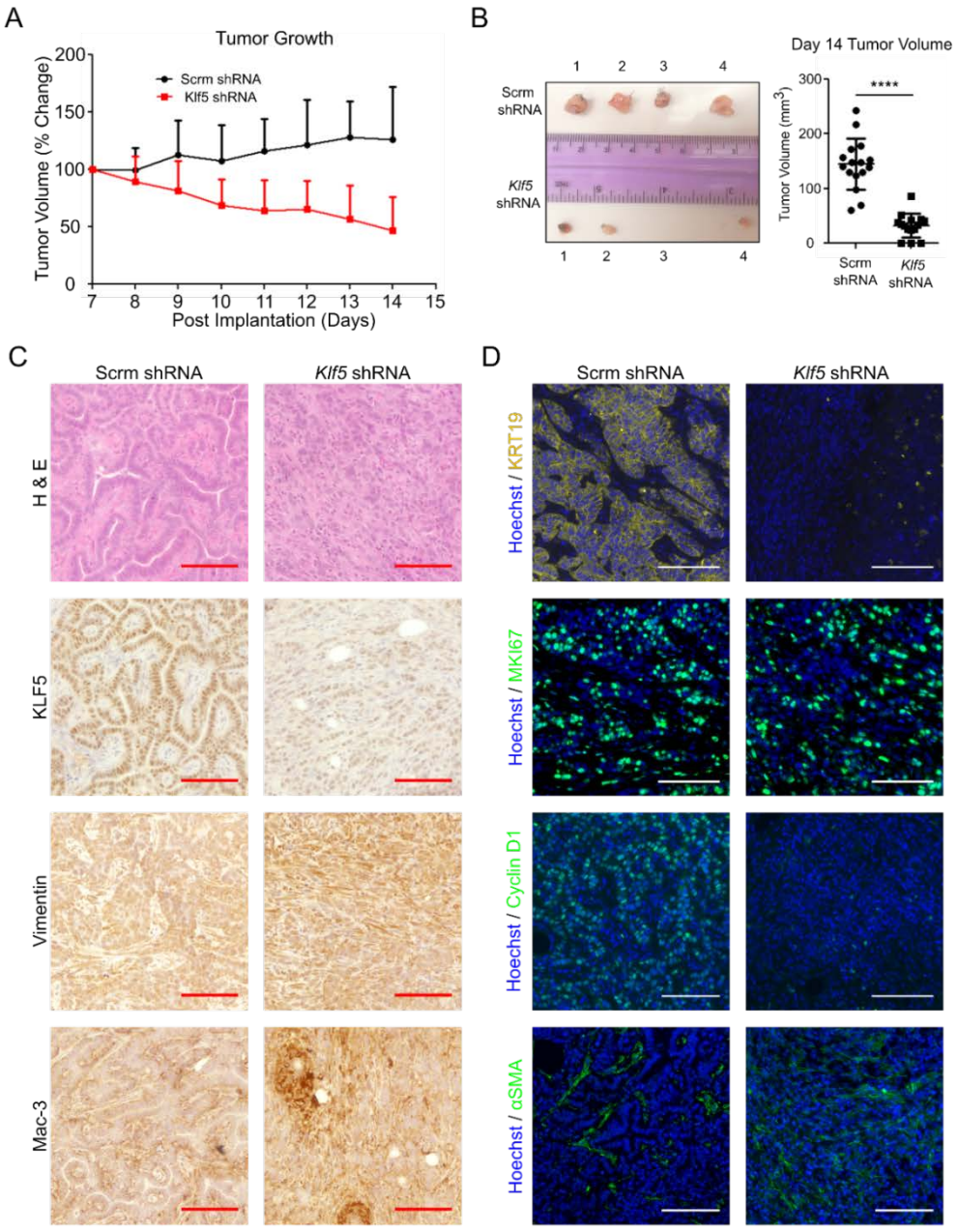

Figure 4.9. Reduction in Tumor Growth after *Klf5* Knockdown

Klf5 shRNA cells were injected s.c. in C57BL/6 mouse and the Scrm shRNA cells were injected s.c. in the opposite flank of the same mouse. Tumors were grown for 7 days, at which point shRNA expression was induced. **(A)** Percent change in tumor volume from 7 days to 14 days after implantation (n = 16, *P < 0.0001* by linear mixed model for longitudinal data). **(B)** Representative photograph of paired Scrm shRNA (top) and *Klf5* shRNA (bottom) tumors collected at 14 days after implantation. Graph represent tumor volume at time of collection. **(C)** H&E staining, IHC staining for KLF5, vimentin, and Mac-3 of paired Scrm shRNA and *Klf5* shRNA tumors. **(D)** IF staining of KRT19, MKI67, Cyclin D1 (CCND1), and αSMA in paired Scrm shRNA and *Klf5* shRNA tumors. Scale Bar = 100μm for **(C)** and **(D)**. Data represent mean ± SD for **(A)** and **(B)**. **** *P < 0.0001* by two-sided, parametric t-test.

4.7 Discussion

The high expression level of KLF5 in human pancreatic cancer cells suggests that it continues to be an important factor during pancreatic cancer progression in addition to its essential role during early pancreatic tumorigenesis. Previous study on KLF5 level in human pancreatic tumors using IHC staining for KLF5 in tissue microarray (TMA) showed that KLF5 level is associated with low-grade PDAC and is almost completely absent in high-grade PDAC (144). Since low-grade pancreatic cancer correlates with better survival outcome (177), the result suggests that patient with KLF5 positive tumors will have better outcome. However, TCGA data on *KLF5* expression and patient survival contradict this hypothesis and shows that higher expression of *KLF5* correlates with worse patient survival (Figure 4.1). This inconsistency could be caused either by the difference in the cohorts that were used or by the lack of validation for the antibody used for TMA study. To address this inconsistency in the existing data, my colleague Jong Won Yang and I conducted an immunohistochemistry staining analysis on human tissue microarrays containing 96 cases of human PDAC using commercially available anti-KLF5 antibody, and the results showed that 73% of the tumors are positive for KLF5 (70/96 cases) (Figure 4.1A). Furthermore, the results did not show significant correlation between tumor grade and KLF5 level, and 76% of high-grade PDAC tumor samples (26/34 cases) express KLF5 (Figure 4.1A).

MEK signaling pathway and PI3K signaling pathway are two critical pathways downstream of oncogenic KRAS signaling that are necessary and sufficient for ADM and PanIN formation (101, 102, 104). Interestingly, both pathways upregulate KLF5 in other pathological and physiological context (138, 157). Here, I demonstrated that pharmacological inhibition of MEK and PI3K kinases in UN-KC-6141 mouse pancreatic cancer cell line reduced KLF5 protein levels

(Figure 4.2). The data suggest that KLF5 is a common signaling target for both pathways in the presence of *Kras*^{G12D} mutation.

To better understand the mechanism of KLF5 in regulating proliferation and ductal phenotype of pancreatic cancer cells demonstrated by previous studies (143, 144), I established a mouse pancreatic cancer cell line with doxycycline-inducible expression of *Klf5*-specific shRNA (Figure 4.3). KLF5 depletion in UN-KC-6141 cells also resulted in decreased cancer cell proliferation (Figure 4.3). Cell cycle analysis showed marked accumulation of S phase cells and G2/M phase cells (Figure 4.3), consistent with previous report of S phase arrest in human colorectal cancer cell lines treated with ML264, a small molecular inhibitor of KLF5 expression (178). *CCND1* is a known gene target of KLF5, and loss of CCND1 protein after KLF5 depletion is commonly associated with arrest at G1/S checkpoint (179). However, prolonged arrest of mammalian cells at G1/S transition can result in permanent S phase stasis (180), and this could explain the increase in S phase cells after *Klf5* knockdown. Furthermore, western blot analysis of levels of different species of cyclins showed changes in cyclin levels that reflected the changes in distributions of cells in the cell cycle phases after *Klf5* knockdown (Figure 4.3B). This result suggests that the changes in cyclin levels were a consequence of cell cycle changes rather than a cause. More detailed analysis using qPCR array for genes involved in cell cycle showed upregulation of several genes involved in DNA damage response (i.e. *Sfn* (181), *Gpr132* (182), *Gadd45a* (183), and *Rb1* (184)). This implicates DNA damage as the cause for the decrease in cell proliferation after *Klf5* knockdown, and this hypothesis can be examined in future studies.

Previous study showed that KLF5 can regulate ductal phenotype of pancreatic cancer cells by regulating expression of a cluster of keratin genes located on human chromosome 17 (144). One of those keratin genes, *KRT19*, codes for keratin-19, which is commonly used as a biomarker

for pancreatic ductal epithelial cells and is upregulated in PDAC (185). Our result corroborated with the previous finding by showing that KRT19 level is decreased after *Klf5* knockdown (Figure 4.6C) and that KLF5 physically interacts with *Krt19* promoter (Figure 4.8A). Interestingly, *KRT19* expression is also regulated by KLF4, another Krüppel-like factor, and SP1 (97). To examine whether KLF5 and KLF4 have redundant function in promoting *KRT19* expression, I performed luciferase promoter activity assay, and the results showed that KLF4 and KLF5 promotes *KRT19* expression in a cooperative manner (Figure 4.8B). The results suggest that KLF4 and KLF5 can compensate for each other in regulation of common gene targets, but they cannot be directly substituted for each other. This cooperative model of regulation of target genes by KLF4 and KLF5 may explain their similarly roles in promoting ADM and PanIN formation and opposite roles during cancer progression.

Klf5 deletion in the UN-KC-6141 by CRISPR/Cas9 method caused moderate decrease in cell proliferation (Figure 4.5C). Cell cycle analysis on *Klf5* KO cells compared to the control cells showed accumulate of S phase cells (Figure 4.5D), but no significant change in the proportion of cells in G2/M phase. *Klf5* deletion decreased the level of CCND1 (Figure 4.7A), but cells still retained KRT19 (Figure 4.7B). The results show that *Klf5* deletion can partially recapitulate the changes in proliferation and ductal phenotype after *Klf5* knockdown. The differences in characteristics of cells after KLF5 is either depleted by RNAi or CRISPR/Cas9 could be caused by nonspecific off target effects of each of these techniques or intrinsic difference between *Klf5* knockdown and *Klf5* knockout. Each of those differences will need to be explored in future studies.

Engraftment of mouse pancreatic cancer cells into wild-type immunocompetent host further supported the *in vitro* finding by demonstrating that *Klf5* inactivation decreases both cellular growth and ductal phenotype *in vivo* (Figure 4.9). Increased infiltration of immune cells

into the tumor after *Klf5* inactivation suggests that tumor regression may be mediated by the immune system (Figure 4.9C), and the role of KLF5 in tumor immune evasion can be explored in future studies. Tumors with *Klf5* inactivation also had increased fibrosis, possibly mediated by changes in the expression of connective tissue growth factors (186).

Chapter 5. Summary and Future Directions

Pancreatic cancer is the fourth leading cause of cancer-related death in United States (187). More than 90% of pancreatic cancer have ductal morphology and is classified as pancreatic ductal adenocarcinoma (PDAC) (188). Pancreatic intraepithelial neoplasia (PanINs) are the most important type of PDAC precursors. Tumorigenesis is believed to be a step-wise progression from low-grade PanINs to high-grade PanINs and then to invasive adenocarcinoma (189). Detailed genomic analysis has produced a corresponding genetic model of tumorigenic progression with activating mutations in Kirsten rat sarcoma viral oncogene homolog (KRAS) as the major initiator followed by loss of function mutations in tumor suppressors (190). Furthermore, oncogenic *Kras* expression specifically targeted to pancreatic progenitor cells is sufficient for the spontaneous formation of PanIN lesions in mouse models (65, 66).

Chronic pancreatitis is a significant risk factor for developing PDAC (163). This relationship is recapitulated in in vivo models in which PanIN formation is accelerated when pancreatitis is induced (66). During pancreatitis, injury leads to partial dedifferentiation of the acinar cells, which acquire ductal epithelial identity. The acquired phenotype is characterized by upregulation of genes associated with embryonic pancreatic progenitor cells (66). This transformation, termed acinar-to-ductal metaplasia (ADM), precedes PanIN formation and PDAC tumorigenesis (66, 164).

Krüppel-like factor 5 (KLF5) is a member of family of transcription factors. KLF5 is highly expressed in many types of cancer (191). Meta-analysis study of microarray data on differential

expression of pancreatic tumor compared to normal tissue show a differential overexpression of KLF5 mRNA in pancreatic cancer (142). Studies using human pancreatic cancer cell lines and mouse models have shown that KLF5 promotes pancreatic cancer cell survival (132, 143) and epithelial phenotype in low-grade PDAC (144). In addition, I have previously shown that KLF5 expression is upregulated by MEK signaling pathway and promotes tumorigenesis in colorectal cancer with mutated KRAS (141). Given the importance of oncogenic KRAS signaling in pancreatic tumorigenesis, I hypothesized that KLF5 may be required for oncogenic KRAS-induced PanIN formation *in vivo*. I generated a mouse model with spatiotemporal control of oncogenic $Kras^{G12D}$ expression and *Klf5* deletion and demonstrated that *Klf5* inactivation reduces ADM and PanIN formation both spontaneously and after pancreatitis. Furthermore, I demonstrated additional role played by KLF5 in cancer cell maintenance by providing evidences showing that *Klf5* depletion in oncogenic *Kras*-expressing mouse pancreatic cancer cell line reduces cell proliferation *in vitro* and causes tumor regression *in vivo*.

RNA sequencing of pancreas from the mouse model identified *Ndrg2* as a direct target gene of KLF5 and a potential suppressor of pancreatitis-induced ADM. Previous studies have shown that STAT3 signaling activation (90, 91) is important for ADM and NDRG2 protein can inhibit STAT3 activation (166, 170). However, the physiological role of NDRG2 in the pancreas has not been studied. In adult mouse, NDRG2 protein is expressed at highly levels in the brain and heart and is expressed at low levels in the pancreas (192). I hypothesized that NDRG2 inhibits ADM through inhibition of STAT3 activation. However, further experiment will be needed to test this hypothesis and show either *Ndrg2* overexpression in mouse pancreas can prevent ADM or *Ndrg2* deletion in mouse pancreas promotes ADM *in vivo*. Alternatively, NDRG2 protein could inhibit ADM through inhibition of NFkB signaling (70, 193). Furthermore, the mechanism by

which KLF5 protein downregulate *Ndrg2* expression need to be explored. KLF5 protein could be recruiting Miz-1 to promote c-Myc mediated repression of *Ndrg2* expression (171, 172), or it could be recruiting HDAC to epigenetically silence *Ndrg2* expression (169, 173). Which mechanism is responsible for KLF5-mediated repression of *Ndrg2* remains to be determined.

In addition to *Ndrg2*, the RNA sequencing data also showed *Rec8* to be a potential target gene of KLF5. REC8 is a protein responsible for the cohesion of sister chromatids during meiosis (194). From the RNA sequencing data, *Rec8* expression is decreased with *Klf5* deletion following acute pancreatitis. What functions a meiosis-specific protein could play in the pancreas remains a mystery. Several studies suggest that REC8 functions as a tumor suppressor and is epigenetically silencing in many types of cancers (195, 196). Potential role of REC8 as a tumor suppressor in pancreatic cancer is further supported by publicly available analysis of TCGA survival data on Human Protein Atlas, which suggests that high REC8 expression is a favorable prognostic factor (175). However, overexpression of REC8 during mitosis causes chromosome missegregation (197). The role of REC8 in pancreatic cancer has not been studied. One hypothesis to explore is whether overexpression of REC8 downstream of oncogenic KRAS signaling in ADM can cause mitotic errors leading to the polyploidization and chromothripsis events (35). If this hypothesis is true, then it will further cement the role of oncogenic KRAS signaling as the initiation event for pancreatic tumorigenesis and will provide us with better understand of the progression process from low grade PanINs to high grade PanINs.

A typical feature of pancreatic cancer is the formation of a dense stroma, a process known as desmoplastic reaction, composed of cellular and fibrillary elements (198). One of the limitations of the RNA sequencing experiments I have performed is that sequencing of total RNA extracted from the whole pancreas do not distinguish the transcriptome of the transforming cells that give

rise to the PanINs and the transcriptome of the stromal cells. To overcome this limitation, single-cell RNA sequencing can be performed on individual acinar cells sorted by the expression of a lineage-tracing fluorescent protein (199). This strategy will provide the cellular resolution required to examine the cell-type specific changes in the transcriptome and address several important questions: what is the fate of the acinar cells after *Klf5* deletion, which transcriptional changes are unique to *Klf5* deletion in the presence of oncogenic KRAS signaling, and why does a subpopulation of acinar cells undergo transformation and give rise to PanINs when all of the acinar cells express oncogenic form of KRAS protein.

The relationship between KLF4, KLF5, and SOX9 in the context of ADM need to be better defined. All three transcription factor have been shown to promote ADM and PanIN formation in genetically engineered mouse models (78, 96). However, in the context of intestinal tissue, KLF5 negatively regulates the expression of *Klf4* and *Sox9* (123, 200). One hypothesis on how the transcription factors are being co-expressed in the cells during ADM and PanIN is that the presence of a fourth unknown factor in pancreatic tissue might be switching KLF5 from a repressor to an activator of *Klf4* and *Sox9* (123, 200). This is supported by the data showing that *Klf5* deletion decreased KLF4 and SOX9 protein levels even when oncogenic $Kras^{G12D}$ is being expressed. Alternatively, KLF4, KLF5 and SOX9 could be acting cooperatively in the transcriptional regulation of the same gene target. This is supported by the study showing that KLF4 and KLF5 can induce *KRT19* expression in a cooperative manner.

Previous studies showed that KLF5 depletion in human pancreatic cancer cell line reduce cancer cell proliferation and tumor growth (143, 144). To understand the underlying mechanisms, I established stable mouse pancreatic cancer cell lines with inducible *Klf5* knockdown through RNAi or with constitutive *Klf5* knockout through CRISPR/Cas9. Depletion of KLF5 protein in

mouse pancreatic cancer cell line showed cell cycle changes characterized by decrease in G0/G1 phase cells and increase in S phase cells. The data suggest that in addition to its role in promoting ADM and PanIN during early pathogenesis, KLF5 plays a separate role in promoting cell cycle progression during pancreatic cancer cell proliferation. The accumulation of cells in S phase could be due to prolonged arrest of mammalian cells at G1/S transition leading to permanent S phase stasis (180). However, analysis of gene expression alterations suggests that DNA damage signaling is activated after KLF5 depletion. Based on these findings, one potential hypothesis is that KLF5 depletion increases DNA damage in cancer cells leading to the activation of DNA damage response pathways and cell cycle arrest. To test this hypothesis, increased DNA damage in cancer cells with KLF5 depletion need to be validated and extended to human pancreatic cancer cell lines. Engraftment of mouse pancreatic cancer cell lines with KLF5 depletion into syngeneic host showed reduced tumor growth with increased immune cell infiltration and fibrosis. These results suggest that KLF5 depletion have effects on the tumor microenvironment in addition to the cell-autonomous effect on proliferation. Further characterization of the fibroblasts and immune cells in the tumor will be required to understand these interactions, since fibroblasts and immune cells can be either positive regulators or negative regulators of tumor progression depending on their differentiation status (64, 201).

The experiments in which KLF5 protein was depleted in mouse pancreatic cancer cell line suggest that KLF5 is critical for maintaining cancer cell proliferation and survival. Hence, pancreatic cancer cells may be “addicted” to high levels of KLF5 protein. To validate this hypothesis, *Klf5* can be deleted in pancreatic cells that have undergone spontaneous malignant transformation using a dual-recombinase mouse model (202). In this model, oncogenic $Kras^{G12D}$ and mutant $Trp53^{R172H}$ can be expressed specifically in the mouse acinar cells through the Flp-

FRT recombination system, and expression of oncogenic KRAS and p53 protein will drive spontaneous oncogenesis in the pancreas of the mouse. After the mouse has developed cancer, *Klf5* deletion can be induced upon tamoxifen injections in the cancer cells through a Cre^{ERT2}-LoxP system. If the pancreatic cancer cells are "addicted" to KLF5, *Klf5* deletion will prevent further progression of cancer and mouse with *Klf5* deletion will have better survival compared to control mouse with intact *Klf5*.

Finally, the most important question to answer is: What is the importance of KLF5 in human disease? From mouse model, we learned that KLF5 promotes ADM and PanIN during early pancreatic tumorigenesis. Based on this, I hypothesize that KLF5 may also promote initiation of human pancreatic cancer. Genome-wide association (GWAS) studies showed that SNPs in intergenic region between *KLF5* and *KLF12* genes are strongly associated with increased risk of pancreatic cancer (145, 203). Recent analysis of TCGA data showed that this region is frequently amplified in multiple types of cancers, and functional analysis of this region showed that it contained super-enhancers that drive *KLF5* expression (146). Molecular analysis of 3 of the strongest individual enhancers (designated e1, e3, and e4 in the research article) in the super-enhancer region showed that these enhancers physically interact with KLF5 protein and deletion of these enhancers reduced *KLF5* promoter activity (146). Using JASPAR online tool, I searched for potential binding site of transcription factors at each of these enhancers (204). Using threshold relative score of 95%, JASPAR identified several potential binding sites for AT-rich interaction domain 3A (ARID3A) in enhancer e1. Analysis of TCGA survival data on Human Protein Atlas showed that ARID3A is a significant favorable prognostic factors for pancreatic cancer (175). Similar methods can be applied to enhancer e3 and e4. JASPAR show e3 and e4 also contained ARID3A binding sites. From these data, I hypothesize that SNPs in super-enhancer region affect

the binding of ARID3A and the expression of KLF5 in the cells. Functional analysis could be done to test this hypothesis, and the role of ARID3A in human PDAC can be explored.

Certain cancer cells, despite of plethora of genomic changes, are dependent on the function of a single oncogene to maintain their malignant phenotype (205). This phenomenon has become the basis of a concept known as "oncogene addiction" (205). The results of my experiments demonstrated that depleting KLF5 in mouse pancreatic cancer cells can reduce cancer cell proliferation and tumor growth. The results suggest that pancreatic cancer cells may be "addicted" to high levels of KLF5 protein. To validate this hypothesis in future experiments, *Klf5* can be deleted in pancreatic cells that have undergone spontaneous malignant transformation using a dual-recombinase mouse model (202). In this model, oncogenic $Kras^{G12D}$ and mutant $Trp53^{R172H}$ can be expressed specifically in the mouse acinar cells through the Flp-FRT recombination system to drive the spontaneous transformation of acinar cells to pancreatic cancer cells. After the mouse has developed pancreatic cancer, *Klf5* deletion can be induced upon tamoxifen injections in the cancer cells through a Cre^{ERT2}-LoxP system. If the pancreatic cancer cells are "addicted" to KLF5, *Klf5* deletion will prevent further progression of cancer and mouse with *Klf5* deletion will have better survival compared to control mouse with intact *Klf5*. KLF5 "addiction" in pancreatic cancer can also provide a strong rationale for development of molecular targeted therapy against KLF5. Previously, our lab demonstrated that ML264, a small molecular drug that inhibit *KLF5* expression, efficiently inhibits growth of the tumor in colorectal cancer xenograft model within 5 days of treatment (150). KLF5 as a novel therapeutic target for pancreatic ductal adenocarcinoma should be further explored.

Bibliography

1. Beger HG. The pancreas : an integrated textbook of basic science, medicine, and surgery. 2nd ed. Malden, Mass. ; Oxford: Blackwell Pub.; 2008. xv, 1006 p. p.

2. Mulley JF, Hargreaves AD, Hegarty MJ, Heller RS, Swain MT. Transcriptomic analysis of the lesser spotted catshark (Scyliorhinus canicula) pancreas, liver and brain reveals molecular level conservation of vertebrate pancreas function. BMC genomics. 2014;15:1074. doi: 10.1186/1471-2164-15-1074. PubMed PMID: 25480530; PubMed Central PMCID: PMC4362833.

3. Leung PS, Ip SP. Pancreatic acinar cell: its role in acute pancreatitis. The international journal of biochemistry & cell biology. 2006;38(7):1024-30. doi: 10.1016/j.biocel.2005.12.001. PubMed PMID: 16423553.

4. Grapin-Botton A. Ductal cells of the pancreas. The international journal of biochemistry & cell biology. 2005;37(3):504-10. doi: 10.1016/j.biocel.2004.07.010. PubMed PMID: 15618005.

5. Jennings RE, Berry AA, Strutt JP, Gerrard DT, Hanley NA. Human pancreas development. Development. 2015;142(18):3126-37. doi: 10.1242/dev.120063. PubMed PMID: 26395141.

6. Gittes GK. Developmental biology of the pancreas: a comprehensive review. Developmental biology. 2009;326(1):4-35. doi: 10.1016/j.ydbio.2008.10.024. PubMed PMID: 19013144.

7. Cano DA, Soria B, Martin F, Rojas A. Transcriptional control of mammalian pancreas organogenesis. Cellular and molecular life sciences : CMLS. 2014;71(13):2383-402. doi: 10.1007/s00018-013-1510-2. PubMed PMID: 24221136.

8. Zorn AM, Wells JM. Vertebrate endoderm development and organ formation. Annual review of cell and developmental biology. 2009;25:221-51. doi: 10.1146/annurev.cellbio.042308.113344. PubMed PMID: 19575677; PubMed Central PMCID: PMC2861293.

9. Offield MF, Jetton TL, Labosky PA, Ray M, Stein RW, Magnuson MA, Hogan BL, Wright CV. PDX-1 is required for pancreatic outgrowth and differentiation of the rostral duodenum. Development. 1996;122(3):983-95. PubMed PMID: 8631275.

10. Jonsson J, Carlsson L, Edlund T, Edlund H. Insulin-promoter-factor 1 is required for pancreas development in mice. Nature. 1994;371(6498):606-9. doi: 10.1038/371606a0. PubMed PMID: 7935793.

11. Svensson P, Williams C, Lundeberg J, Ryden P, Bergqvist I, Edlund H. Gene array identification of Ipf1/Pdx1-/- regulated genes in pancreatic progenitor cells. BMC developmental biology. 2007;7:129. doi: 10.1186/1471-213X-7-129. PubMed PMID: 18036209; PubMed Central PMCID: PMC2212654.

12. Seymour PA, Shih HP, Patel NA, Freude KK, Xie R, Lim CJ, Sander M. A Sox9/Fgf feed-forward loop maintains pancreatic organ identity. Development. 2012;139(18):3363-72. doi: 10.1242/dev.078733. PubMed PMID: 22874919; PubMed Central PMCID: PMC3424044.

13. Oliver-Krasinski JM, Kasner MT, Yang J, Crutchlow MF, Rustgi AK, Kaestner KH, Stoffers DA. The diabetes gene Pdx1 regulates the transcriptional network of pancreatic endocrine progenitor cells in mice. The Journal of clinical investigation. 2009;119(7):1888-98. doi: 10.1172/JCI37028. PubMed PMID: 19487809; PubMed Central PMCID: PMC2701861.

14. Marshak S, Totary H, Cerasi E, Melloul D. Purification of the beta-cell glucose-sensitive factor that transactivates the insulin gene differentially in normal and transformed islet cells. Proceedings of the National Academy of Sciences of the United States of America. 1996;93(26):15057-62. PubMed PMID: 8986763; PubMed Central PMCID: PMC26355.

15. Holland AM, Hale MA, Kagami H, Hammer RE, MacDonald RJ. Experimental control of pancreatic development and maintenance. Proceedings of the National Academy of Sciences of the United States of America. 2002;99(19):12236-41. doi: 10.1073/pnas.192255099. PubMed PMID: 12221286; PubMed Central PMCID: PMC129428.

16. Kawaguchi Y, Cooper B, Gannon M, Ray M, MacDonald RJ, Wright CV. The role of the transcriptional regulator Ptf1a in converting intestinal to pancreatic progenitors. Nature genetics. 2002;32(1):128-34. doi: 10.1038/ng959. PubMed PMID: 12185368.

17. Jacquemin P, Yoshitomi H, Kashima Y, Rousseau GG, Lemaigre FP, Zaret KS. An endothelial-mesenchymal relay pathway regulates early phases of pancreas development. Developmental biology. 2006;290(1):189-99. doi: 10.1016/j.ydbio.2005.11.023. PubMed PMID: 16386727.

18. Beres TM, Masui T, Swift GH, Shi L, Henke RM, MacDonald RJ. PTF1 is an organ-specific and Notch-independent basic helix-loop-helix complex containing the mammalian Suppressor of Hairless (RBP-J) or its paralogue, RBP-L. Molecular and cellular biology. 2006;26(1):117-30. doi: 10.1128/MCB.26.1.117-130.2006. PubMed PMID: 16354684; PubMed Central PMCID: PMC1317634.

19. Masui T, Long Q, Beres TM, Magnuson MA, MacDonald RJ. Early pancreatic development requires the vertebrate Suppressor of Hairless (RBPJ) in the PTF1 bHLH complex. Genes & development. 2007;21(20):2629-43. doi: 10.1101/gad.1575207. PubMed PMID: 17938243; PubMed Central PMCID: PMC2000326.

20. Thompson N, Gesina E, Scheinert P, Bucher P, Grapin-Botton A. RNA profiling and chromatin immunoprecipitation-sequencing reveal that PTF1a stabilizes pancreas progenitor identity via the control of MNX1/HLXB9 and a network of other transcription factors. Molecular and cellular biology. 2012;32(6):1189-99. doi: 10.1128/MCB.06318-11. PubMed PMID: 22232429; PubMed Central PMCID: PMC3295004.

21. Masui T, Swift GH, Hale MA, Meredith DM, Johnson JE, Macdonald RJ. Transcriptional autoregulation controls pancreatic Ptf1a expression during development and adulthood. Molecular and cellular biology. 2008;28(17):5458-68. doi: 10.1128/MCB.00549-08. PubMed PMID: 18606784; PubMed Central PMCID: PMC2519732.

22. Esni F, Ghosh B, Biankin AV, Lin JW, Albert MA, Yu X, MacDonald RJ, Civin CI, Real FX, Pack MA, Ball DW, Leach SD. Notch inhibits Ptf1 function and acinar cell differentiation in developing mouse and zebrafish pancreas. Development. 2004;131(17):4213-24. doi: 10.1242/dev.01280. PubMed PMID: 15280211.

23. Masui T, Swift GH, Deering T, Shen C, Coats WS, Long Q, Elsasser HP, Magnuson MA, MacDonald RJ. Replacement of Rbpj with Rbpjl in the PTF1 complex controls the final maturation of pancreatic acinar cells. Gastroenterology. 2010;139(1):270-80. doi: 10.1053/j.gastro.2010.04.003. PubMed PMID: 20398665; PubMed Central PMCID: PMC2902682.

24. Pan FC, Bankaitis ED, Boyer D, Xu X, Van de Casteele M, Magnuson MA, Heimberg H, Wright CV. Spatiotemporal patterns of multipotentiality in Ptf1a-expressing cells during pancreas organogenesis and injury-induced facultative restoration. Development. 2013;140(4):751-64. doi: 10.1242/dev.090159. PubMed PMID: 23325761; PubMed Central PMCID: PMC3557774.

25. Lynn FC, Smith SB, Wilson ME, Yang KY, Nekrep N, German MS. Sox9 coordinates a transcriptional network in pancreatic progenitor cells. Proceedings of the National Academy of Sciences of the United States of America. 2007;104(25):10500-5. doi: 10.1073/pnas.0704054104. PubMed PMID: 17563382; PubMed Central PMCID: PMC1965542.

26. Murtaugh LC. Pancreas and beta-cell development: from the actual to the possible. Development. 2007;134(3):427-38. doi: 10.1242/dev.02770. PubMed PMID: 17185316.

27. Rahib L, Smith BD, Aizenberg R, Rosenzweig AB, Fleshman JM, Matrisian LM. Projecting cancer incidence and deaths to 2030: the unexpected burden of thyroid, liver, and pancreas cancers in the United States. Cancer research. 2014;74(11):2913-21. doi: 10.1158/0008-5472.CAN-14-0155. PubMed PMID: 24840647.

28. Kleeff J, Korc M, Apte M, La Vecchia C, Johnson CD, Biankin AV, Neale RE, Tempero M, Tuveson DA, Hruban RH, Neoptolemos JP. Pancreatic cancer. Nature reviews Disease primers. 2016;2:16022. doi: 10.1038/nrdp.2016.22. PubMed PMID: 27158978.

29. Kamisawa T, Wood LD, Itoi T, Takaori K. Pancreatic cancer. Lancet. 2016;388(10039):73-85. doi: 10.1016/S0140-6736(16)00141-0. PubMed PMID: 26830752.

30. Iacobuzio-Donahue CA, van der Heijden MS, Baumgartner MR, Troup WJ, Romm JM, Doheny K, Pugh E, Yeo CJ, Goggins MG, Hruban RH, Kern SE. Large-scale allelotype of pancreaticobiliary carcinoma provides quantitative estimates of genome-wide allelic loss. Cancer research. 2004;64(3):871-5. PubMed PMID: 14871814.

31. Kowalski J, Morsberger LA, Blackford A, Hawkins A, Yeo CJ, Hruban RH, Griffin CA. Chromosomal abnormalities of adenocarcinoma of the pancreas: identifying early and late changes. Cancer genetics and cytogenetics. 2007;178(1):26-35. doi: 10.1016/j.cancergencyto.2007.06.004. PubMed PMID: 17889705.

32. Jones S, Zhang X, Parsons DW, Lin JC, Leary RJ, Angenendt P, Mankoo P, Carter H, Kamiyama H, Jimeno A, Hong SM, Fu B, Lin MT, Calhoun ES, Kamiyama M, Walter K, Nikolskaya T, Nikolsky Y, Hartigan J, Smith DR, Hidalgo M, Leach SD, Klein AP, Jaffee EM, Goggins M, Maitra A, Iacobuzio-Donahue C, Eshleman JR, Kern SE, Hruban RH, Karchin R, Papadopoulos N, Parmigiani G, Vogelstein B, Velculescu VE, Kinzler KW. Core signaling pathways in human pancreatic cancers revealed by global genomic analyses. Science. 2008;321(5897):1801-6. doi: 10.1126/science.1164368. PubMed PMID: 18772397; PubMed Central PMCID: PMC2848990.

33. Biankin AV, Waddell N, Kassahn KS, Gingras MC, Muthuswamy LB, Johns AL, Miller DK, Wilson PJ, Patch AM, Wu J, Chang DK, Cowley MJ, Gardiner BB, Song S, Harliwong I, Idrisoglu S, Nourse C, Nourbakhsh E, Manning S, Wani S, Gongora M, Pajic M, Scarlett CJ, Gill AJ, Pinho AV, Rooman I, Anderson M, Holmes O, Leonard C, Taylor D, Wood S, Xu Q, Nones K, Fink JL, Christ A, Bruxner T, Cloonan N, Kolle G, Newell F, Pinese M, Mead RS, Humphris JL, Kaplan W, Jones MD, Colvin EK, Nagrial AM, Humphrey ES, Chou A, Chin VT, Chantrill LA, Mawson A, Samra JS, Kench JG, Lovell JA, Daly RJ, Merrett ND, Toon C, Epari K, Nguyen NQ, Barbour A, Zeps N, Australian Pancreatic Cancer Genome I, Kakkar N, Zhao F, Wu YQ, Wang M, Muzny DM, Fisher WE, Brunicardi FC, Hodges SE, Reid JG, Drummond J, Chang K, Han Y, Lewis LR, Dinh H, Buhay CJ, Beck T, Timms L, Sam M, Begley K, Brown A, Pai D, Panchal A, Buchner N, De Borja R, Denroche RE, Yung CK, Serra S, Onetto N, Mukhopadhyay D, Tsao MS, Shaw PA, Petersen GM, Gallinger S, Hruban RH, Maitra A, Iacobuzio-Donahue CA, Schulick RD, Wolfgang CL, Morgan RA, Lawlor RT, Capelli P, Corbo V, Scardoni M, Tortora G, Tempero MA, Mann KM, Jenkins NA, Perez-Mancera PA, Adams DJ, Largaespada DA, Wessels LF, Rust AG, Stein LD, Tuveson DA, Copeland NG, Musgrove EA, Scarpa A, Eshleman JR, Hudson TJ, Sutherland RL, Wheeler DA, Pearson JV, McPherson JD, Gibbs RA, Grimmond SM. Pancreatic cancer genomes reveal aberrations in axon guidance pathway genes. Nature. 2012;491(7424):399-405. doi: 10.1038/nature11547. PubMed PMID: 23103869; PubMed Central PMCID: PMC3530898.

34. Yachida S, Jones S, Bozic I, Antal T, Leary R, Fu B, Kamiyama M, Hruban RH, Eshleman JR, Nowak MA, Velculescu VE, Kinzler KW, Vogelstein B, Iacobuzio-Donahue CA. Distant metastasis occurs late during the genetic evolution of pancreatic cancer. Nature. 2010;467(7319):1114-7. doi: 10.1038/nature09515. PubMed PMID: 20981102; PubMed Central PMCID: PMC3148940.

35. Notta F, Chan-Seng-Yue M, Lemire M, Li Y, Wilson GW, Connor AA, Denroche RE, Liang SB, Brown AM, Kim JC, Wang T, Simpson JT, Beck T, Borgida A, Buchner N, Chadwick

D, Hafezi-Bakhtiari S, Dick JE, Heisler L, Hollingsworth MA, Ibrahimov E, Jang GH, Johns J, Jorgensen LG, Law C, Ludkovski O, Lungu I, Ng K, Pasternack D, Petersen GM, Shlush LI, Timms L, Tsao MS, Wilson JM, Yung CK, Zogopoulos G, Bartlett JM, Alexandrov LB, Real FX, Cleary SP, Roehrl MH, McPherson JD, Stein LD, Hudson TJ, Campbell PJ, Gallinger S. A renewed model of pancreatic cancer evolution based on genomic rearrangement patterns. Nature. 2016;538(7625):378-82. doi: 10.1038/nature19823. PubMed PMID: 27732578; PubMed Central PMCID: PMC5446075.

36. Yachida S, White CM, Naito Y, Zhong Y, Brosnan JA, Macgregor-Das AM, Morgan RA, Saunders T, Laheru DA, Herman JM, Hruban RH, Klein AP, Jones S, Velculescu V, Wolfgang CL, Iacobuzio-Donahue CA. Clinical significance of the genetic landscape of pancreatic cancer and implications for identification of potential long-term survivors. Clinical cancer research : an official journal of the American Association for Cancer Research. 2012;18(22):6339-47. doi: 10.1158/1078-0432.CCR-12-1215. PubMed PMID: 22991414; PubMed Central PMCID: PMC3500447.

37. Oshima M, Okano K, Muraki S, Haba R, Maeba T, Suzuki Y, Yachida S. Immunohistochemically detected expression of 3 major genes (CDKN2A/p16, TP53, and SMAD4/DPC4) strongly predicts survival in patients with resectable pancreatic cancer. Annals of surgery. 2013;258(2):336-46. doi: 10.1097/SLA.0b013e3182827a65. PubMed PMID: 23470568.

38. Hruban RH, Goggins M, Parsons J, Kern SE. Progression model for pancreatic cancer. Clinical cancer research : an official journal of the American Association for Cancer Research. 2000;6(8):2969-72. PubMed PMID: 10955772.

39. Matthaei H, Schulick RD, Hruban RH, Maitra A. Cystic precursors to invasive pancreatic cancer. Nature reviews Gastroenterology & hepatology. 2011;8(3):141-50. doi: 10.1038/nrgastro.2011.2. PubMed PMID: 21383670; PubMed Central PMCID: PMC3236705.

40. Hruban RH, Wilentz RE, Kern SE. Genetic progression in the pancreatic ducts. The American journal of pathology. 2000;156(6):1821-5. doi: 10.1016/S0002-9440(10)65054-7. PubMed PMID: 10854204; PubMed Central PMCID: PMC1850064.

41. Hruban RH, Wilentz RE, Maitra A. Identification and analysis of precursors to invasive pancreatic cancer. Methods in molecular medicine. 2005;103:1-13. PubMed PMID: 15542896.

42. Hruban RH, Maitra A, Kern SE, Goggins M. Precursors to pancreatic cancer. Gastroenterology clinics of North America. 2007;36(4):831-49, vi. doi: 10.1016/j.gtc.2007.08.012. PubMed PMID: 17996793; PubMed Central PMCID: PMC2194627.

43. Hruban RH, Takaori K, Klimstra DS, Adsay NV, Albores-Saavedra J, Biankin AV, Biankin SA, Compton C, Fukushima N, Furukawa T, Goggins M, Kato Y, Kloppel G, Longnecker DS, Luttges J, Maitra A, Offerhaus GJ, Shimizu M, Yonezawa S. An illustrated consensus on the classification of pancreatic intraepithelial neoplasia and intraductal papillary mucinous neoplasms. The American journal of surgical pathology. 2004;28(8):977-87. PubMed PMID: 15252303.

44. Konstantinidis IT, Vinuela EF, Tang LH, Klimstra DS, D'Angelica MI, Dematteo RP, Kingham TP, Fong Y, Jarnagin WR, Allen PJ. Incidentally discovered pancreatic intraepithelial neoplasia: what is its clinical significance? Annals of surgical oncology. 2013;20(11):3643-7. doi: 10.1245/s10434-013-3042-2. PubMed PMID: 23748606.

45. van Heek NT, Meeker AK, Kern SE, Yeo CJ, Lillemoe KD, Cameron JL, Offerhaus GJ, Hicks JL, Wilentz RE, Goggins MG, De Marzo AM, Hruban RH, Maitra A. Telomere shortening is nearly universal in pancreatic intraepithelial neoplasia. The American journal of pathology. 2002;161(5):1541-7. doi: 10.1016/S0002-9440(10)64432-X. PubMed PMID: 12414502; PubMed Central PMCID: PMC1850788.

46. Kanda M, Matthaei H, Wu J, Hong SM, Yu J, Borges M, Hruban RH, Maitra A, Kinzler K, Vogelstein B, Goggins M. Presence of somatic mutations in most early-stage pancreatic intraepithelial neoplasia. Gastroenterology. 2012;142(4):730-3 e9. doi: 10.1053/j.gastro.2011.12.042. PubMed PMID: 22226782; PubMed Central PMCID: PMC3321090.

47. Lohr M, Kloppel G, Maisonneuve P, Lowenfels AB, Luttges J. Frequency of K-ras mutations in pancreatic intraductal neoplasias associated with pancreatic ductal adenocarcinoma and chronic pancreatitis: a meta-analysis. Neoplasia. 2005;7(1):17-23. doi: 10.1593/neo.04445. PubMed PMID: 15720814; PubMed Central PMCID: PMC1490318.

48. Wilentz RE, Geradts J, Maynard R, Offerhaus GJ, Kang M, Goggins M, Yeo CJ, Kern SE, Hruban RH. Inactivation of the p16 (INK4A) tumor-suppressor gene in pancreatic duct lesions: loss of intranuclear expression. Cancer research. 1998;58(20):4740-4. PubMed PMID: 9788631.

49. Schutte M, Hruban RH, Geradts J, Maynard R, Hilgers W, Rabindran SK, Moskaluk CA, Hahn SA, Schwarte-Waldhoff I, Schmiegel W, Baylin SB, Kern SE, Herman JG. Abrogation of the Rb/p16 tumor-suppressive pathway in virtually all pancreatic carcinomas. Cancer research. 1997;57(15):3126-30. PubMed PMID: 9242437.

50. Wilentz RE, Iacobuzio-Donahue CA, Argani P, McCarthy DM, Parsons JL, Yeo CJ, Kern SE, Hruban RH. Loss of expression of Dpc4 in pancreatic intraepithelial neoplasia: evidence that DPC4 inactivation occurs late in neoplastic progression. Cancer research. 2000;60(7):2002-6. PubMed PMID: 10766191.

51. Luttges J, Galehdari H, Brocker V, Schwarte-Waldhoff I, Henne-Bruns D, Kloppel G, Schmiegel W, Hahn SA. Allelic loss is often the first hit in the biallelic inactivation of the p53 and DPC4 genes during pancreatic carcinogenesis. The American journal of pathology. 2001;158(5):1677-83. doi: 10.1016/S0002-9440(10)64123-5. PubMed PMID: 11337365; PubMed Central PMCID: PMC1891939.

52. Murphy SJ, Hart SN, Lima JF, Kipp BR, Klebig M, Winters JL, Szabo C, Zhang L, Eckloff BW, Petersen GM, Scherer SE, Gibbs RA, McWilliams RR, Vasmatzis G, Couch FJ. Genetic alterations associated with progression from pancreatic intraepithelial neoplasia to invasive pancreatic tumor. Gastroenterology. 2013;145(5):1098-109 e1. doi:

10.1053/j.gastro.2013.07.049. PubMed PMID: 23912084; PubMed Central PMCID: PMC3926442.

53. Matthaei H, Hong SM, Mayo SC, dal Molin M, Olino K, Venkat R, Goggins M, Herman JM, Edil BH, Wolfgang CL, Cameron JL, Schulick RD, Maitra A, Hruban RH. Presence of pancreatic intraepithelial neoplasia in the pancreatic transection margin does not influence outcome in patients with R0 resected pancreatic cancer. Annals of surgical oncology. 2011;18(12):3493-9. doi: 10.1245/s10434-011-1745-9. PubMed PMID: 21537863; PubMed Central PMCID: PMC3166423.

54. Brugge WR, Lauwers GY, Sahani D, Fernandez-del Castillo C, Warshaw AL. Cystic neoplasms of the pancreas. The New England journal of medicine. 2004;351(12):1218-26. doi: 10.1056/NEJMra031623. PubMed PMID: 15371579.

55. Furukawa T, Kloppel G, Volkan Adsay N, Albores-Saavedra J, Fukushima N, Horii A, Hruban RH, Kato Y, Klimstra DS, Longnecker DS, Luttges J, Offerhaus GJ, Shimizu M, Sunamura M, Suriawinata A, Takaori K, Yonezawa S. Classification of types of intraductal papillary-mucinous neoplasm of the pancreas: a consensus study. Virchows Archiv : an international journal of pathology. 2005;447(5):794-9. doi: 10.1007/s00428-005-0039-7. PubMed PMID: 16088402.

56. Adsay NV, Merati K, Basturk O, Iacobuzio-Donahue C, Levi E, Cheng JD, Sarkar FH, Hruban RH, Klimstra DS. Pathologically and biologically distinct types of epithelium in intraductal papillary mucinous neoplasms: delineation of an "intestinal" pathway of carcinogenesis in the pancreas. The American journal of surgical pathology. 2004;28(7):839-48. PubMed PMID: 15223952.

57. Wu J, Jiao Y, Dal Molin M, Maitra A, de Wilde RF, Wood LD, Eshleman JR, Goggins MG, Wolfgang CL, Canto MI, Schulick RD, Edil BH, Choti MA, Adsay V, Klimstra DS, Offerhaus GJ, Klein AP, Kopelovich L, Carter H, Karchin R, Allen PJ, Schmidt CM, Naito Y, Diaz LA, Jr., Kinzler KW, Papadopoulos N, Hruban RH, Vogelstein B. Whole-exome sequencing of neoplastic cysts of the pancreas reveals recurrent mutations in components of ubiquitin-dependent pathways. Proceedings of the National Academy of Sciences of the United States of America. 2011;108(52):21188-93. doi: 10.1073/pnas.1118046108. PubMed PMID: 22158988; PubMed Central PMCID: PMC3248495.

58. Wu J, Matthaei H, Maitra A, Dal Molin M, Wood LD, Eshleman JR, Goggins M, Canto MI, Schulick RD, Edil BH, Wolfgang CL, Klein AP, Diaz LA, Jr., Allen PJ, Schmidt CM, Kinzler KW, Papadopoulos N, Hruban RH, Vogelstein B. Recurrent GNAS mutations define an unexpected pathway for pancreatic cyst development. Science translational medicine. 2011;3(92):92ra66. doi: 10.1126/scitranslmed.3002543. PubMed PMID: 21775669; PubMed Central PMCID: PMC3160649.

59. Amato E, Molin MD, Mafficini A, Yu J, Malleo G, Rusev B, Fassan M, Antonello D, Sadakari Y, Castelli P, Zamboni G, Maitra A, Salvia R, Hruban RH, Bassi C, Capelli P, Lawlor RT, Goggins M, Scarpa A. Targeted next-generation sequencing of cancer genes dissects the molecular profiles of intraductal papillary neoplasms of the pancreas. The Journal of pathology.

2014;233(3):217-27. doi: 10.1002/path.4344. PubMed PMID: 24604757; PubMed Central PMCID: PMC4057302.

60. Hosoda W, Chianchiano P, Griffin JF, Pittman ME, Brosens LA, Noe M, Yu J, Shindo K, Suenaga M, Rezaee N, Yonescu R, Ning Y, Albores-Saavedra J, Yoshizawa N, Harada K, Yoshizawa A, Hanada K, Yonehara S, Shimizu M, Uehara T, Samra JS, Gill AJ, Wolfgang CL, Goggins MG, Hruban RH, Wood LD. Genetic analyses of isolated high-grade pancreatic intraepithelial neoplasia (HG-PanIN) reveal paucity of alterations in TP53 and SMAD4. The Journal of pathology. 2017;242(1):16-23. doi: 10.1002/path.4884. PubMed PMID: 28188630; PubMed Central PMCID: PMC5553451.

61. Bailey P, Chang DK, Nones K, Johns AL, Patch AM, Gingras MC, Miller DK, Christ AN, Bruxner TJ, Quinn MC, Nourse C, Murtaugh LC, Harliwong I, Idrisoglu S, Manning S, Nourbakhsh E, Wani S, Fink L, Holmes O, Chin V, Anderson MJ, Kazakoff S, Leonard C, Newell F, Waddell N, Wood S, Xu Q, Wilson PJ, Cloonan N, Kassahn KS, Taylor D, Quek K, Robertson A, Pantano L, Mincarelli L, Sanchez LN, Evers L, Wu J, Pinese M, Cowley MJ, Jones MD, Colvin EK, Nagrial AM, Humphrey ES, Chantrill LA, Mawson A, Humphris J, Chou A, Pajic M, Scarlett CJ, Pinho AV, Giry-Laterriere M, Rooman I, Samra JS, Kench JG, Lovell JA, Merrett ND, Toon CW, Epari K, Nguyen NQ, Barbour A, Zeps N, Moran-Jones K, Jamieson NB, Graham JS, Duthie F, Oien K, Hair J, Grutzmann R, Maitra A, Iacobuzio-Donahue CA, Wolfgang CL, Morgan RA, Lawlor RT, Corbo V, Bassi C, Rusev B, Capelli P, Salvia R, Tortora G, Mukhopadhyay D, Petersen GM, Australian Pancreatic Cancer Genome I, Munzy DM, Fisher WE, Karim SA, Eshleman JR, Hruban RH, Pilarsky C, Morton JP, Sansom OJ, Scarpa A, Musgrove EA, Bailey UM, Hofmann O, Sutherland RL, Wheeler DA, Gill AJ, Gibbs RA, Pearson JV, Waddell N, Biankin AV, Grimmond SM. Genomic analyses identify molecular subtypes of pancreatic cancer. Nature. 2016;531(7592):47-52. doi: 10.1038/nature16965. PubMed PMID: 26909576.

62. Springer S, Wang Y, Dal Molin M, Masica DL, Jiao Y, Kinde I, Blackford A, Raman SP, Wolfgang CL, Tomita T, Niknafs N, Douville C, Ptak J, Dobbyn L, Allen PJ, Klimstra DS, Schattner MA, Schmidt CM, Yip-Schneider M, Cummings OW, Brand RE, Zeh HJ, Singhi AD, Scarpa A, Salvia R, Malleo G, Zamboni G, Falconi M, Jang JY, Kim SW, Kwon W, Hong SM, Song KB, Kim SC, Swan N, Murphy J, Geoghegan J, Brugge W, Fernandez-Del Castillo C, Mino-Kenudson M, Schulick R, Edil BH, Adsay V, Paulino J, van Hooft J, Yachida S, Nara S, Hiraoka N, Yamao K, Hijioka S, van der Merwe S, Goggins M, Canto MI, Ahuja N, Hirose K, Makary M, Weiss MJ, Cameron J, Pittman M, Eshleman JR, Diaz LA, Jr., Papadopoulos N, Kinzler KW, Karchin R, Hruban RH, Vogelstein B, Lennon AM. A combination of molecular markers and clinical features improve the classification of pancreatic cysts. Gastroenterology. 2015;149(6):1501-10. doi: 10.1053/j.gastro.2015.07.041. PubMed PMID: 26253305; PubMed Central PMCID: PMC4782782.

63. Fukushima N, Zamboni G. Mucinous cystic neoplasms of the pancreas: update on the surgical pathology and molecular genetics. Seminars in diagnostic pathology. 2014;31(6):467-74. doi: 10.1053/j.semdp.2014.08.007. PubMed PMID: 25441310.

64. Kalluri R. The biology and function of fibroblasts in cancer. Nature reviews Cancer. 2016;16(9):582-98. doi: 10.1038/nrc.2016.73. PubMed PMID: 27550820.

65. Hingorani SR, Petricoin EF, Maitra A, Rajapakse V, King C, Jacobetz MA, Ross S, Conrads TP, Veenstra TD, Hitt BA, Kawaguchi Y, Johann D, Liotta LA, Crawford HC, Putt ME, Jacks T, Wright CV, Hruban RH, Lowy AM, Tuveson DA. Preinvasive and invasive ductal pancreatic cancer and its early detection in the mouse. Cancer cell. 2003;4(6):437-50. PubMed PMID: 14706336.

66. Guerra C, Schuhmacher AJ, Canamero M, Grippo PJ, Verdaguer L, Perez-Gallego L, Dubus P, Sandgren EP, Barbacid M. Chronic pancreatitis is essential for induction of pancreatic ductal adenocarcinoma by K-Ras oncogenes in adult mice. Cancer Cell. 2007;11(3):291-302. doi: 10.1016/j.ccr.2007.01.012. PubMed PMID: 17349585.

67. Malka D, Hammel P, Maire F, Rufat P, Madeira I, Pessione F, Levy P, Ruszniewski P. Risk of pancreatic adenocarcinoma in chronic pancreatitis. Gut. 2002;51(6):849-52. PubMed PMID: 12427788; PubMed Central PMCID: PMC1773474.

68. Habbe N, Shi G, Meguid RA, Fendrich V, Esni F, Chen H, Feldmann G, Stoffers DA, Konieczny SF, Leach SD, Maitra A. Spontaneous induction of murine pancreatic intraepithelial neoplasia (mPanIN) by acinar cell targeting of oncogenic Kras in adult mice. Proceedings of the National Academy of Sciences of the United States of America. 2008;105(48):18913-8. doi: 10.1073/pnas.0810097105. PubMed PMID: 19028870; PubMed Central PMCID: PMC2596215.

69. Bardeesy N, Sharpless NE. RAS unplugged: negative feedback and oncogene-induced senescence. Cancer cell. 2006;10(6):451-3. doi: 10.1016/j.ccr.2006.11.015. PubMed PMID: 17157783.

70. Liou GY, Doppler H, Necela B, Krishna M, Crawford HC, Raimondo M, Storz P. Macrophage-secreted cytokines drive pancreatic acinar-to-ductal metaplasia through NF-kappaB and MMPs. The Journal of cell biology. 2013;202(3):563-77. doi: 10.1083/jcb.201301001. PubMed PMID: 23918941; PubMed Central PMCID: PMC3734091.

71. Houbracken I, de Waele E, Lardon J, Ling Z, Heimberg H, Rooman I, Bouwens L. Lineage tracing evidence for transdifferentiation of acinar to duct cells and plasticity of human pancreas. Gastroenterology. 2011;141(2):731-41, 41 e1-4. doi: 10.1053/j.gastro.2011.04.050. PubMed PMID: 21703267.

72. Liou GY, Doppler H, DelGiorno KE, Zhang L, Leitges M, Crawford HC, Murphy MP, Storz P. Mutant KRas-Induced Mitochondrial Oxidative Stress in Acinar Cells Upregulates EGFR Signaling to Drive Formation of Pancreatic Precancerous Lesions. Cell reports. 2016;14(10):2325-36. doi: 10.1016/j.celrep.2016.02.029. PubMed PMID: 26947075; PubMed Central PMCID: PMC4794374.

73. Liou GY, Doppler H, Braun UB, Panayiotou R, Scotti Buzhardt M, Radisky DC, Crawford HC, Fields AP, Murray NR, Wang QJ, Leitges M, Storz P. Protein kinase D1 drives pancreatic acinar cell reprogramming and progression to intraepithelial neoplasia. Nature communications. 2015;6:6200. doi: 10.1038/ncomms7200. PubMed PMID: 25698580; PubMed Central PMCID: PMC4394184.

74. Means AL, Meszoely IM, Suzuki K, Miyamoto Y, Rustgi AK, Coffey RJ, Jr., Wright CV, Stoffers DA, Leach SD. Pancreatic epithelial plasticity mediated by acinar cell transdifferentiation and generation of nestin-positive intermediates. Development. 2005;132(16):3767-76. doi: 10.1242/dev.01925. PubMed PMID: 16020518.

75. Shi G, DiRenzo D, Qu C, Barney D, Miley D, Konieczny SF. Maintenance of acinar cell organization is critical to preventing Kras-induced acinar-ductal metaplasia. Oncogene. 2013;32(15):1950-8. doi: 10.1038/onc.2012.210. PubMed PMID: 22665051; PubMed Central PMCID: PMC3435479.

76. Reichert M, Rustgi AK. Pancreatic ductal cells in development, regeneration, and neoplasia. The Journal of clinical investigation. 2011;121(12):4572-8. doi: 10.1172/JCI57131. PubMed PMID: 22133881; PubMed Central PMCID: PMC3225990.

77. Liu J, Akanuma N, Liu C, Naji A, Halff GA, Washburn WK, Sun L, Wang P. TGF-beta1 promotes acinar to ductal metaplasia of human pancreatic acinar cells. Scientific reports. 2016;6:30904. doi: 10.1038/srep30904. PubMed PMID: 27485764; PubMed Central PMCID: PMC4971483.

78. Kopp JL, von Figura G, Mayes E, Liu FF, Dubois CL, Morris JPt, Pan FC, Akiyama H, Wright CV, Jensen K, Hebrok M, Sander M. Identification of Sox9-dependent acinar-to-ductal reprogramming as the principal mechanism for initiation of pancreatic ductal adenocarcinoma. Cancer cell. 2012;22(6):737-50. doi: 10.1016/j.ccr.2012.10.025. PubMed PMID: 23201164; PubMed Central PMCID: PMC3568632.

79. Benitz S, Regel I, Reinhard T, Popp A, Schaffer I, Raulefs S, Kong B, Esposito I, Michalski CW, Kleeff J. Polycomb repressor complex 1 promotes gene silencing through H2AK119 mono-ubiquitination in acinar-to-ductal metaplasia and pancreatic cancer cells. Oncotarget. 2016;7(10):11424-33. doi: 10.18632/oncotarget.6717. PubMed PMID: 26716510; PubMed Central PMCID: PMC4905483.

80. Krah NM, De La OJ, Swift GH, Hoang CQ, Willet SG, Chen Pan F, Cash GM, Bronner MP, Wright CV, MacDonald RJ, Murtaugh LC. The acinar differentiation determinant PTF1A inhibits initiation of pancreatic ductal adenocarcinoma. eLife. 2015;4. doi: 10.7554/eLife.07125. PubMed PMID: 26151762; PubMed Central PMCID: PMC4536747.

81. Kopp JL, Dubois CL, Schaffer AE, Hao E, Shih HP, Seymour PA, Ma J, Sander M. Sox9+ ductal cells are multipotent progenitors throughout development but do not produce new endocrine cells in the normal or injured adult pancreas. Development. 2011;138(4):653-65. doi: 10.1242/dev.056499. PubMed PMID: 21266405; PubMed Central PMCID: PMC3026412.

82. Furuyama K, Kawaguchi Y, Akiyama H, Horiguchi M, Kodama S, Kuhara T, Hosokawa S, Elbahrawy A, Soeda T, Koizumi M, Masui T, Kawaguchi M, Takaori K, Doi R, Nishi E, Kakinoki R, Deng JM, Behringer RR, Nakamura T, Uemoto S. Continuous cell supply from a Sox9-expressing progenitor zone in adult liver, exocrine pancreas and intestine. Nature genetics. 2011;43(1):34-41. doi: 10.1038/ng.722. PubMed PMID: 21113154.

83. Prevot PP, Simion A, Grimont A, Colletti M, Khalaileh A, Van den Steen G, Sempoux C, Xu X, Roelants V, Hald J, Bertrand L, Heimberg H, Konieczny SF, Dor Y, Lemaigre FP, Jacquemin P. Role of the ductal transcription factors HNF6 and Sox9 in pancreatic acinar-to-ductal metaplasia. Gut. 2012;61(12):1723-32. doi: 10.1136/gutjnl-2011-300266. PubMed PMID: 22271799; PubMed Central PMCID: PMC3898034.

84. Shroff S, Rashid A, Wang H, Katz MH, Abbruzzese JL, Fleming JB, Wang H. SOX9: a useful marker for pancreatic ductal lineage of pancreatic neoplasms. Human pathology. 2014;45(3):456-63. doi: 10.1016/j.humpath.2013.10.008. PubMed PMID: 24418153; PubMed Central PMCID: PMC3945019.

85. Grimont A, Pinho AV, Cowley MJ, Augereau C, Mawson A, Giry-Laterriere M, Van den Steen G, Waddell N, Pajic M, Sempoux C, Wu J, Grimmond SM, Biankin AV, Lemaigre FP, Rooman I, Jacquemin P. SOX9 regulates ERBB signalling in pancreatic cancer development. Gut. 2015;64(11):1790-9. doi: 10.1136/gutjnl-2014-307075. PubMed PMID: 25336113.

86. Park JY, Hong SM, Klimstra DS, Goggins MG, Maitra A, Hruban RH. Pdx1 expression in pancreatic precursor lesions and neoplasms. Applied immunohistochemistry & molecular morphology : AIMM. 2011;19(5):444-9. doi: 10.1097/PAI.0b013e318206d958. PubMed PMID: 21297446; PubMed Central PMCID: PMC3123421.

87. Rose SD, Swift GH, Peyton MJ, Hammer RE, MacDonald RJ. The role of PTF1-P48 in pancreatic acinar gene expression. The Journal of biological chemistry. 2001;276(47):44018-26. doi: 10.1074/jbc.M106264200. PubMed PMID: 11562365.

88. Gu G, Dubauskaite J, Melton DA. Direct evidence for the pancreatic lineage: NGN3+ cells are islet progenitors and are distinct from duct progenitors. Development. 2002;129(10):2447-57. PubMed PMID: 11973276.

89. Miyatsuka T, Kaneto H, Shiraiwa T, Matsuoka TA, Yamamoto K, Kato K, Nakamura Y, Akira S, Takeda K, Kajimoto Y, Yamasaki Y, Sandgren EP, Kawaguchi Y, Wright CV, Fujitani Y. Persistent expression of PDX-1 in the pancreas causes acinar-to-ductal metaplasia through Stat3 activation. Genes & development. 2006;20(11):1435-40. doi: 10.1101/gad.1412806. PubMed PMID: 16751181; PubMed Central PMCID: PMC1475756.

90. Corcoran RB, Contino G, Deshpande V, Tzatsos A, Conrad C, Benes CH, Levy DE, Settleman J, Engelman JA, Bardeesy N. STAT3 plays a critical role in KRAS-induced pancreatic tumorigenesis. Cancer research. 2011;71(14):5020-9. doi: 10.1158/0008-5472.CAN-11-0908. PubMed PMID: 21586612; PubMed Central PMCID: PMC3693754.

91. Gruber R, Panayiotou R, Nye E, Spencer-Dene B, Stamp G, Behrens A. YAP1 and TAZ Control Pancreatic Cancer Initiation in Mice by Direct Up-regulation of JAK-STAT3 Signaling. Gastroenterology. 2016;151(3):526-39. doi: 10.1053/j.gastro.2016.05.006. PubMed PMID: 27215660; PubMed Central PMCID: PMC5007286.

92. Zhang W, Nandakumar N, Shi Y, Manzano M, Smith A, Graham G, Gupta S, Vietsch EE, Laughlin SZ, Wadhwa M, Chetram M, Joshi M, Wang F, Kallakury B, Toretsky J, Wellstein A, Yi C. Downstream of mutant KRAS, the transcription regulator YAP is essential for

neoplastic progression to pancreatic ductal adenocarcinoma. Science signaling. 2014;7(324):ra42. doi: 10.1126/scisignal.2005049. PubMed PMID: 24803537; PubMed Central PMCID: PMC4175524.

93. McConnell BB, Yang VW. Mammalian Kruppel-like factors in health and diseases. Physiological reviews. 2010;90(4):1337-81. doi: 10.1152/physrev.00058.2009. PubMed PMID: 20959618; PubMed Central PMCID: PMC2975554.

94. Bialkowska AB, Yang VW, Mallipattu SK. Kruppel-like factors in mammalian stem cells and development. Development. 2017;144(5):737-54. doi: 10.1242/dev.145441. PubMed PMID: 28246209; PubMed Central PMCID: PMC5374354.

95. Kim CK, He P, Bialkowska AB, Yang VW. SP and KLF Transcription Factors in Digestive Physiology and Diseases. Gastroenterology. 2017;152(8):1845-75. doi: 10.1053/j.gastro.2017.03.035. PubMed PMID: 28366734.

96. Wei D, Wang L, Yan Y, Jia Z, Gagea M, Li Z, Zuo X, Kong X, Huang S, Xie K. KLF4 Is Essential for Induction of Cellular Identity Change and Acinar-to-Ductal Reprogramming during Early Pancreatic Carcinogenesis. Cancer Cell. 2016;29(3):324-38. doi: 10.1016/j.ccell.2016.02.005. PubMed PMID: 26977883; PubMed Central PMCID: PMC4794756.

97. Brembeck FH, Rustgi AK. The tissue-dependent keratin 19 gene transcription is regulated by GKLF/KLF4 and Sp1. The Journal of biological chemistry. 2000;275(36):28230-9. doi: 10.1074/jbc.M004013200. PubMed PMID: 10859317.

98. Zammarchi F, Morelli M, Menicagli M, Di Cristofano C, Zavaglia K, Paolucci A, Campani D, Aretini P, Boggi U, Mosca F, Cavazzana A, Cartegni L, Bevilacqua G, Mazzanti CM. KLF4 is a novel candidate tumor suppressor gene in pancreatic ductal carcinoma. The American journal of pathology. 2011;178(1):361-72. doi: 10.1016/j.ajpath.2010.11.021. PubMed PMID: 21224073; PubMed Central PMCID: PMC3069861.

99. Yan Y, Li Z, Kong X, Jia Z, Zuo X, Gagea M, Huang S, Wei D, Xie K. KLF4-Mediated Suppression of CD44 Signaling Negatively Impacts Pancreatic Cancer Stemness and Metastasis. Cancer research. 2016;76(8):2419-31. doi: 10.1158/0008-5472.CAN-15-1691. PubMed PMID: 26880805; PubMed Central PMCID: PMC4876033.

100. Ardito CM, Gruner BM, Takeuchi KK, Lubeseder-Martellato C, Teichmann N, Mazur PK, Delgiorno KE, Carpenter ES, Halbrook CJ, Hall JC, Pal D, Briel T, Herner A, Trajkovic-Arsic M, Sipos B, Liou GY, Storz P, Murray NR, Threadgill DW, Sibilia M, Washington MK, Wilson CL, Schmid RM, Raines EW, Crawford HC, Siveke JT. EGF receptor is required for KRAS-induced pancreatic tumorigenesis. Cancer cell. 2012;22(3):304-17. doi: 10.1016/j.ccr.2012.07.024. PubMed PMID: 22975374; PubMed Central PMCID: PMC3443395.

101. Collins MA, Yan W, Sebolt-Leopold JS, Pasca di Magliano M. MAPK signaling is required for dedifferentiation of acinar cells and development of pancreatic intraepithelial neoplasia in mice. Gastroenterology. 2014;146(3):822-34 e7. doi: 10.1053/j.gastro.2013.11.052. PubMed PMID: 24315826; PubMed Central PMCID: PMC4037403.

102. Halbrook CJ, Wen HJ, Ruggeri JM, Takeuchi KK, Zhang Y, di Magliano MP, Crawford HC. Mitogen-activated Protein Kinase Kinase Activity Maintains Acinar-to-Ductal Metaplasia and Is Required for Organ Regeneration in Pancreatitis. Cellular and molecular gastroenterology and hepatology. 2017;3(1):99-118. doi: 10.1016/j.jcmgh.2016.09.009. PubMed PMID: 28090569.

103. Baer R, Cintas C, Dufresne M, Cassant-Sourdy S, Schonhuber N, Planque L, Lulka H, Couderc B, Bousquet C, Garmy-Susini B, Vanhaesebroeck B, Pyronnet S, Saur D, Guillermet-Guibert J. Pancreatic cell plasticity and cancer initiation induced by oncogenic Kras is completely dependent on wild-type PI 3-kinase p110alpha. Genes & development. 2014;28(23):2621-35. doi: 10.1101/gad.249409.114. PubMed PMID: 25452273; PubMed Central PMCID: PMC4248293.

104. Wu CY, Carpenter ES, Takeuchi KK, Halbrook CJ, Peverley LV, Bien H, Hall JC, DelGiorno KE, Pal D, Song Y, Shi C, Lin RZ, Crawford HC. PI3K regulation of RAC1 is required for KRAS-induced pancreatic tumorigenesis in mice. Gastroenterology. 2014;147(6):1405-16 e7. doi: 10.1053/j.gastro.2014.08.032. PubMed PMID: 25311989; PubMed Central PMCID: PMC4252806.

105. Payne SN, Maher ME, Tran NH, Van De Hey DR, Foley TM, Yueh AE, Leystra AA, Pasch CA, Jeffrey JJ, Clipson L, Matkowskyj KA, Deming DA. PIK3CA mutations can initiate pancreatic tumorigenesis and are targetable with PI3K inhibitors. Oncogenesis. 2015;4:e169. doi: 10.1038/oncsis.2015.28. PubMed PMID: 26436951; PubMed Central PMCID: PMC4632089.

106. Heid I, Lubeseder-Martellato C, Sipos B, Mazur PK, Lesina M, Schmid RM, Siveke JT. Early requirement of Rac1 in a mouse model of pancreatic cancer. Gastroenterology. 2011;141(2):719-30, 30 e1-7. doi: 10.1053/j.gastro.2011.04.043. PubMed PMID: 21684285.

107. Xu HN, Nioka S, Chance B, Li LZ. Heterogeneity of mitochondrial redox state in premalignant pancreas in a PTEN null transgenic mouse model. Advances in experimental medicine and biology. 2011;701:207-13. doi: 10.1007/978-1-4419-7756-4_28. PubMed PMID: 21445789; PubMed Central PMCID: PMC5679089.

108. Hill R, Calvopina JH, Kim C, Wang Y, Dawson DW, Donahue TR, Dry S, Wu H. PTEN loss accelerates KrasG12D-induced pancreatic cancer development. Cancer research. 2010;70(18):7114-24. doi: 10.1158/0008-5472.CAN-10-1649. PubMed PMID: 20807812; PubMed Central PMCID: PMC2940963.

109. Eser S, Reiff N, Messer M, Seidler B, Gottschalk K, Dobler M, Hieber M, Arbeiter A, Klein S, Kong B, Michalski CW, Schlitter AM, Esposito I, Kind AJ, Rad L, Schnieke AE, Baccarini M, Alessi DR, Rad R, Schmid RM, Schneider G, Saur D. Selective requirement of PI3K/PDK1 signaling for Kras oncogene-driven pancreatic cell plasticity and cancer. Cancer cell. 2013;23(3):406-20. doi: 10.1016/j.ccr.2013.01.023. PubMed PMID: 23453624.

110. Elghazi L, Weiss AJ, Barker DJ, Callaghan J, Staloch L, Sandgren EP, Gannon M, Adsay VN, Bernal-Mizrachi E. Regulation of pancreas plasticity and malignant transformation by Akt signaling. Gastroenterology. 2009;136(3):1091-103. doi: 10.1053/j.gastro.2008.11.043. PubMed PMID: 19121634; PubMed Central PMCID: PMC2739876.

111. Albury TM, Pandey V, Gitto SB, Dominguez L, Spinel LP, Talarchek J, Klein-Szanto AJ, Testa JR, Altomare DA. Constitutively active Akt1 cooperates with KRas(G12D) to accelerate in vivo pancreatic tumor onset and progression. Neoplasia. 2015;17(2):175-82. doi: 10.1016/j.neo.2014.12.006. PubMed PMID: 25748236; PubMed Central PMCID: PMC4351297.

112. Weiss GA, Rossi MR, Khushalani NI, Lo K, Gibbs JF, Bharthuar A, Cowell JK, Iyer R. Evaluation of phosphatidylinositol-3-kinase catalytic subunit (PIK3CA) and epidermal growth factor receptor (EGFR) gene mutations in pancreaticobiliary adenocarcinoma. Journal of gastrointestinal oncology. 2013;4(1):20-9. doi: 10.3978/j.issn.2078-6891.2012.012. PubMed PMID: 23450128; PubMed Central PMCID: PMC3562624.

113. Basturk O, Hong SM, Wood LD, Adsay NV, Albores-Saavedra J, Biankin AV, Brosens LA, Fukushima N, Goggins M, Hruban RH, Kato Y, Klimstra DS, Kloppel G, Krasinskas A, Longnecker DS, Matthaei H, Offerhaus GJ, Shimizu M, Takaori K, Terris B, Yachida S, Esposito I, Furukawa T, Baltimore Consensus M. A Revised Classification System and Recommendations From the Baltimore Consensus Meeting for Neoplastic Precursor Lesions in the Pancreas. The American journal of surgical pathology. 2015;39(12):1730-41. doi: 10.1097/PAS.0000000000000533. PubMed PMID: 26559377; PubMed Central PMCID: PMC4646710.

114. Newman K, Stahl-Herz J, Kabiawu O, Newman E, Wieczorek R, Wang B, Pei Z, Bannan M, Lee P, Xu R. Pancreatic carcinoma with multilineage (acinar, neuroendocrine, and ductal) differentiation. International journal of clinical and experimental pathology. 2009;2(6):602-7. PubMed PMID: 19636408; PubMed Central PMCID: PMC2713457.

115. Palagani V, Bozko P, El Khatib M, Belahmer H, Giese N, Sipos B, Malek NP, Plentz RR. Combined inhibition of Notch and JAK/STAT is superior to monotherapies and impairs pancreatic cancer progression. Carcinogenesis. 2014;35(4):859-66. doi: 10.1093/carcin/bgt394. PubMed PMID: 24293409.

116. Aichler M, Seiler C, Tost M, Siveke J, Mazur PK, Da Silva-Buttkus P, Bartsch DK, Langer P, Chiblak S, Durr A, Hofler H, Kloppel G, Muller-Decker K, Brielmeier M, Esposito I. Origin of pancreatic ductal adenocarcinoma from atypical flat lesions: a comparative study in transgenic mice and human tissues. The Journal of pathology. 2012;226(5):723-34. doi: 10.1002/path.3017. PubMed PMID: 21984419.

117. Donahue TR, Dawson DW. Leveraging Mechanisms Governing Pancreatic Tumorigenesis To Reduce Pancreatic Cancer Mortality. Trends in endocrinology and metabolism: TEM. 2016;27(11):770-81. doi: 10.1016/j.tem.2016.06.009. PubMed PMID: 27461042; PubMed Central PMCID: PMC5075262.

118. Noe M, Brosens LA. Pathology of Pancreatic Cancer Precursor Lesions. Surgical pathology clinics. 2016;9(4):561-80. doi: 10.1016/j.path.2016.05.004. PubMed PMID: 27926360.

119. Shindo T, Manabe I, Fukushima Y, Tobe K, Aizawa K, Miyamoto S, Kawai-Kowase K, Moriyama N, Imai Y, Kawakami H, Nishimatsu H, Ishikawa T, Suzuki T, Morita H, Maemura K, Sata M, Hirata Y, Komukai M, Kagechika H, Kadowaki T, Kurabayashi M, Nagai R.

Kruppel-like zinc-finger transcription factor KLF5/BTEB2 is a target for angiotensin II signaling and an essential regulator of cardiovascular remodeling. Nature medicine. 2002;8(8):856-63. doi: 10.1038/nm738. PubMed PMID: 12101409.

120. Conkright MD, Wani MA, Anderson KP, Lingrel JB. A gene encoding an intestinal-enriched member of the Kruppel-like factor family expressed in intestinal epithelial cells. Nucleic acids research. 1999;27(5):1263-70. PubMed PMID: 9973612; PubMed Central PMCID: PMC148310.

121. McConnell BB, Kim SS, Yu K, Ghaleb AM, Takeda N, Manabe I, Nusrat A, Nagai R, Yang VW. Kruppel-like factor 5 is important for maintenance of crypt architecture and barrier function in mouse intestine. Gastroenterology. 2011;141(4):1302-13, 13 e1-6. doi: 10.1053/j.gastro.2011.06.086. PubMed PMID: 21763241; PubMed Central PMCID: PMC3186863.

122. Bell SM, Zhang L, Xu Y, Besnard V, Wert SE, Shroyer N, Whitsett JA. Kruppel-like factor 5 controls villus formation and initiation of cytodifferentiation in the embryonic intestinal epithelium. Developmental biology. 2013;375(2):128-39. doi: 10.1016/j.ydbio.2012.12.010. PubMed PMID: 23266329; PubMed Central PMCID: PMC3582784.

123. Nandan MO, Ghaleb AM, Liu Y, Bialkowska AB, McConnell BB, Shroyer KR, Robine S, Yang VW. Inducible intestine-specific deletion of Kruppel-like factor 5 is characterized by a regenerative response in adult mouse colon. Developmental biology. 2014;387(2):191-202. doi: 10.1016/j.ydbio.2014.01.002. PubMed PMID: 24440658; PubMed Central PMCID: PMC3949508.

124. McConnell BB, Klapproth JM, Sasaki M, Nandan MO, Yang VW. Kruppel-like factor 5 mediates transmissible murine colonic hyperplasia caused by Citrobacter rodentium infection. Gastroenterology. 2008;134(4):1007-16. doi: 10.1053/j.gastro.2008.01.013. PubMed PMID: 18395082; PubMed Central PMCID: PMC2336106.

125. McConnell BB, Kim SS, Bialkowska AB, Yu K, Sitaraman SV, Yang VW. Kruppel-like factor 5 protects against dextran sulfate sodium-induced colonic injury in mice by promoting epithelial repair. Gastroenterology. 2011;140(2):540-9 e2. doi: 10.1053/j.gastro.2010.10.061. PubMed PMID: 21078320; PubMed Central PMCID: PMC3031670.

126. Tetreault MP, Alrabaa R, McGeehan M, Katz JP. Kruppel-like factor 5 protects against murine colitis and activates JAK-STAT signaling in vivo. PloS one. 2012;7(5):e38338. doi: 10.1371/journal.pone.0038338. PubMed PMID: 22675454; PubMed Central PMCID: PMC3364979.

127. Zhao Y, Hamza MS, Leong HS, Lim CB, Pan YF, Cheung E, Soo KC, Iyer NG. Kruppel-like factor 5 modulates p53-independent apoptosis through Pim1 survival kinase in cancer cells. Oncogene. 2008;27(1):1-8. doi: 10.1038/sj.onc.1210625. PubMed PMID: 17603560.

128. Li M, Gu Y, Ma YC, Shang ZF, Wang C, Liu FJ, Cao JP, Wan HJ, Zhang XG. Kruppel-Like Factor 5 Promotes Epithelial Proliferation and DNA Damage Repair in the Intestine of

Irradiated Mice. International journal of biological sciences. 2015;11(12):1458-68. doi: 10.7150/ijbs.13444. PubMed PMID: 26681925; PubMed Central PMCID: PMC4672003.

129. Shibata M, Chiba T, Matsuoka T, Mihara N, Kawashiri S, Imai K. Kruppel-like factors 4 and 5 expression and their involvement in differentiation of oral carcinomas. International journal of clinical and experimental pathology. 2015;8(4):3701-9. PubMed PMID: 26097551; PubMed Central PMCID: PMC4466938.

130. Noto JM, Khizanishvili T, Chaturvedi R, Piazuelo MB, Romero-Gallo J, Delgado AG, Khurana SS, Sierra JC, Krishna US, Suarez G, Powell AE, Goldenring JR, Coffey RJ, Yang VW, Correa P, Mills JC, Wilson KT, Peek RM, Jr. Helicobacter pylori promotes the expression of Kruppel-like factor 5, a mediator of carcinogenesis, in vitro and in vivo. PloS one. 2013;8(1):e54344. doi: 10.1371/journal.pone.0054344. PubMed PMID: 23372710; PubMed Central PMCID: PMC3553174.

131. Mori A, Moser C, Lang SA, Hackl C, Gottfried E, Kreutz M, Schlitt HJ, Geissler EK, Stoeltzing O. Up-regulation of Kruppel-like factor 5 in pancreatic cancer is promoted by interleukin-1beta signaling and hypoxia-inducible factor-1alpha. Molecular cancer research : MCR. 2009;7(8):1390-8. doi: 10.1158/1541-7786.MCR-08-0525. PubMed PMID: 19671674.

132. David CJ, Huang YH, Chen M, Su J, Zou Y, Bardeesy N, Iacobuzio-Donahue CA, Massague J. TGF-beta Tumor Suppression through a Lethal EMT. Cell. 2016;164(5):1015-30. doi: 10.1016/j.cell.2016.01.009. PubMed PMID: 26898331; PubMed Central PMCID: PMC4801341.

133. Chanchevalap S, Nandan MO, Merlin D, Yang VW. All-trans retinoic acid inhibits proliferation of intestinal epithelial cells by inhibiting expression of the gene encoding Kruppel-like factor 5. FEBS letters. 2004;578(1-2):99-105. doi: 10.1016/j.febslet.2004.10.079. PubMed PMID: 15581624; PubMed Central PMCID: PMC1599793.

134. Du JX, Yun CC, Bialkowska A, Yang VW. Protein inhibitor of activated STAT1 interacts with and up-regulates activities of the pro-proliferative transcription factor Kruppel-like factor 5. The Journal of biological chemistry. 2007;282(7):4782-93. doi: 10.1074/jbc.M603413200. PubMed PMID: 17178721; PubMed Central PMCID: PMC2212600.

135. Zhang H, Bialkowska A, Rusovici R, Chanchevalap S, Shim H, Katz JP, Yang VW, Yun CC. Lysophosphatidic acid facilitates proliferation of colon cancer cells via induction of Kruppel-like factor 5. The Journal of biological chemistry. 2007;282(21):15541-9. doi: 10.1074/jbc.M700702200. PubMed PMID: 17430902; PubMed Central PMCID: PMC2000347.

136. Guo L, He P, No YR, Yun CC. Kruppel-like factor 5 incorporates into the beta-catenin/TCF complex in response to LPA in colon cancer cells. Cellular signalling. 2015;27(5):961-8. doi: 10.1016/j.cellsig.2015.02.005. PubMed PMID: 25683913; PubMed Central PMCID: PMC4361321.

137. McConnell BB, Bialkowska AB, Nandan MO, Ghaleb AM, Gordon FJ, Yang VW. Haploinsufficiency of Kruppel-like factor 5 rescues the tumor-initiating effect of the Apc(Min)

mutation in the intestine. Cancer research. 2009;69(10):4125-33. doi: 10.1158/0008-5472.CAN-08-4402. PubMed PMID: 19435907; PubMed Central PMCID: PMC2702486.

138. Nandan MO, Yoon HS, Zhao W, Ouko LA, Chanchevalap S, Yang VW. Kruppel-like factor 5 mediates the transforming activity of oncogenic H-Ras. Oncogene. 2004;23(19):3404-13. doi: 10.1038/sj.onc.1207397. PubMed PMID: 15077182; PubMed Central PMCID: PMC1351030.

139. Nandan MO, Chanchevalap S, Dalton WB, Yang VW. Kruppel-like factor 5 promotes mitosis by activating the cyclin B1/Cdc2 complex during oncogenic Ras-mediated transformation. FEBS letters. 2005;579(21):4757-62. doi: 10.1016/j.febslet.2005.07.053. PubMed PMID: 16102754; PubMed Central PMCID: PMC1626271.

140. Nandan MO, Ghaleb AM, McConnell BB, Patel NV, Robine S, Yang VW. Kruppel-like factor 5 is a crucial mediator of intestinal tumorigenesis in mice harboring combined ApcMin and KRASV12 mutations. Molecular cancer. 2010;9:63. doi: 10.1186/1476-4598-9-63. PubMed PMID: 20298593; PubMed Central PMCID: PMC2856552.

141. Nandan MO, McConnell BB, Ghaleb AM, Bialkowska AB, Sheng H, Shao J, Babbin BA, Robine S, Yang VW. Kruppel-like factor 5 mediates cellular transformation during oncogenic KRAS-induced intestinal tumorigenesis. Gastroenterology. 2008;134(1):120-30. doi: 10.1053/j.gastro.2007.10.023. PubMed PMID: 18054006; PubMed Central PMCID: PMC2194652.

142. Grutzmann R, Boriss H, Ammerpohl O, Luttges J, Kalthoff H, Schackert HK, Kloppel G, Saeger HD, Pilarsky C. Meta-analysis of microarray data on pancreatic cancer defines a set of commonly dysregulated genes. Oncogene. 2005;24(32):5079-88. doi: 10.1038/sj.onc.1208696. PubMed PMID: 15897887.

143. Shain AH, Salari K, Giacomini CP, Pollack JR. Integrative genomic and functional profiling of the pancreatic cancer genome. BMC genomics. 2013;14:624. doi: 10.1186/1471-2164-14-624. PubMed PMID: 24041470; PubMed Central PMCID: PMC3848637.

144. Diaferia GR, Balestrieri C, Prosperini E, Nicoli P, Spaggiari P, Zerbi A, Natoli G. Dissection of transcriptional and cis-regulatory control of differentiation in human pancreatic cancer. The EMBO journal. 2016;35(6):595-617. doi: 10.15252/embj.201592404. PubMed PMID: 26769127; PubMed Central PMCID: PMC4801945.

145. Wu C, Miao X, Huang L, Che X, Jiang G, Yu D, Yang X, Cao G, Hu Z, Zhou Y, Zuo C, Wang C, Zhang X, Zhou Y, Yu X, Dai W, Li Z, Shen H, Liu L, Chen Y, Zhang S, Wang X, Zhai K, Chang J, Liu Y, Sun M, Cao W, Gao J, Ma Y, Zheng X, Cheung ST, Jia Y, Xu J, Tan W, Zhao P, Wu T, Wang C, Lin D. Genome-wide association study identifies five loci associated with susceptibility to pancreatic cancer in Chinese populations. Nature genetics. 2011;44(1):62-6. doi: 10.1038/ng.1020. PubMed PMID: 22158540.

146. Zhang X, Choi PS, Francis JM, Gao GF, Campbell JD, Ramachandran A, Mitsuishi Y, Ha G, Shih J, Vazquez F, Tsherniak A, Taylor AM, Zhou J, Wu Z, Berger AC, Giannakis M, Hahn WC, Cherniack AD, Meyerson M. Somatic super-enhancer duplications and hotspot

mutations lead to oncogenic activation of the KLF5 transcription factor. Cancer discovery. 2017. doi: 10.1158/2159-8290.CD-17-0532. PubMed PMID: 28963353.

147. Takeda N, Manabe I, Uchino Y, Eguchi K, Matsumoto S, Nishimura S, Shindo T, Sano M, Otsu K, Snider P, Conway SJ, Nagai R. Cardiac fibroblasts are essential for the adaptive response of the murine heart to pressure overload. The Journal of clinical investigation. 2010;120(1):254-65. doi: 10.1172/JCI40295. PubMed PMID: 20038803; PubMed Central PMCID: PMC2798693.

148. Tuveson DA, Shaw AT, Willis NA, Silver DP, Jackson EL, Chang S, Mercer KL, Grochow R, Hock H, Crowley D, Hingorani SR, Zaks T, King C, Jacobetz MA, Wang L, Bronson RT, Orkin SH, DePinho RA, Jacks T. Endogenous oncogenic K-ras(G12D) stimulates proliferation and widespread neoplastic and developmental defects. Cancer cell. 2004;5(4):375-87. PubMed PMID: 15093544.

149. Schneider CA, Rasband WS, Eliceiri KW. NIH Image to ImageJ: 25 years of image analysis. Nature methods. 2012;9(7):671-5. PubMed PMID: 22930834; PubMed Central PMCID: PMC5554542.

150. Ruiz de Sabando A, Wang C, He Y, Garcia-Barros M, Kim J, Shroyer KR, Bannister TD, Yang VW, Bialkowska AB. ML264, A Novel Small-Molecule Compound That Potently Inhibits Growth of Colorectal Cancer. Molecular cancer therapeutics. 2016;15(1):72-83. doi: 10.1158/1535-7163.MCT-15-0600. PubMed PMID: 26621868; PubMed Central PMCID: PMC4707060.

151. Torres MP, Rachagani S, Souchek JJ, Mallya K, Johansson SL, Batra SK. Novel pancreatic cancer cell lines derived from genetically engineered mouse models of spontaneous pancreatic adenocarcinoma: applications in diagnosis and therapy. PloS one. 2013;8(11):e80580. doi: 10.1371/journal.pone.0080580. PubMed PMID: 24278292; PubMed Central PMCID: PMC3835415.

152. Wiederschain D, Wee S, Chen L, Loo A, Yang G, Huang A, Chen Y, Caponigro G, Yao YM, Lengauer C, Sellers WR, Benson JD. Single-vector inducible lentiviral RNAi system for oncology target validation. Cell cycle. 2009;8(3):498-504. doi: 10.4161/cc.8.3.7701. PubMed PMID: 19177017.

153. Reiser J, Harmison G, Kluepfel-Stahl S, Brady RO, Karlsson S, Schubert M. Transduction of nondividing cells using pseudotyped defective high-titer HIV type 1 particles. Proceedings of the National Academy of Sciences of the United States of America. 1996;93(26):15266-71. PubMed PMID: 8986799; PubMed Central PMCID: PMC26392.

154. Zhang XY, La Russa VF, Reiser J. Transduction of bone-marrow-derived mesenchymal stem cells by using lentivirus vectors pseudotyped with modified RD114 envelope glycoproteins. Journal of virology. 2004;78(3):1219-29. PubMed PMID: 14722277; PubMed Central PMCID: PMC321376.

155. Sarbassov DD, Guertin DA, Ali SM, Sabatini DM. Phosphorylation and regulation of Akt/PKB by the rictor-mTOR complex. Science. 2005;307(5712):1098-101. doi: 10.1126/science.1106148. PubMed PMID: 15718470.

156. Cong L, Zhang F. Genome engineering using CRISPR-Cas9 system. Methods in molecular biology. 2015;1239:197-217. doi: 10.1007/978-1-4939-1862-1_10. PubMed PMID: 25408407.

157. Bialkowska AB, Crisp M, Bannister T, He Y, Chowdhury S, Schurer S, Chase P, Spicer T, Madoux F, Tian C, Hodder P, Zaharevitz D, Yang VW. Identification of small-molecule inhibitors of the colorectal cancer oncogene Kruppel-like factor 5 expression by ultrahigh-throughput screening. Molecular cancer therapeutics. 2011;10(11):2043-51. doi: 10.1158/1535-7163.MCT-11-0550. PubMed PMID: 21885866; PubMed Central PMCID: PMC3213326.

158. Bray NL, Pimentel H, Melsted P, Pachter L. Near-optimal probabilistic RNA-seq quantification. Nature biotechnology. 2016;34(5):525-7. doi: 10.1038/nbt.3519. PubMed PMID: 27043002.

159. Wang L, Wang S, Li W. RSeQC: quality control of RNA-seq experiments. Bioinformatics. 2012;28(16):2184-5. doi: 10.1093/bioinformatics/bts356. PubMed PMID: 22743226.

160. Love MI, Huber W, Anders S. Moderated estimation of fold change and dispersion for RNA-seq data with DESeq2. Genome biology. 2014;15(12):550. doi: 10.1186/s13059-014-0550-8. PubMed PMID: 25516281; PubMed Central PMCID: PMC4302049.

161. Bialkowska AB, Liu Y, Nandan MO, Yang VW. A colon cancer-derived mutant of Kruppel-like factor 5 (KLF5) is resistant to degradation by glycogen synthase kinase 3beta (GSK3beta) and the E3 ubiquitin ligase F-box and WD repeat domain-containing 7alpha (FBW7alpha). The Journal of biological chemistry. 2014;289(9):5997-6005. doi: 10.1074/jbc.M113.508549. PubMed PMID: 24398687; PubMed Central PMCID: PMC3937667.

162. Zeitouni D, Pylayeva-Gupta Y, Der CJ, Bryant KL. KRAS Mutant Pancreatic Cancer: No Lone Path to an Effective Treatment. Cancers. 2016;8(4). doi: 10.3390/cancers8040045. PubMed PMID: 27096871; PubMed Central PMCID: PMC4846854.

163. Raimondi S, Lowenfels AB, Morselli-Labate AM, Maisonneuve P, Pezzilli R. Pancreatic cancer in chronic pancreatitis; aetiology, incidence, and early detection. Best practice & research Clinical gastroenterology. 2010;24(3):349-58. doi: 10.1016/j.bpg.2010.02.007. PubMed PMID: 20510834.

164. Morris JPt, Cano DA, Sekine S, Wang SC, Hebrok M. Beta-catenin blocks Kras-dependent reprogramming of acini into pancreatic cancer precursor lesions in mice. The Journal of clinical investigation. 2010;120(2):508-20. doi: 10.1172/JCI40045. PubMed PMID: 20071774; PubMed Central PMCID: PMC2810083.

165. Hu W, Fan C, Jiang P, Ma Z, Yan X, Di S, Jiang S, Li T, Cheng Y, Yang Y. Emerging role of N-myc downstream-regulated gene 2 (NDRG2) in cancer. Oncotarget. 2016;7(1):209-23.

doi: 10.18632/oncotarget.6228. PubMed PMID: 26506239; PubMed Central PMCID: PMC4807993.

166. Kim MJ, Lim J, Yang Y, Lee MS, Lim JS. N-myc downstream-regulated gene 2 (NDRG2) suppresses the epithelial-mesenchymal transition (EMT) in breast cancer cells via STAT3/Snail signaling. Cancer letters. 2014;354(1):33-42. doi: 10.1016/j.canlet.2014.06.023. PubMed PMID: 25153349.

167. Ji B, Tsou L, Wang H, Gaiser S, Chang DZ, Daniluk J, Bi Y, Grote T, Longnecker DS, Logsdon CD. Ras activity levels control the development of pancreatic diseases. Gastroenterology. 2009;137(3):1072-82, 82 e1-6. doi: 10.1053/j.gastro.2009.05.052. PubMed PMID: 19501586; PubMed Central PMCID: PMC2789008.

168. Hu XL, Liu XP, Lin SX, Deng YC, Liu N, Li X, Yao LB. NDRG2 expression and mutation in human liver and pancreatic cancers. World journal of gastroenterology. 2004;10(23):3518-21. PubMed PMID: 15526377; PubMed Central PMCID: PMC4576239.

169. Yamamura A, Miura K, Karasawa H, Morishita K, Abe K, Mizuguchi Y, Saiki Y, Fukushige S, Kaneko N, Sase T, Nagase H, Sunamura M, Motoi F, Egawa S, Shibata C, Unno M, Sasaki I, Horii A. Suppressed expression of NDRG2 correlates with poor prognosis in pancreatic cancer. Biochem Biophys Res Commun. 2013;441(1):102-7. doi: 10.1016/j.bbrc.2013.10.010. PubMed PMID: 24134849.

170. Park Y, Shon SK, Kim A, Kim KI, Yang Y, Cho DH, Lee MS, Lim JS. SOCS1 induced by NDRG2 expression negatively regulates STAT3 activation in breast cancer cells. Biochemical and biophysical research communications. 2007;363(2):361-7. doi: 10.1016/j.bbrc.2007.08.195. PubMed PMID: 17888401.

171. Guo P, Zhao KW, Dong XY, Sun X, Dong JT. Acetylation of KLF5 alters the assembly of p15 transcription factors in transforming growth factor-beta-mediated induction in epithelial cells. The Journal of biological chemistry. 2009;284(27):18184-93. doi: 10.1074/jbc.M109.007096. PubMed PMID: 19419955; PubMed Central PMCID: PMC2709394.

172. Zhang J, Li F, Liu X, Shen L, Liu J, Su J, Zhang W, Deng Y, Wang L, Liu N, Han W, Zhang J, Ji S, Yang A, Han H, Yao L. The repression of human differentiation-related gene NDRG2 expression by Myc via Miz-1-dependent interaction with the NDRG2 core promoter. J Biol Chem. 2006;281(51):39159-68. doi: 10.1074/jbc.M605820200. PubMed PMID: 17050536.

173. Matsumura T, Suzuki T, Aizawa K, Munemasa Y, Muto S, Horikoshi M, Nagai R. The deacetylase HDAC1 negatively regulates the cardiovascular transcription factor Kruppel-like factor 5 through direct interaction. The Journal of biological chemistry. 2005;280(13):12123-9. doi: 10.1074/jbc.M410578200. PubMed PMID: 15668237.

174. Nakagawa M, Koyanagi M, Tanabe K, Takahashi K, Ichisaka T, Aoi T, Okita K, Mochiduki Y, Takizawa N, Yamanaka S. Generation of induced pluripotent stem cells without Myc from mouse and human fibroblasts. Nature biotechnology. 2008;26(1):101-6. doi: 10.1038/nbt1374. PubMed PMID: 18059259.

175. Uhlen M, Zhang C, Lee S, Sjostedt E, Fagerberg L, Bidkhori G, Benfeitas R, Arif M, Liu Z, Edfors F, Sanli K, von Feilitzen K, Oksvold P, Lundberg E, Hober S, Nilsson P, Mattsson J, Schwenk JM, Brunnstrom H, Glimelius B, Sjoblom T, Edqvist PH, Djureinovic D, Micke P, Lindskog C, Mardinoglu A, Ponten F. A pathology atlas of the human cancer transcriptome. Science. 2017;357(6352). doi: 10.1126/science.aan2507. PubMed PMID: 28818916.

176. Ran FA, Hsu PD, Lin CY, Gootenberg JS, Konermann S, Trevino AE, Scott DA, Inoue A, Matoba S, Zhang Y, Zhang F. Double nicking by RNA-guided CRISPR Cas9 for enhanced genome editing specificity. Cell. 2013;154(6):1380-9. doi: 10.1016/j.cell.2013.08.021. PubMed PMID: 23992846; PubMed Central PMCID: PMC3856256.

177. Wasif N, Ko CY, Farrell J, Wainberg Z, Hines OJ, Reber H, Tomlinson JS. Impact of tumor grade on prognosis in pancreatic cancer: should we include grade in AJCC staging? Annals of surgical oncology. 2010;17(9):2312-20. doi: 10.1245/s10434-010-1071-7. PubMed PMID: 20422460; PubMed Central PMCID: PMC2924500.

178. Bialkowska A, Crisp M, Madoux F, Spicer T, Knapinska A, Mercer B, Bannister TD, He Y, Chowdhury S, Cameron M, Yang VW, Hodder P. ML264: An Antitumor Agent that Potently and Selectively Inhibits Kruppel-like Factor Five (KLF5) Expression: A Probe for Studying Colon Cancer Development and Progression. Probe Reports from the NIH Molecular Libraries Program. Bethesda (MD)2010.

179. Suzuki T, Sawaki D, Aizawa K, Munemasa Y, Matsumura T, Ishida J, Nagai R. Kruppel-like factor 5 shows proliferation-specific roles in vascular remodeling, direct stimulation of cell growth, and inhibition of apoptosis. The Journal of biological chemistry. 2009;284(14):9549-57. doi: 10.1074/jbc.M806230200. PubMed PMID: 19189969; PubMed Central PMCID: PMC2666607.

180. Borel F, Lacroix FB, Margolis RL. Prolonged arrest of mammalian cells at the G1/S boundary results in permanent S phase stasis. Journal of cell science. 2002;115(Pt 14):2829-38. PubMed PMID: 12082144.

181. Ford JC, al-Khodairy F, Fotou E, Sheldrick KS, Griffiths DJ, Carr AM. 14-3-3 protein homologs required for the DNA damage checkpoint in fission yeast. Science. 1994;265(5171):533-5. PubMed PMID: 8036497.

182. Weng Z, Fluckiger AC, Nisitani S, Wahl MI, Le LQ, Hunter CA, Fernal AA, Le Beau MM, Witte ON. A DNA damage and stress inducible G protein-coupled receptor blocks cells in G2/M. Proceedings of the National Academy of Sciences of the United States of America. 1998;95(21):12334-9. PubMed PMID: 9770487; PubMed Central PMCID: PMC22832.

183. Niehrs C, Schafer A. Active DNA demethylation by Gadd45 and DNA repair. Trends in cell biology. 2012;22(4):220-7. doi: 10.1016/j.tcb.2012.01.002. PubMed PMID: 22341196.

184. Knudsen KE, Booth D, Naderi S, Sever-Chroneos Z, Fribourg AF, Hunton IC, Feramisco JR, Wang JY, Knudsen ES. RB-dependent S-phase response to DNA damage. Molecular and cellular biology. 2000;20(20):7751-63. PubMed PMID: 11003670; PubMed Central PMCID: PMC86358.

185. Jain R, Fischer S, Serra S, Chetty R. The use of Cytokeratin 19 (CK19) immunohistochemistry in lesions of the pancreas, gastrointestinal tract, and liver. Applied immunohistochemistry & molecular morphology : AIMM. 2010;18(1):9-15. doi: 10.1097/PAI.0b013e3181ad36ea. PubMed PMID: 19956064.

186. Noda S, Asano Y, Nishimura S, Taniguchi T, Fujiu K, Manabe I, Nakamura K, Yamashita T, Saigusa R, Akamata K, Takahashi T, Ichimura Y, Toyama T, Tsuruta D, Trojanowska M, Nagai R, Sato S. Simultaneous downregulation of KLF5 and Fli1 is a key feature underlying systemic sclerosis. Nature communications. 2014;5:5797. doi: 10.1038/ncomms6797. PubMed PMID: 25504335; PubMed Central PMCID: PMC4268882.

187. Howlader N, Noone AM, Krapcho M, Garshell J, Miller D, Altekruse SF, Kosary CL, Yu M, Ruhl J, Tatalovich Z, Mariotto AB, Lewis DR, Chen HS, Feuer EJ, Cronin KA. SEER Cancer Statistics Review, 1975-2012 based on November 2014 SEER data submission, posted to the SEER web site, April 2015. Available from: http://seer.cancer.gov/csr/1975_2012/.

188. Singh D, Upadhyay G, Srivastava RK, Shankar S. Recent advances in pancreatic cancer: biology, treatment, and prevention. Biochimica et biophysica acta. 2015;1856(1):13-27. doi: 10.1016/j.bbcan.2015.04.003. PubMed PMID: 25977074.

189. Distler M, Aust D, Weitz J, Pilarsky C, Grutzmann R. Precursor lesions for sporadic pancreatic cancer: PanIN, IPMN, and MCN. BioMed research international. 2014;2014:474905. doi: 10.1155/2014/474905. PubMed PMID: 24783207; PubMed Central PMCID: PMC3982269.

190. Ischenko I, Petrenko O, Hayman MJ. Analysis of the tumor-initiating and metastatic capacity of PDX1-positive cells from the adult pancreas. Proceedings of the National Academy of Sciences of the United States of America. 2014;111(9):3466-71. doi: 10.1073/pnas.1319911111. PubMed PMID: 24550494; PubMed Central PMCID: PMC3948305.

191. Dong JT, Chen C. Essential role of KLF5 transcription factor in cell proliferation and differentiation and its implications for human diseases. Cellular and molecular life sciences : CMLS. 2009;66(16):2691-706. doi: 10.1007/s00018-009-0045-z. PubMed PMID: 19448973.

192. Hu XL, Liu XP, Deng YC, Lin SX, Wu L, Zhang J, Wang LF, Wang XB, Li X, Shen L, Zhang YQ, Yao LB. Expression analysis of the NDRG2 gene in mouse embryonic and adult tissues. Cell and tissue research. 2006;325(1):67-76. doi: 10.1007/s00441-005-0137-5. PubMed PMID: 16520977.

193. Kim A, Kim MJ, Yang Y, Kim JW, Yeom YI, Lim JS. Suppression of NF-kappaB activity by NDRG2 expression attenuates the invasive potential of highly malignant tumor cells. Carcinogenesis. 2009;30(6):927-36. doi: 10.1093/carcin/bgp072. PubMed PMID: 19336468.

194. Stoop-Myer C, Amon A. Meiosis: Rec8 is the reason for cohesion. Nature cell biology. 1999;1(5):E125-7. doi: 10.1038/12956. PubMed PMID: 10559953.

195. Yu J, Liang Q, Wang J, Wang K, Gao J, Zhang J, Zeng Y, Chiu PW, Ng EK, Sung JJ. REC8 functions as a tumor suppressor and is epigenetically downregulated in gastric cancer,

especially in EBV-positive subtype. Oncogene. 2017;36(2):182-93. doi: 10.1038/onc.2016.187. PubMed PMID: 27212034; PubMed Central PMCID: PMC5241426.

196. Liu D, Shen X, Zhu G, Xing M. REC8 is a novel tumor suppressor gene epigenetically robustly targeted by the PI3K pathway in thyroid cancer. Oncotarget. 2015;6(36):39211-24. doi: 10.18632/oncotarget.5391. PubMed PMID: 26472282; PubMed Central PMCID: PMC4770767.

197. Ishiguro T, Tanaka K, Sakuno T, Watanabe Y. Shugoshin-PP2A counteracts casein-kinase-1-dependent cleavage of Rec8 by separase. Nature cell biology. 2010;12(5):500-6. doi: 10.1038/ncb2052. PubMed PMID: 20383139.

198. Sousa CM, Biancur DE, Wang X, Halbrook CJ, Sherman MH, Zhang L, Kremer D, Hwang RF, Witkiewicz AK, Ying H, Asara JM, Evans RM, Cantley LC, Lyssiotis CA, Kimmelman AC. Pancreatic stellate cells support tumour metabolism through autophagic alanine secretion. Nature. 2016;536(7617):479-83. doi: 10.1038/nature19084. PubMed PMID: 27509858; PubMed Central PMCID: PMC5228623.

199. Kolodziejczyk AA, Kim JK, Svensson V, Marioni JC, Teichmann SA. The technology and biology of single-cell RNA sequencing. Molecular cell. 2015;58(4):610-20. doi: 10.1016/j.molcel.2015.04.005. PubMed PMID: 26000846.

200. Dang DT, Zhao W, Mahatan CS, Geiman DE, Yang VW. Opposing effects of Kruppel-like factor 4 (gut-enriched Kruppel-like factor) and Kruppel-like factor 5 (intestinal-enriched Kruppel-like factor) on the promoter of the Kruppel-like factor 4 gene. Nucleic acids research. 2002;30(13):2736-41. PubMed PMID: 12087155; PubMed Central PMCID: PMC117055.

201. Chang JH, Jiang Y, Pillarisetty VG. Role of immune cells in pancreatic cancer from bench to clinical application: An updated review. Medicine. 2016;95(49):e5541. doi: 10.1097/MD.0000000000005541. PubMed PMID: 27930550; PubMed Central PMCID: PMC5266022.

202. Schonhuber N, Seidler B, Schuck K, Veltkamp C, Schachtler C, Zukowska M, Eser S, Feyerabend TB, Paul MC, Eser P, Klein S, Lowy AM, Banerjee R, Yang F, Lee CL, Moding EJ, Kirsch DG, Scheideler A, Alessi DR, Varela I, Bradley A, Kind A, Schnieke AE, Rodewald HR, Rad R, Schmid RM, Schneider G, Saur D. A next-generation dual-recombinase system for time- and host-specific targeting of pancreatic cancer. Nature medicine. 2014;20(11):1340-7. doi: 10.1038/nm.3646. PubMed PMID: 25326799; PubMed Central PMCID: PMC4270133.

203. Childs EJ, Mocci E, Campa D, Bracci PM, Gallinger S, Goggins M, Li D, Neale RE, Olson SH, Scelo G, Amundadottir LT, Bamlet WR, Bijlsma MF, Blackford A, Borges M, Brennan P, Brenner H, Bueno-de-Mesquita HB, Canzian F, Capurso G, Cavestro GM, Chaffee KG, Chanock SJ, Cleary SP, Cotterchio M, Foretova L, Fuchs C, Funel N, Gazouli M, Hassan M, Herman JM, Holcatova I, Holly EA, Hoover RN, Hung RJ, Janout V, Key TJ, Kupcinskas J, Kurtz RC, Landi S, Lu L, Malecka-Panas E, Mambrini A, Mohelnikova-Duchonova B, Neoptolemos JP, Oberg AL, Orlow I, Pasquali C, Pezzilli R, Rizzato C, Saldia A, Scarpa A, Stolzenberg-Solomon RZ, Strobel O, Tavano F, Vashist YK, Vodicka P, Wolpin BM, Yu H, Petersen GM, Risch HA, Klein AP. Common variation at 2p13.3, 3q29, 7p13 and 17q25.1

associated with susceptibility to pancreatic cancer. Nature genetics. 2015;47(8):911-6. doi: 10.1038/ng.3341. PubMed PMID: 26098869; PubMed Central PMCID: PMC4520746.

204. Khan A, Fornes O, Stigliani A, Gheorghe M, Castro-Mondragon JA, van der Lee R, Bessy A, Cheneby J, Kulkarni SR, Tan G, Baranasic D, Arenillas DJ, Sandelin A, Vandepoele K, Lenhard B, Ballester B, Wasserman WW, Parcy F, Mathelier A. JASPAR 2018: update of the open-access database of transcription factor binding profiles and its web framework. Nucleic acids research. 2017. doi: 10.1093/nar/gkx1126. PubMed PMID: 29140473.

205. Weinstein IB, Joe A. Oncogene addiction. Cancer research. 2008;68(9):3077-80; discussion 80. doi: 10.1158/0008-5472.CAN-07-3293. PubMed PMID: 18451130.

Appendix A. Differentially Expressed Genes from RNA Sequencing

Differentially Expressed Genes in Pairwise Comparison between *Ptf1a-Cre^{ERTM};Klf5$^{fl/fl}$* and *Ptf1a-Cre^{ERTM}* at 2 days after Cerulein Treatment

Gene Name	Description	log2(FC)	*P*adj
Slc15a2	solute carrier family 15 (H+/peptide transporter), member 2	2.14	8.10E-11
Rec8	REC8 meiotic recombination protein	-1.73	7.73E-07
1500015A07Rik	RIKEN cDNA 1500015A07 gene	1.78	2.43E-06
Gm6472	predicted pseudogene 6472	1.99	4.04E-06
Glo1	glyoxalase 1	1.06	4.80E-06
Gm7666	predicted pseudogene 7666	2.41	0.000403
Gm13835	predicted gene 13835	1.77	0.003341
Cdk5rap1	CDK5 regulatory subunit associated protein 1	1.17	0.004172
Fmo2	flavin containing monooxygenase 2	1.18	0.008215
5830444B04Rik	RIKEN cDNA 5830444B04 gene	-4.01	0.010168
Zfp458	zinc finger protein 458	1.41	0.012686
2610035D17Rik	RIKEN cDNA 2610035D17 gene	-1.77	0.020163
Ndrg2	N-myc downstream regulated gene 2	1.05	0.021226
Gm13453	predicted gene 13453	3.56	0.026845
Ighv1-11	NA	-4.13	0.028305
Tmem181b-ps	transmembrane protein 181B, pseudogene	0.89	0.034145
Xlr3a	X-linked lymphocyte-regulated 3A	-1.74	0.038196
Olfr1372-ps1	olfactory receptor 1372, pseudogene 1	2.13	0.044578
Gcnt4	beta-1,6-N-acetylglucosaminyltransferase	1.84	0.045909

Differentially Expressed Genes in Pairwise Comparison between *Ptf1a-Cre^{ERTM};LSL-Kras^{G12D};Klf5$^{fl/fl}$* and *Ptf1a-Cre^{ERTM};LSL-Kras^{G12D}* at 2 days after Cerulein Treatment

Gene Name	Description	log2(FC)	*P*adj
Rpgrip1	retinitis pigmentosa GTPase regulator interacting protein 1	-3.168122091	1.51E-09
Gm6472	predicted pseudogene 6472	2.322621921	5.71E-09
Glo1	glyoxalase 1	1.199719124	4.17E-08
Gm7666	predicted pseudogene 7666	3.187184778	4.79E-08
1500015A07Rik	RIKEN cDNA 1500015A07 gene	1.736593085	2.80E-06
F830016B08Rik	RIKEN cDNA F830016B08 gene	-2.128551541	6.43E-05
Nat8	N-acetyltransferase 8 (GCN5-related, putative)	2.359732583	8.41E-05
Ndrg2	N-myc downstream regulated gene 2	1.287186322	0.000366997
Upp2	uridine phosphorylase 2	1.895630634	0.000400758

Gm26782	predicted gene, 26782	-1.552372368	0.00113584
Try10	trypsin 10	1.198119948	0.001573129
Rnf212	ring finger protein 212	1.540462472	0.002362912
2610035D17Rik	RIKEN cDNA 2610035D17 gene	-1.977040562	0.003149319
Rec8	REC8 meiotic recombination protein	-1.264794607	0.004137236
Npas2	neuronal PAS domain protein 2	-2.909073547	0.005900257
Gm13453	predicted gene 13453	3.65963997	0.005900257
Gm13835	predicted gene 13835	1.718109605	0.005900257
Arntl	aryl hydrocarbon receptor nuclear translocator-like	-2.290323267	0.006068246
Rprl3	ribonuclease P RNA-like 3	7.842341383	0.006068246

Appendix B. qPCR Array for Expression of Cell Cycle Regulator Genes

Position	Gene	Klf5 shRNA vs. Scrm shRNA (fold-change)	Standard Deviation	*P*-Value
A1	*Abl1*	1.74	0.12	0.002
A2	*Atm*	1.31	0.19	0.721
A3	*Atr*	1.48	0.22	0.932
A4	*Aurka*	0.62	0.02	0.003
A5	*Aurkb*	0.97	0.10	0.726
A6	*Bcl2*	1.84	0.12	0.001
A7	*Birc5*	1.08	0.09	0.704
A8	*Brca1*	1.35	0.12	0.480
A9	*Brca2*	1.16	0.20	0.804
A10	*Casp3*	1.25	0.11	0.462
A11	*Ccna1*	3.98	1.15	0.186
A12	*Ccna2*	0.95	0.08	0.672
B1	*Ccnb1*	2.44	0.16	0.002
B2	*Ccnb2*	1.05	0.10	0.462
B3	*Ccnc*	0.99	0.23	0.604
B4	*Ccnd1*	1.09	0.12	0.864
B5	*Ccnd2*	0.14	0.01	0.029
B6	*Ccnd3*	1.55	0.14	0.006
B7	*Ccne1*	2.22	0.16	0.000
B8	*Ccnf*	1.13	0.13	0.965
B9	*Cdc20*	1.27	0.06	0.062
B10	*Cdc25a*	5.06	0.38	0.000
B11	*Cdc25c*	1.08	0.09	0.439
B12	*Cdc6*	1.08	0.04	0.286
C1	*Cdc7*	1.93	0.20	0.298
C2	*Cdk1*	0.92	0.06	0.433
C3	*Cdk2*	5.71	0.36	0.000
C4	*Cdk4*	2.18	0.16	0.006
C5	*Cdk5rap1*	1.39	0.06	0.010
C6	*Cdk6*	1.42	0.11	0.039
C7	*Cdkn1a*	1.47	0.15	0.088
C8	*Cdkn1b*	0.65	0.05	0.148
C9	*Cdkn2a*	Undetermined	NA	NA
C10	*Cdkn2b*	Undetermined	NA	NA
C11	*Cdkn3*	0.64	0.08	0.018
C12	*Chek1*	1.34	0.27	0.932

D1	*Chek2*	0.64	0.05	0.135
D2	*Cks1b*	1.41	0.30	0.509
D3	*Ddit3*	1.05	0.08	0.604
D4	*Dst*	1.93	0.19	0.007
D5	*E2f1*	1.94	0.39	0.069
D6	*E2f2*	1.29	0.09	0.008
D7	*E2f3*	1.33	0.07	0.057
D8	*E2f4*	1.02	0.02	0.910
D9	*Gadd45a*	3.67	0.16	0.000
D10	*Gpr132*	3.43	1.49	0.048
D11	*Hus1*	0.84	0.03	0.406
D12	*Itgb1*	1.93	0.20	0.029
E1	*Mad2l1*	0.82	0.11	0.399
E2	*Mcm2*	1.02	0.05	0.880
E3	*Mcm3*	1.13	0.08	0.391
E4	*Mcm4*	1.48	0.10	0.020
E5	*Mdm2*	1.31	0.11	0.312
E6	*Mki67*	1.08	0.04	0.298
E7	*Mre11a*	1.02	0.07	0.926
E8	*Msh2*	0.94	0.13	0.487
E9	*Myb*	1.98	0.32	0.022
E10	*Nbn*	0.81	0.05	0.335
E11	*Nek2*	1.22	0.07	0.018
E12	*Notch2*	1.82	0.14	0.001
F1	*Pkd1*	1.12	0.20	0.381
F2	*Pmp22*	11.88	2.75	0.003
F3	*Ppm1d*	1.21	0.16	0.335
F4	*Rad17*	0.86	0.06	0.017
F5	*Rad21*	1.25	0.23	0.740
F6	*Rad51*	1.42	0.53	0.770
F7	*Rad9a*	0.95	0.09	0.577
F8	*Ran*	1.44	0.32	0.663
F9	*Rb1*	4.58	0.43	0.001
F10	*Rbl1*	1.15	0.06	0.749
F11	*Rbl2*	1.12	0.09	0.159
F12	*Sfn*	2.80	0.43	0.002
G1	*Shc1*	1.00	0.14	0.895
G2	*Skp2*	1.56	0.20	0.070
G3	*Slfn1*	Undetermined	NA	NA
G4	*Smc1a*	5.31	0.20	0.000
G5	*Stag1*	1.02	0.13	0.969

G6	*Stmn1*	1.75	0.17	0.075
G7	*Terf1*	0.88	0.13	0.463
G8	*Tfdp1*	1.01	0.06	0.972
G9	*Trp53*	0.77	0.02	0.032
G10	*Trp63*	Undetermined	NA	NA
G11	*Tsg101*	1.15	0.03	0.285
G12	*Wee1*	1.19	0.08	0.529
H1	*Actb*	0.97	0.04	0.394
H2	*B2m*	2.72	0.45	0.027
H3	*Gapdh*	0.76	0.08	0.230
H4	*Gusb*	1.11	0.06	0.471
H5	*Hsp90ab1*	1.23	0.07	0.111